

DECOMPOSITION
WITH
SOFT SPECIFICATIONS

LARGE SYSTEM OPTIMIZATION

USING

DECOMPOSITION

WITH

SOFT SPECIFICATIONS

by

WAHID K. MICHAEL^o, B.Sc. (ENG.)

A Thesis

Submitted to the Faculty of Graduate Studies

in Partial Fulfilment of the Requirements

for the Degree

Master of Engineering

McMaster University

Master of Engineering (1977)
(Mechanical Engineering)

McMaster University
Hamilton, Ontario

TITLE : LARGE SYSTEM OPTIMIZATION USING
DECOMPOSITION WITH SOFT SPECIFICATIONS.
AUTHOR : WAHID K. MICHAEL, B.Sc. (Eng.), Cairo Univ.
SUPERVISOR : PROFESSOR J.N. SIDDALL.
NUMBER OF PAGES : viii , 187

ABSTRACT

The problem considered is that of obtaining an optimum solution to large nonlinear engineering system by coordinated optimum solutions of smaller sub-systems. The technique produces a way of displaying graphically and numerically the trade-offs between each sub-system design objective and the sub-system joint design specifications. A nonlinear multi-variable fitting model is developed to represent the trade-off hypersurface. Shape, potential and advantages of the trade-off surfaces also are illustrated.

ACKNOWLEDGMENTS

The author wishes to express his sincere gratitude to his supervisor Professor J.N. Siddall for his constant guidance and encouragement.

The interest and advice of Professor B. Latta and Professor D.R. Woods are gratefully acknowledged.

Thanks are due to Mr. Tom Pal and Mr. S. Ziada for their kind help.

Further the author is indebted to the Department of Mechanical Engineering for the scholarship award and the teaching assistantship and to McMaster Computer Centre for the good service.

TABLE OF CONTENTS

<u>CHAPTER</u>		<u>PAGE</u>
1	INTRODUCTION	1
2	TRADE-OFF CURVES	3
2.1	Definition	3
2.2	Generation	3
2.3	Examples	15
	2.3.1 Shrink Fitted Cylinders	15
	2.3.2 Axial Flow Fan	20
2.4	Results	30
2.5	Conclusion	48
3	DECOMPOSITION	64
3.1	General	64
3.2	Approach	65
3.3	Example: Heat Exchanger and Fan System	70
3.4	Results	83
3.5	Conclusion	85
4	DISCUSSION AND RECOMMENDATIONS	89
4.1	Evaluation and Conclusions	89
4.2	Future Research	91
	REFERENCES	92
	APPENDICES	
A.	Cost or Profit as an Optimization Criterion	96
B.	Design Procedures of an Axial Flow Duct Fan	102
C.	Design Procedures of a Multipass Counter Flow Recuperator	121

D.	Some Physical Properties	135
E.	Nonlinear Curve Fitting	154
F.	User's Manual to Generate and Plot a Trade-off Surface	177

LIST OF FIGURES

		<u>PAGE</u>
Figure 2.1	Type A trade-off curve	7
Figure 2.2	Type A trade-off surface	9
Figure 2.3	Constrained objective function contour lines	11
Figure 2.4	Type B trade-off surface, Section 1	12
Figure 2.5	Type B trade-off surface, Section 2	12
Figure 2.6	Type A TOC-Local minima	14
Figure 2.7	Shrink fitted cylinders subjected to internal pressure	17
Figure 2.8	Axial flow fan	21
Figure 2.9 & 2.10	Internal pressure and maximum inter- ference trade-off surface.	35-36
Figure 2.11	Associating value curves with shrink fitted cylinders trade-off curves	37
Figure 2.12 to 2.20	Two shrink fitted cylinders example trade-off surfaces	39-47
Figure 2.21 to 2.32	Axial flow fan example trade-off surfaces	52-63
Figure 3.1	The hierarchial structure of a de- composed system into a multiple sub- system	68

		<u>PAGE</u>
Figure 3.2	Decomposed recuperator fan system	71
Figure 3.3	Two-pass counterflow recuperator	75
Figure A.1	Changes in arrest value with time for different methods of depreciation	97
Figure A.2	Cash position diagram	100
Figure A.3	Cash flow diagram	100
Figure B.1	Components of ducted fan unit	103
Figure B.2	Velocity vectors for rotor and straightener blade element	108
Figure B.3	Force vector diagram for rotor blade element	110
Figure B.4	Geometric details of rotor blades element, cascade method	113
Figure B.5	Geometric details of straightener blade element, cascade method	114
Figure B.6	Assumed blades cross section for stresses calculations	118
Figure C.1	Variation in gases temperature in counterflow recuperator	122
Figure C.2	Two-pass overall-counterflow exchanger	123
Figure C.3	Staggered tube banks	126
Figure C.4	Pressure drop in two-pass exchanger	132
Figure D.1	Friction factors for commercial pipe	142
Figure D.2	Friction factor for staggered tube banks	146

		<u>PAGE</u>
Figure D.3	Entrance and exit pressure loss coefficients for a heat exchanger	146
Figure D.4	Two-pass overall-counter-flow recuperator volume flow rate distribution	150
Figure D.5	Block diagram of leakage	150
Figure D.6	Friction factors for stacks.	152
Figure E.1	Surface generated by the empirical formula "Model 4"	167
Figure E.2	Confidence limits of the "Model 4" friction value	168
Figure E.3	Comparison between Model 4 and bi-cubic spline fits.	169

CHAPTER 1
INTRODUCTION

In recent years, much has been published concerning the optimum design problem in engineering [1,2]*. Fundamentally, the problem is one of optimizing a design with respect to one or more optimization criteria [7]. However, in complex design systems, there are often several sub-systems that can be considered as a separate design problem governed by some specifications and usually they all will have the same objective (minimum cost and/or maximum profit). It is to this topic that this research is directed.

An objective of this thesis will be to explore the use of soft specifications in optimization by relaxing the hard ones and generating a set of trade-off curves [3]. Moreover, it is evident that the problems of large systems optimization, which involves large numbers of design variables and constraints, is still a subject under consideration [4, 5]. Therefore, this investigation attempts to study the use of trade-off curves, after representing them in a convenient empirical formula, in a decomposed system.

* Numbers in brackets refer to similarly numbered references at the end of the paper.

This thesis in particular examines the following questions: how and why does the designer generate and represent trade-off curves, and how might he determine the "optimum" design of a large complex system by decomposing it?

Chapter 2 describes a way of generating and representing trade-off curves with a brief discussion of their use applied to two design examples. Chapter 3 is devoted to describing the use of the trade off technique in combining a decomposed large design system with the aid of an example. Conclusions and further research suggestions are given in Chapter 4. Appendices A through E are devoted to illustrating related indispensable topics. Cost as an objective is discussed in Appendix A. Ducted axial flow fan design is presented in Appendix B. Appendix C and D describe a recuperator design and the needed physical properties. A non-linear fitting model is demonstrated, with a brief statistical comparison, in Appendix E. Finally, a user's manual and program listing is attached in Appendix F.

CHAPTER 2

TRADE - OFF CURVES

2.1 Definition

A trade-off curve (interaction curve) can be defined as the locus of all of the optimum design points for a given configuration. It may represent the relation between the configuration optimization criteria and a relaxed design specification [3] or a competing design objective [7]. The generalization to more than one specification introduces trade-off surfaces (hypersurfaces).

2.2 Generation

In formulating the optimum design problem, the designer must consider the application and the desired objective or objectives of the design. Then, he must identify the design variables, objective functions, and constraints. In such design problems, solutions by trial and error or empirical approaches may not be good enough, and efficient numerical techniques are needed to do the complex analysis and optimization.

"OPTISEP" is an optimization subroutines package

[27] , which was efficiently used through this piece of work. In general, in an optimization problem, a solution is sought that minimizes (maximizes) some numerical objective function U , of one or more design variables, subject to a set of equality and/or inequality design constraints ψ and ϕ . In the mathematical optimization programming employed by OPTISEP, the techniques are generally iterative. The design variables are altered at each iteration in accordance with some strategy until the objective function can no longer be improved without violating the constraints.

Moreover, there is a point about application of OPTISEP to solve problems like (2.3.1) and (2.3.2)

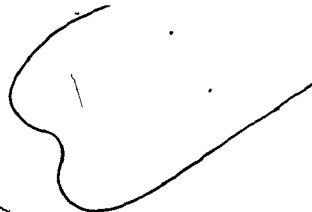
that requires further comment. First of all, in generating the trade-off curve (TOC), new estimates for the design variables are required each time the optimization problem is solved. The new design estimates were obtained in two ways. First, the optimum found from one iteration was used as a starting point for the next iteration. This method worked best when the relaxed design specification changes were relatively small. Secondly, a linear curve fit based on previously obtained optima was used to estimate the new starting point. Thus, in these two ways, new estimates can be made accurately to aid convergence and increase overall efficiency.

Furthermore, a special problem of local minima

can arise in optimization. If the design objective is a non-convex one or if a design space is a non-convex region, then there is a possibility of local minima. In any complex design, it is difficult to show that a design objective is a convex function over the feasible region, or that the feasible region is convex. Consequently, the designer must be aware of the possibility of local minima. The existence of local minima has an interesting effect on the (TOC), as will be illustrated later in this chapter.

The treatment of local minima is a serious problem in optimization. There is usually no way to tell if a minimum is, in fact, the absolute global minimum or just a local minimum. Hence, the designer must try different starting points in an attempt to find other possible minima and to determine what the objective function surface is like.

It is worthwhile to examine the effect of integer and discrete variables in generating a trade-off curve, surface, or hypersurface. Integer variables occur when the quantity of some identical components is a variable, such as the number of rotor and straightener blades in a fan (N_R , and N_S). On the other hand, discrete variables usually arise from discrete standard size such as an electric motor horsepower and revolutions per minute, (HP and RPM). This will be described in the following section through the presentation of two design examples. The most practical approach for optimizing an integer and/or discrete design



problem is to treat the variables as continuous, and after the optimum values are found, round them off to the nearest integer or discrete values with attention to the constraints feasibility. Furthermore, it is good practice to check all integer values adjacent to the unrounded solution to ensure that the optimum has not occurred nearby. However, while generating a trade-off curve, or surface, it is not advisable to round the integer or discrete design variables because an irregular step wise curve will be formed having the same continuous trend. Curve irregularity depends upon the discrete steps and how far they affect the objective function value. It is worth noting that another deviation from the actual optimum may occur due to the optimization stopping criteria, which may be a relative change in the objective function or in the design variables step size.

However, it is worthwhile to discuss and examine additional properties of the TOC, which will be of great help in understanding the behaviour and trend of the ensuing curves. The trade-off curve divides objective function space into two different regions. The region above the TOC represents all feasible designs. The region below the TOC represents designs that are not possible because they violate the governing physical relationships. In this sense, the TOC represents a boundary of the feasible region, where all the points on the TOC are optimum designs. Consider now Figure 2.1. Objective

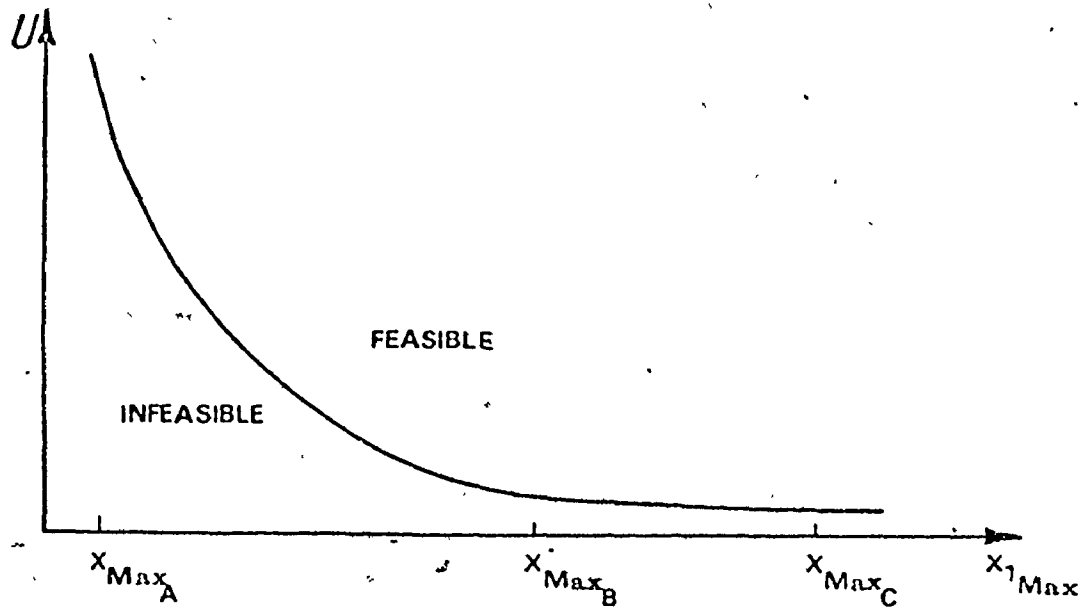
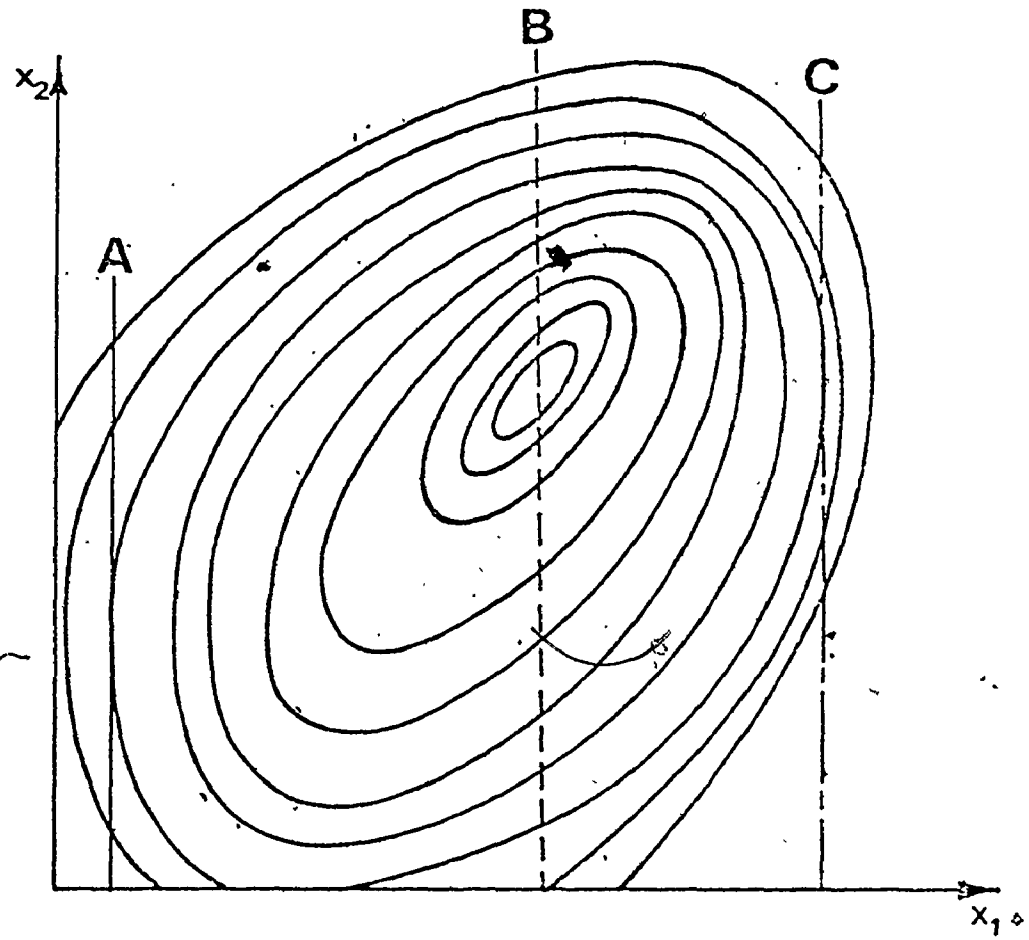


Figure 2.1 Type A Trade-off Curve.

function contours were plotted versus its two design variables x_1 and x_2 . Inequality constraint, ϕ_1 , is assumed to have the form

$$\phi_1 = x_{1\text{Max}} - x_1 \geq 0.0 \quad (2.1)$$

where, $x_{1\text{Max}}$ is the upper limit of the design variables x_1 . Relaxing the constraint by varying $x_{1\text{Max}}$ value between $x_{1\text{MaxA}}$ and $x_{1\text{MaxC}}$, a trade-off curve shown in Figure 2.1 can be generated. The portion of the TOC between A and B represents the smallest value that the function $U(x_1, x_2)$ can attain without violating the constraint (2.1). The points between B and C on the curve, where the constraint is not active, are similar to an unconstrained problem. For a design not on the curve, the objective function can be improved by moving towards the TOC.

In this sense, the shape of TOC, shown in Figure 2.1 is affected by the objective function profile and the constraint equation. However, throughout the procedure of generating the TOC, the objective function shape does not change, only the position of the constraint with respect to the objective function does change. In this stage, we will call this type of TOC's "Type-A". Moreover, a Type-A trade-off surface may also be generated to give more insight into the design. Figure 2.2 represents a two-dimensional objective function $U(x_1, x_2)$, which is subjected to the following two constraints

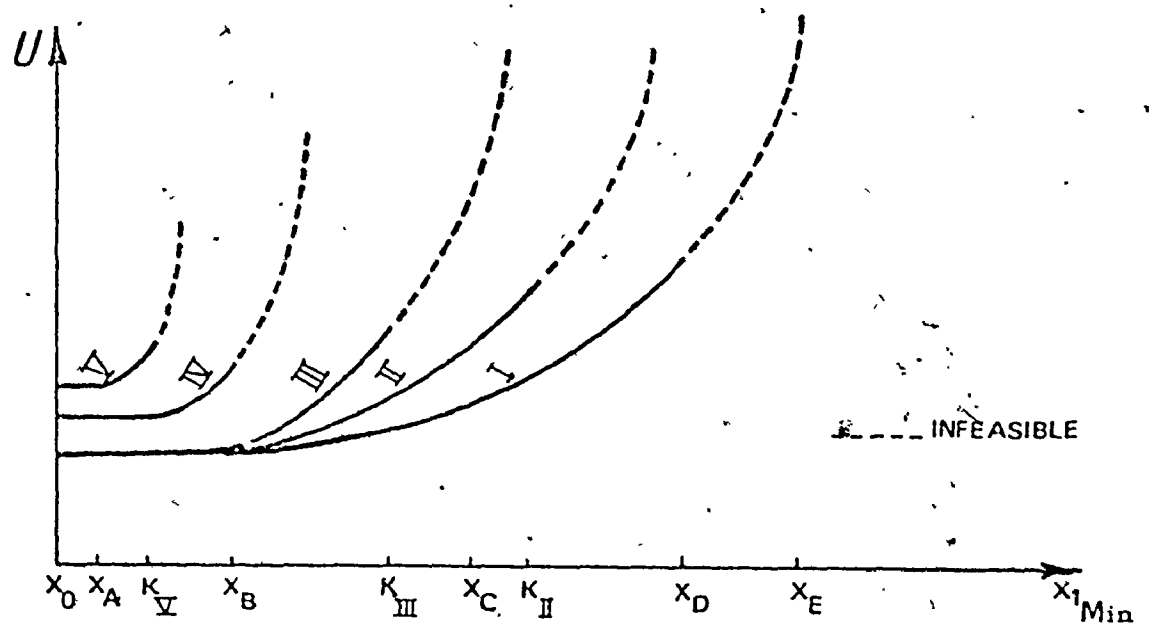
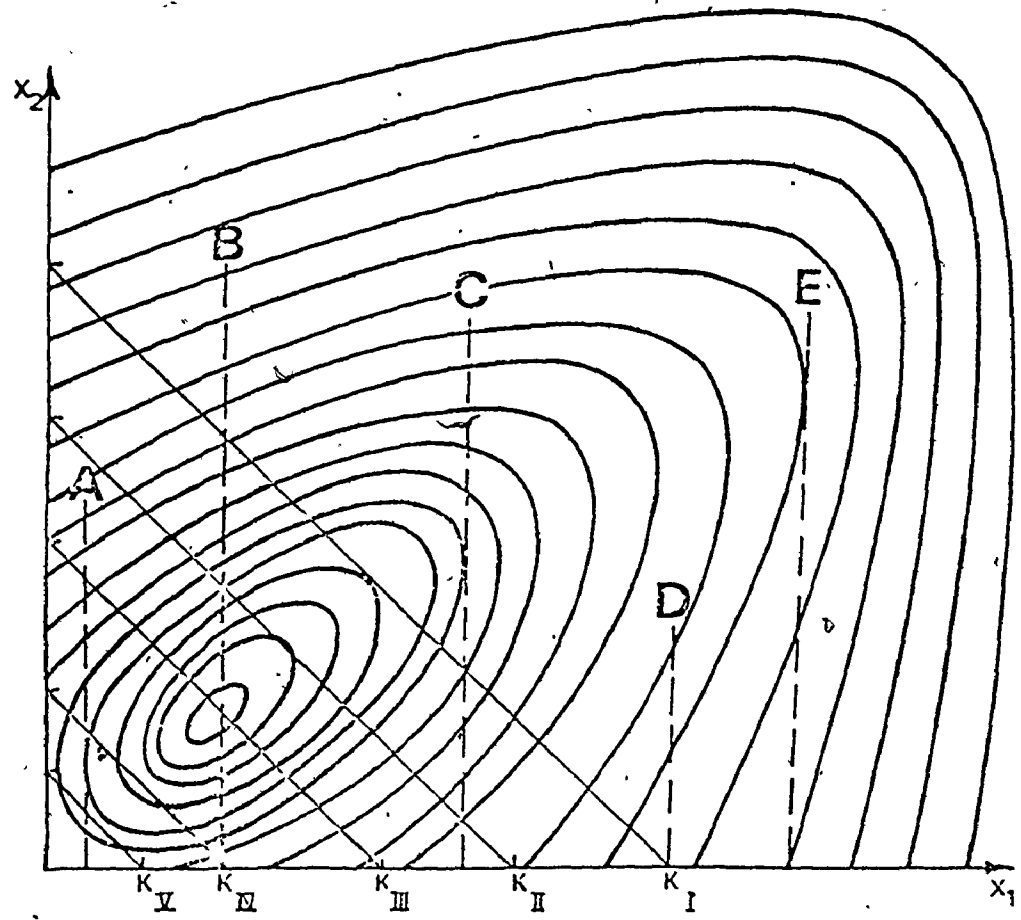


Figure 2.2. Type A Trade-off Surface.

$$\phi_1 = x_1 - x_{1\text{Min}} \geq 0 \quad (2.2)$$

$$\phi_2 = K - (x_1 + x_2) \geq 0 \quad (2.3)$$

where, $x_{1\text{Min}}$ and K are input specifications for the lower limit of x_1 and the upper limit of the sum of x_1 and x_2 , respectively. By relaxing $x_{1\text{Min}}$ and K values, the trade-off surface shown in Figure 2.2 will be created. It is obvious from Figure 2.2 that an infeasible trade-off curve is formed if $x_{1\text{Min}}$ is greater than K specified for this particular curve.

On the other hand, we can define a "Type-B" trade-off curve as the one which is accompanied by a change in the objective function shape during the course of its generation. Thus, this applies to any system in which the objective function is a function of specifications being changed. For illustration, let us assume the following two-dimensional objective function, U , which is subjected to a set of inequality constraints, Figure 2.3

$$\text{Minimum, } U(x_1, x_2) = \alpha x_1^2 + x_2^2 \quad (2.4)$$

$$\text{subjected to } \phi_1 = x_1 + x_2 \geq \beta \quad (2.5)$$

$$\phi_2 = x_1 \geq 0.0 \quad (2.6)$$

$$\phi_3 = x_2 \geq 0.0 \quad (2.7)$$

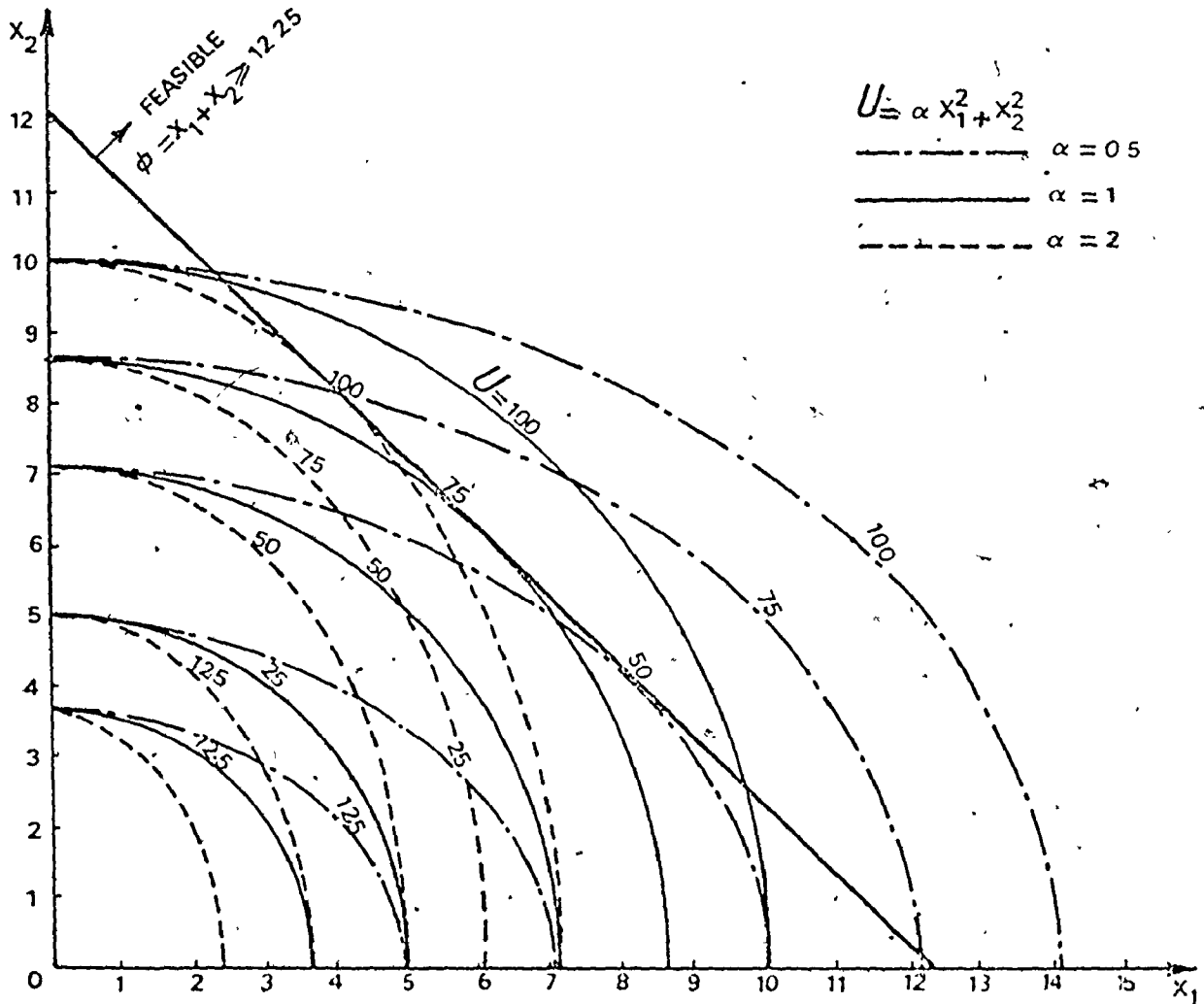


Figure 2.3 Constrained Objective Function Contour Lines.

7

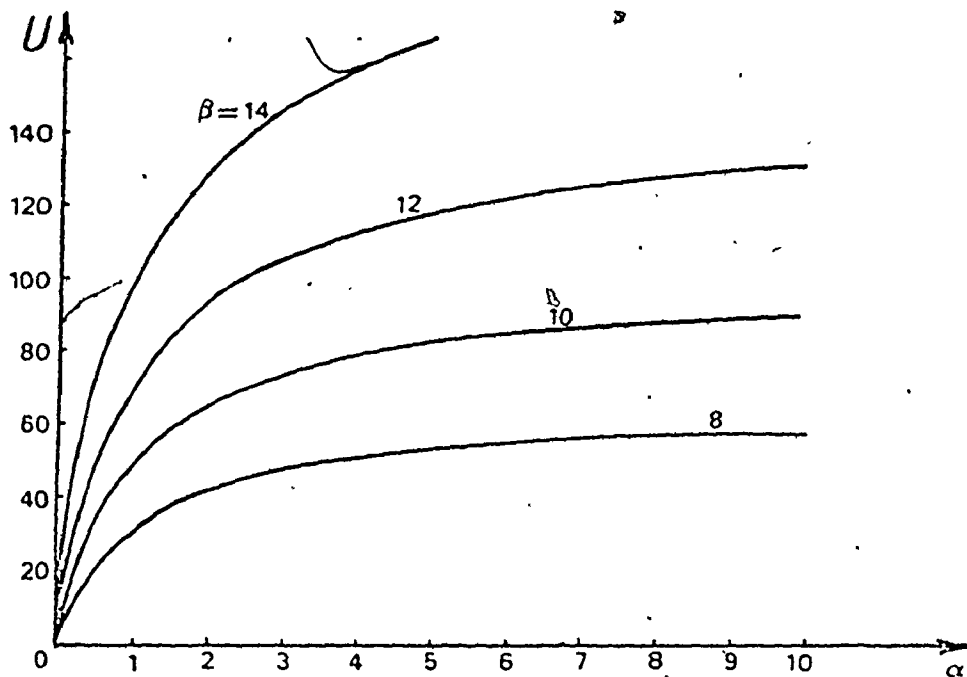


Figure 2.4. Type B Trade-off Surface, Section 1.

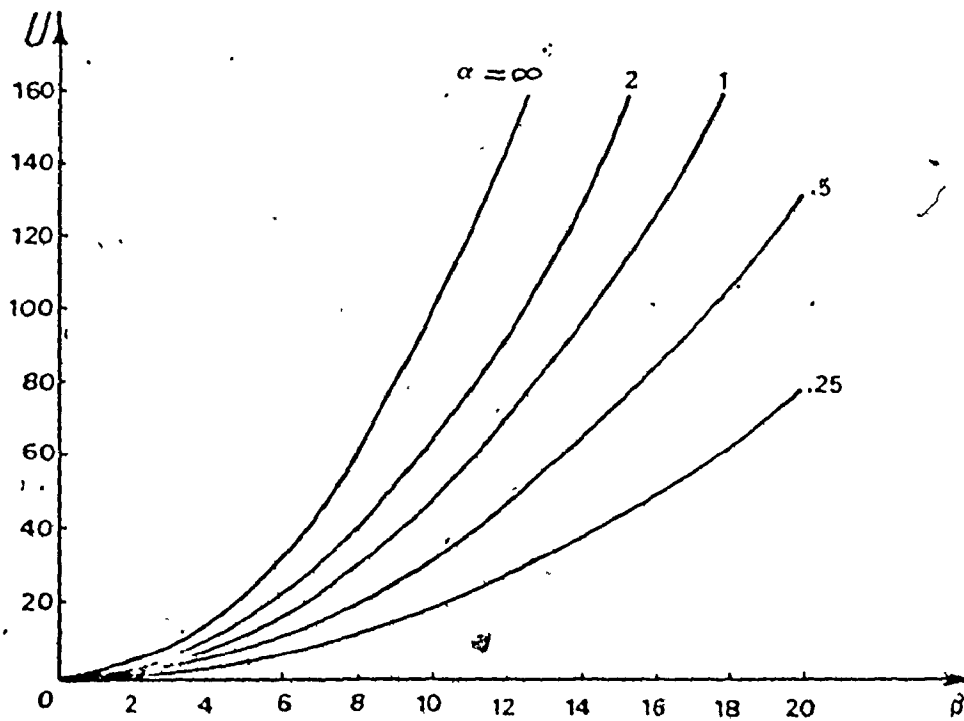


Figure 2.5. Type B Trade-off Surface, Section 2.

in which, α and β are input specifications which by relaxing their values a trade-off surface can be generated, shown in Figures 2.4 and 2.5. The minimum feasible objective function value, U^* , can simply be calculated from

$$U^* = \left[\frac{\alpha}{1 + \alpha} \right] \beta^2 \quad (2.8)$$

where the optimum design variables x_1^* and x_2^* computed by

$$x_1^* = \beta / (1 + \alpha) \quad (2.9)$$

$$x_2^* = \alpha \beta / (1 + \alpha) \quad (2.10)$$

An observation can be made from Figure 2.3. Along the TOC, the gradients of the objective function and the active constraint are in opposite direction since the contours are tangent at these points. However, this is not the case, for the stable region of the TOC type-A where the constraints are not active, as shown in Figure 2.1 between points B and C, and also from Figure 2.2 between x_{1_0} and x_{1_B} for K_I .

Finally, the effect of a local minima on the shape of the TOC is considered. Figure 2.6 shows an assumed two-dimensional objective function, U , with global and local minimums A and B, respectively. It is subjected to a direct constraint, $\phi = x_1 - x_{1_{Min}} \geq 0$. Type-A trade off curves are then generated by relaxing $x_{1_{Min}}$ value. Depending upon

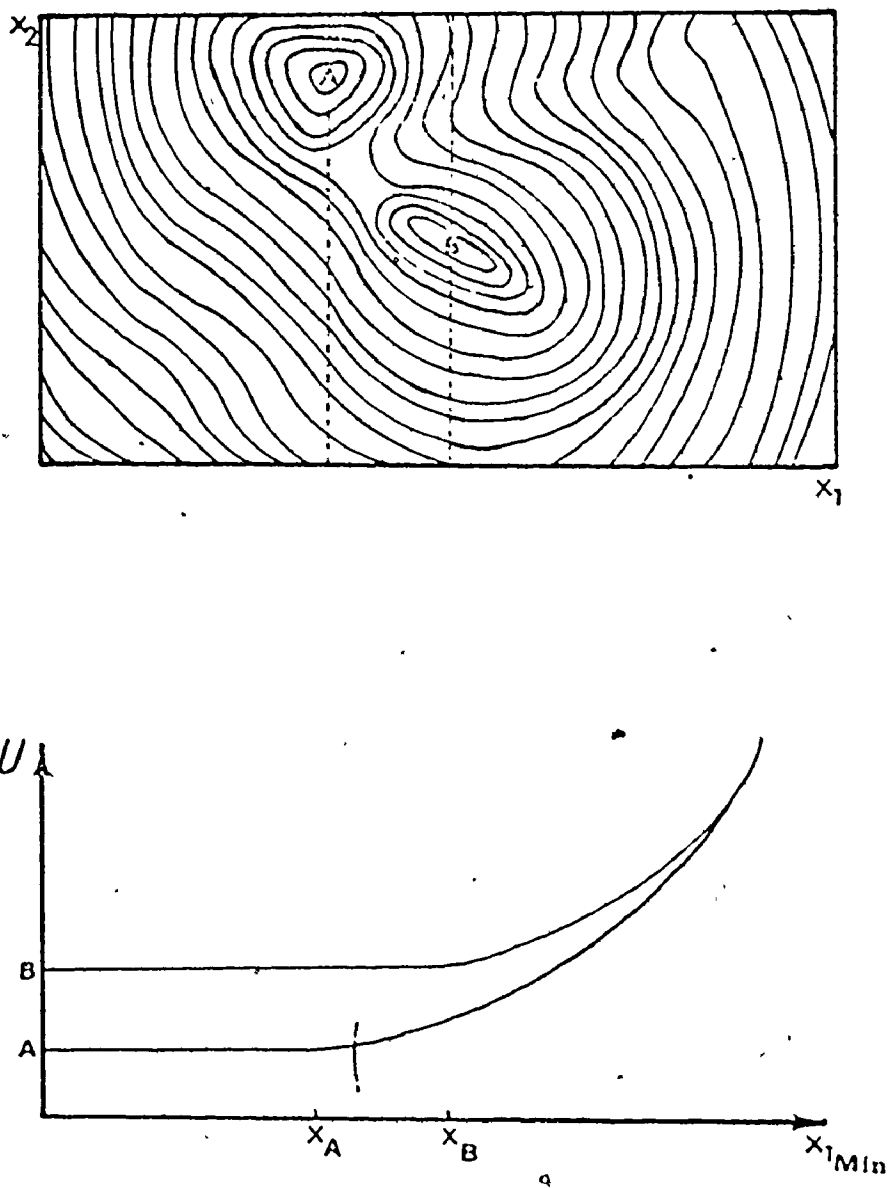


Figure 2.6. Type A TOC-Local Minima.

the starting estimates of the design variables a minimum feasible may be found. In this sense, two TOCs might be plotted as shown in Figure 2.6. Once the TOCs (surfaces) are found, it becomes clear which portion of the curve (surface) produces the more acceptable designs; portion with lower function values is more satisfactory. With knowledge of the types of designs that produce the lower branches, the designer can select an estimate near the proper optimum when finalizing a design.

In this brief illustration and categorization of trade-off curves, objective functions with a maximum of two design variables were used. However, with an increasing number of design variables, the design space becomes difficult to visualize. In the same sense, with an increasing number of input design specifications, a trade-off hyper-surfaces could be formed.

2.3 Examples

In the following section two-design problems are presented to illustrate the application, shape and use of the previously described trade-off curves.

2.3.1 Shrink Fitted Cylinders

2.3.1. a Definition of Problem

Cylinders subjected to extremely high pressures

should be prestressed in order to fulfill strength requirements which cannot be met with increasing the thickness. One of the methods used, is to build up a cylinder of two cylinders or more shrunk together, shown in Figure 2.7, [4,8].

The following hard specifications* are set for the design:

Applied operating pressure	(P_0)	= 13000 psi
Material yield strength	(S_Y)	= 40000 psi
Modulus of elasticity	(E)	= 3×10^7 psi
Factor of safety	(FS)	= 2
Nominal inner radius	(R_0)	= 5.0 in.
Maximum outer radius.....	(R_{Max})	= 25 in.
Minimum cylinder thickness.....	(TH)	= 0.25 in.
Maximum interference between cylinders.....	(\bar{D}_{Max})	= 0.0018 in.

2.3.1 b Formulation for Optimization

The design variables are:

R_1 = intermediate radius, in.

R_2 = outer radius, in.

P_f = shrink-fit pressure, psi

The optimization criterion is to minimize the overall assembly

* Hard specifications are those permitting no deviation from their specified values. In actual design practice, however, some change is usually acceptable, [7].

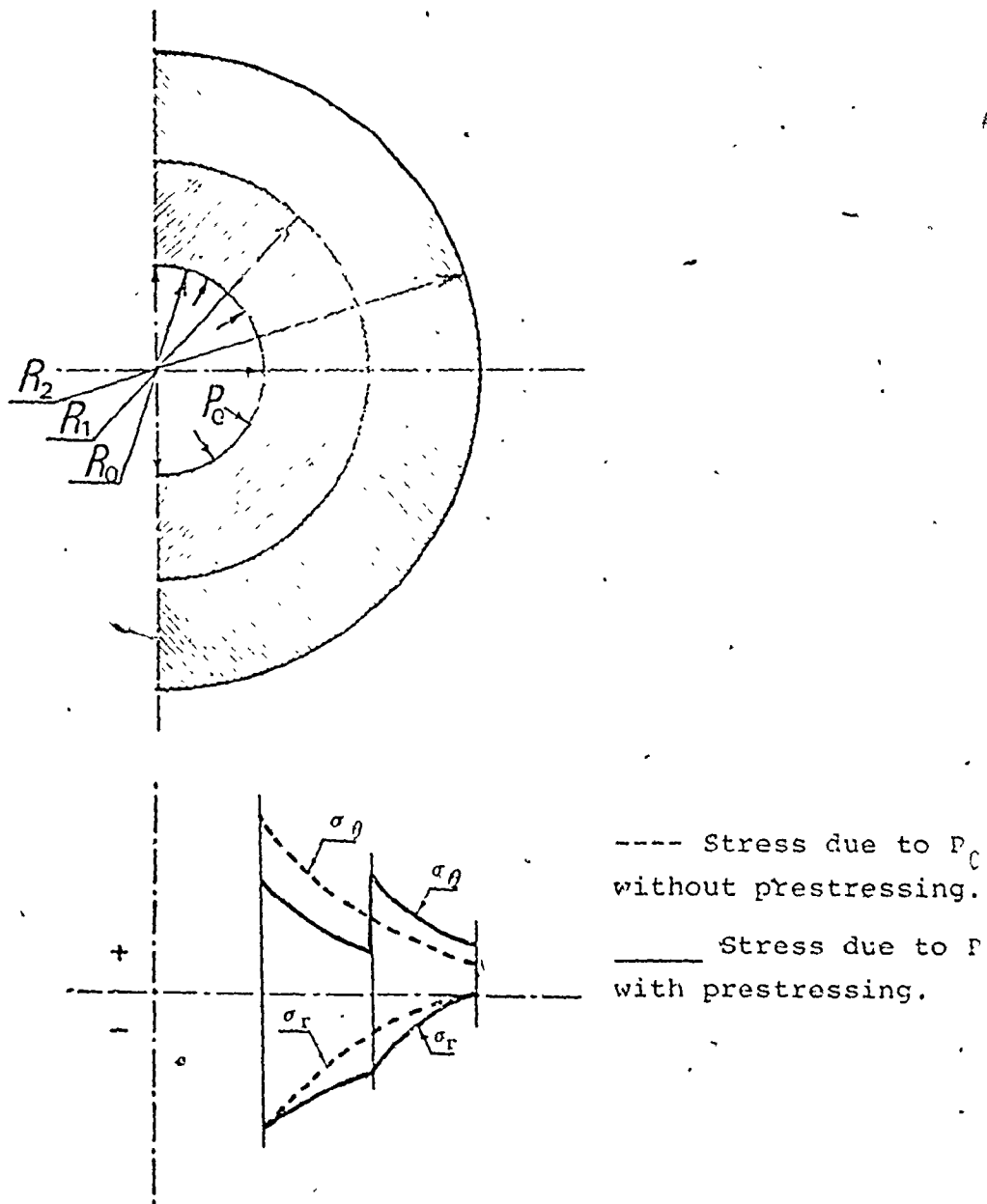


Figure 2.7. Shrink Fitted Cylinders Subjected to Internal Pressure.

volume.

$$U = R_2^2 = \text{minimum} \quad (2.11)$$

System constraints can be divided into two sections, design variables constraints and state variables* constraints. As for the first section, all the design variables have to be positive quantities. To ensure availability of machining and handling of each cylinders, its thickness has to be greater than a certain specific value (TH). Also, the maximum outer radius of the whole assembly may be constrained to a limited maximum value, which depends on the availability of space.

The above constraints can be expressed mathematically as follows:

$$\phi_1 = R_1 \geq 0 \quad (2.12)$$

$$\phi_2 = R_2 \geq 0 \quad (2.13)$$

$$\phi_3 = P_f \geq 0 \quad (2.14)$$

$$\phi_4 = (R_1 - R_0) - TH \geq 0 \quad (2.15)$$

$$\phi_5 = (R_2 - R_1) - TH \geq 0 \quad (2.16)$$

$$\phi_6 = R_{\text{Max}} - R_2 \geq 0 \quad (2.17)$$

Taking the "Tresca Criteria" [8] as a measure of the limit of elasticity under the applied internal and shrink pressures, we can state the following state variables constraints

* State variables describe the state of the system in many ways, and cannot be adjusted directly by the designer. They are functions of the system design variables.

$$\phi_7 = (S_Y/FS) - 2\tau_{R_0} \geq 0 \quad (2.18)$$

$$\phi_8 = (S_Y/FS) - 2\tau_{R_1} \geq 0 \quad (2.19)$$

Where, τ_{R_0} and τ_{R_1} are the applied shear stress at R_0 and R_1 , respectively, and they are equal to, [8] :

$$\tau_{R_0} = P_0 \left(\frac{R_2^2}{R_2^2 - R_0^2} \right) - P_f \left(\frac{R_1^2}{R_1^2 - R_0^2} \right) \quad (2.20)$$

$$\tau_{R_1} = P_0 \left(\frac{R_0^2 R_2^2}{R_1^2 R_2^2 - R_0^2 R_1^2} \right) - P_f \left(\frac{R_2^2}{R_2^2 - R_1^2} \right) \quad (2.21)$$

In the unassembled condition, that is, before the shrinking operation takes place, the radial interference for machining is as follows:

$$D_{Mc} = \frac{2 R_1^3 P_f}{E} \cdot \frac{R_2^2 - R_0^2}{(R_2^2 - R_1^2)(R_1^2 - R_0^2)} \quad (2.22)$$

The radial interference has to be greater than zero and less than a certain specified maximum interference (D_{Max}), which in turn depends on the kind of material used (coefficient of expansion and maximum temperature difference for heating and/or cooling processes needed for the shrinking process). This leads

to the following state constraints

$$\phi_9 = D_{Mc} \geq 0 \quad (2.23)$$

$$\phi_{10} = D_{Max} - D_{Mc} \geq 0 \quad (2.24)$$

2.3.2 Axial Flow Fan

2.3.2 a Definition of Problem

The axial flow fan can be placed in three main categories: free fan, diaphragm mounted fan and ducted fan. The various components of the axial flow duct fan, with which we will be concerned, are indicated in Figure 2.8. The rotor blades are a series of air foils which, owing to their relative motion with the air, add total head to the air stream. A straightener is located downstream of the rotor to remove the swirl. [9]

The following hard specifications are set for the design:

- Air volume flow rate(Q) = 7575 ft³/min.
- Unit total head rise(ΔH) = 5 in. of water
- Blades material yield strength(S_{yB}) = 50,000 psi
- Hub and shaft material yield strength(S_{ysh}) = 50,000 psi
- Design factor of safety.....(FS) = 2
- Minimum and maximum unit radius.....(R_{min}, R_{max}) = 7.5, 36 in.

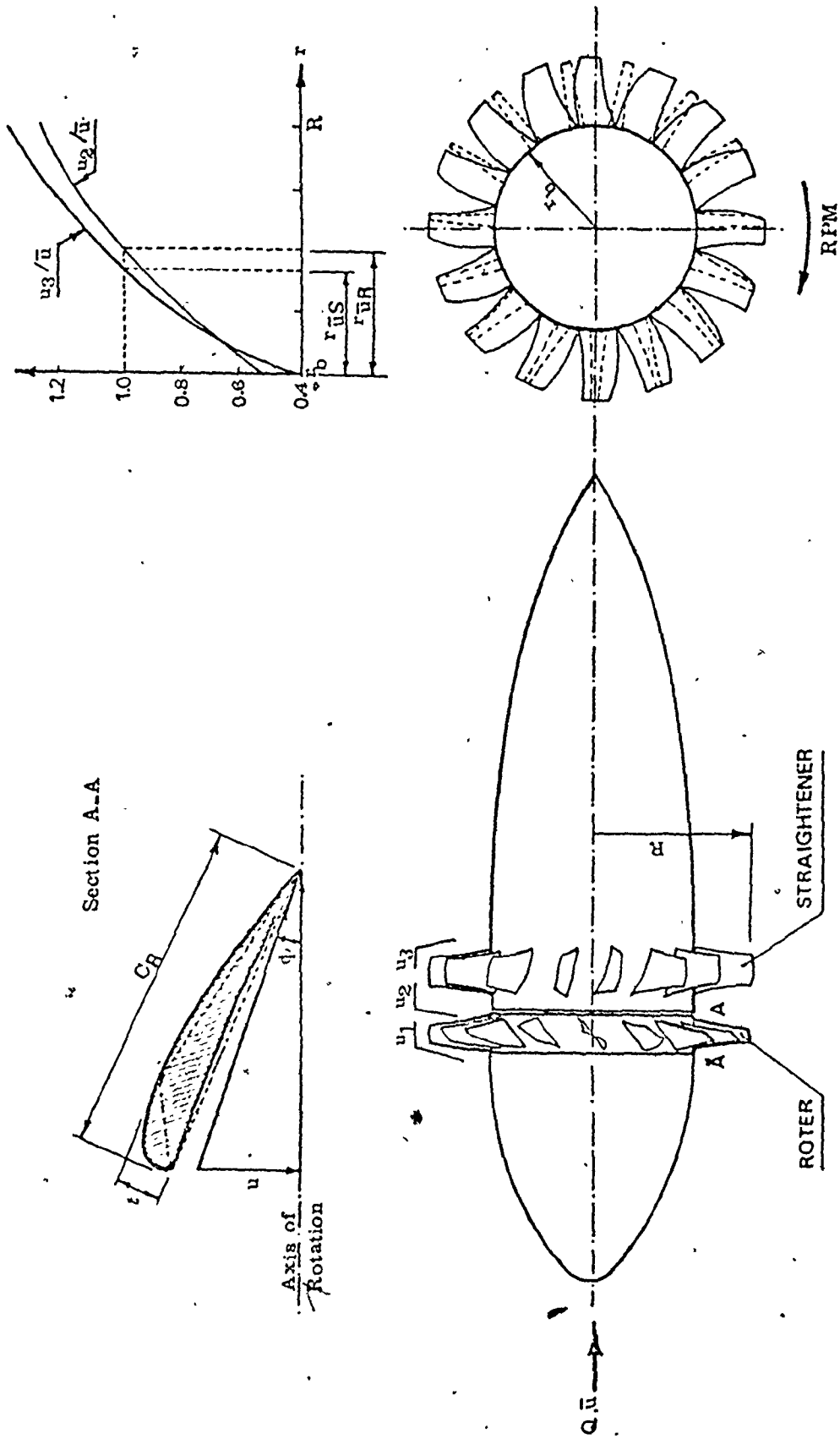


Figure 2.8. Axial Flow Fan.

Maximum boss to duct radius ratio	(β_{\max})	=	0.8
Minimum number of rotor or straightener blades	(N_{\min})	=	3
Minimum feasible horse- power	(HP_{\min})	=	0.25 hp
Upper and lower limits of motors revolutions per minute	$(RPM_{\max} \quad RPM_{\min})$	=	30,000 &400 rpm

other specifications will also be included during the course of presenting the design example.

2.3.2b Formulation for Optimization

The design variables are:

R = duct (= rotor tip) radius

r_b = boss radius, in.

RPM = motor revolutions per minute

N_R = number of rotor blades

N_S = number of straightener blades

\bar{r}_R = radial position at which axial velocity $u(r)$ equals mean axial velocity \bar{u} for the rotor blades, in.

\bar{r}_S = same as \bar{r}_R but for straightener blades, in.

t_R = maximum rotor blade thickness at the boss radius, in.

t_S = maximum straightener blade thickness at the boss radius, in.

The optimization criterion is to minimize the unit present value cost average [Appendix: A]

$$U = \text{P.V.A.C.} = \text{minimum} \quad (2.25)$$

The following input specifications have to be stated:

$$\text{Fan estimated life, } g = 10 \text{ years}$$

$$\text{Fan estimated tax life, } y = 12 \text{ years}$$

$$\text{Estimated interest rate, } i = 9.25 \%$$

Estimated interest rate

$$\text{with risk, } i_m = 12 \%$$

$$\text{Estimated tax rate, } t = 50 \%$$

Initial fixed cost, I_F , is the sum of:

(a) Blades manufacturing cost for both rotor and straightener, I_{F_1} .

(b) Main shaft, bearings, nose and tail fairing and the complete assembly cost, I_{F_2} .

(c) Driving electric motor cost, I_{F_3} .

$$\text{Therefore, } I_{F_1} = K_1 \cdot (\text{rotor blades volume} + \text{straightener blades volume}) \quad (\text{dollars}) \quad (2.26)$$

$$I_{F_2} = K_2 \cdot (\text{fan unit length} \times \text{maximum cross section}) \quad (\text{dollars}) \quad (2.27)$$

$$\begin{aligned} I_{F_3} &= f(\text{motor horsepower, HP}) \\ &= k_i \left[\frac{\text{HP}}{k_{ii}} \right]^{k_{iii}} \quad (\text{dollars}) \quad (2.28) \end{aligned}$$

where, K_1 , K_2 , k_i , k_{ii} and k_{iii} are cost constants to be estimated based on historical correlated data collected from the previous experience of material, machining, assembly and

installation of the unit in question [15, 16]. The following constant values are assumed for the particular case in hand.

$$K_1 = 20 \text{ dollars/in.}^3$$

$$K_2 = 0.5 \text{ dollars/in.}^3$$

Range of horsepower	2 - 30	30 - 100	100 -
k_i (dollars)	140	368	2460
k_{ii} (HP)	10	30	100
k_{iii}	0.88	1.58	2.17

On the other hand, the running cost or the annual gross expenses, $-P^*$, is the maintenance and the electric motor power cost. It is assumed that the maintenance cost is a percentage of the electric power cost.

$$\begin{aligned} \text{Therefore, } -P^* = & \text{ Total unit working hours per year} \\ & \times \text{ Unit kilowatts hours} \times \text{ Estimated} \\ & \text{ cost rate (0.01 dollars/KW is as-} \\ & \text{ sumed)} \times \text{ Percentage increase due} \\ & \text{ to maintenance (1.3 is assumed)} \\ & \hspace{15em} (2.29) \end{aligned}$$

Employing the previous specifications and equations (2.26, 2.27, 2.28 and 2.29) in the present value average cost [Appendix A equation A.5], the optimization criterion could be computed.

System constraints can be divided into two sections, configuration constraints and aerodynamic constraints. As for the first section, duct radius must be kept within upper and lower limits according to the design configuration

$$\phi_1 = R - R_{\min} \geq 0.0 \quad (2.30)$$

$$\phi_2 = R_{\max} - R \geq 0.0 \quad (2.31)$$

Boss radius must also be kept within upper limit proportion with tip radius ($\beta_b = r_b/R$)

$$\phi_3 = \beta_{\max} - \beta_b \geq 0.0 \quad (2.32)$$

Motor revolutions per minute has to be bounded by upper and lower limits.

$$\phi_5 = \text{RPM} - \text{RPM}_{\min} \geq 0.0 \quad (2.34)$$

$$\phi_6 = \text{RPM}_{\max} - \text{RPM} \geq 0.0 \quad (2.35)$$

Number of rotor and straightener blades have to be positive and greater than a minimum limit

$$\phi_7 = N_R - N_{\min} \geq 0.0 \quad (2.36)$$

$$\phi_8 = N_S - N_{\min} \geq 0.0 \quad (2.37)$$

Boss radius has to be greater than shaft radius. However, the shaft radius has to be big enough to withstand the torque and thrust subjected to it. That is to say that shaft material allowable stress has to be greater than applied shaft principal stress ($\bar{\sigma}_{sh}$). Therefore, assuming that shaft radius equals boss radius the following constraint will bound the lower limit of boss radius, [Appendix B],

$$\phi_4 = S_{y_{sh}} / FS - \bar{\sigma}_{sh} \geq 0.0 \quad (2.33)$$

Maximum thickness of a rotor blade at its root has to be big

enough to withstand centrifugal, lift and drag forces. In other words, material allowable stress has to be greater than applied maximum stress ($\bar{\sigma}_R$), [Appendix B].

$$\phi_9 = S_{YB} / F.S - \bar{\sigma}_R \geq 0.0 \quad (2.38)$$

Also, maximum straightener blade thickness at its root has to be big enough to withstand lifting force. Same material is assumed to be used for both rotor and straightener blades.

$$\phi_{10} = S_{YB} / F.S - \bar{\sigma}_s \geq 0.0 \quad (2.39)$$

The sum of blades thickness at its root for both the rotor and straightener has to be less than root circumference.

$$\phi_{11} = 2\pi r_b - t_R \cdot N_R \geq 0.0 \quad (2.40)$$

$$\phi_{12} = 2\pi r_b - t_S \cdot N_S \geq 0.0 \quad (2.41)$$

Electric motor horsepower has to be positive and greater than a minimum value.

$$\phi_{13} = HP - HP_{\min} \geq 0.0 \quad (2.42)$$

The overall unit efficiency has to be less than unity.

$$\phi_{14} = 1 - \eta_t^* \geq 0.0 \quad (2.43)$$

The following is devoted to aerodynamic constraints. We are using the arbitrary vortex flow method, which leads to a small boss tip ratio with a very high efficiency and large mean total

head rise compared with the free vortex method of design. It is suggested, based on experimental evidence [9], that the design difference in total head between root and tip should not exceed 1.5 times $0.5\bar{u}^2$. This can be expressed in a non-dimensional form by

$$\phi_{15} = 1.5 - \frac{2}{\lambda} [\epsilon_R(1) - \beta_b \cdot \epsilon_R(\beta_b)] \geq 0.0 \quad (2.44)$$

$$\phi_{16} = 1.5 - \frac{2}{\lambda} [\epsilon_S(1) - \beta_b \epsilon_S(\beta_b)] \geq 0.0 \quad (2.45)$$

where, β_b , λ and $\epsilon(\beta)$ are dimensionless boss position, mean flow coefficient and swirl coefficient respectively as explained in Appendix B, equations B.3, B.4, B.12 and B.13. The flow coefficient $\lambda(\beta)$ for both the rotor and the straightener must have a lower limit of 0.2 fixed by efficiency considerations and an upper limit of 1.5 due to design difficulties, [Equations B.10 and B.11].

$$\phi_{17} = \lambda_R(\beta_b) - 0.2 \geq 0.0 \quad (2.46)$$

$$\phi_{18} = \lambda_S(\beta_b) - 0.2 \geq 0.0 \quad (2.47)$$

$$\phi_{19} = 1.5 - \lambda_R(1) \geq 0.0 \quad (2.48)$$

$$\phi_{20} = 1.5 - \lambda_S(1) \geq 0.0 \quad (2.49)$$

Swirl coefficient $\epsilon(\beta)$ must have an upper limit of 1.5 fixed

by blade stalling. On the other hand, it has to be positive, and from a practical point of view greater than 0.4, [Equations B.12 and B.13].

$$\phi_{21} = \epsilon_R(1) - 0.4 \geq 0.0 \quad (2.50)$$

$$\phi_{22} = \epsilon_S(1) - 0.4 \geq 0.0 \quad (2.51)$$

$$\phi_{23} = 1.5 - \epsilon_R(\beta_b) \geq 0.0 \quad (2.52)$$

$$\phi_{24} = 1.5 - \epsilon_S(\beta_b) \geq 0.0 \quad (2.53)$$

The aspect ratio* for both rotor and straightener blades must be in the vicinity of 6.

$$\phi_{25} = 6.0 - (1 - \beta) N_R / 2\pi \sigma_R(1) \geq 0.0 \quad (2.54)$$

$$\phi_{26} = 6.0 - (1 - \beta) N_S / 2\pi \sigma_S(1) \geq 0.0 \quad (2.55)$$

Rotor and straightener solidity is limited between 0.15 and 2.0.

$$\phi_{27} = \sigma_R(1) - 0.15 \geq 0.0 \quad (2.56)$$

$$\phi_{28} = \sigma_S(1) - 0.15 \geq 0.0 \quad (2.57)$$

$$\phi_{29} = 2.0 - \sigma_R(\beta_b) \geq 0.0 \quad (2.58)$$

* Aspect ratio is the ratio, span/mean chord, of an air foil blade.

$$\phi_{30} = 2.0 - \sigma_R(\beta_b) \geq 0.0 \quad (2.59)$$

Rotor and straightener lift coefficients have to be greater than 0.7.

$$\phi_{31} = C_{L_R}(\beta_b) - 0.7 \geq 0.0 \quad (2.60)$$

$$\phi_{32} = C_{L_S}(\beta_b) - 0.7 \geq 0.0 \quad (2.61)$$

Maximum axial velocity at both rotor and straightener tips have to be less than sound velocity to prevent flow separation.

$$\phi_{33} = 1116.0 - u_2(1) \geq 0.0 \quad (2.62)$$

$$\phi_{34} = 1116.0 - u_3(1) \geq 0.0 \quad (2.63)$$

The total volume flow rate through the fan for the different sections, downstream of a rotor row of blading and downstream of a straightener row of blading, has to be constant. Therefore, the following integrations have to be satisfied with a reasonable accuracy.

$$\begin{aligned} \bar{U} &= \frac{2^{-1}}{1-\kappa_b} \int_{\beta_b}^1 u_2(\beta) \cdot \beta \, d\beta \\ &= \frac{2}{1-\beta_b} \int_{\beta_b}^1 u_3(\beta) \cdot \beta \, d\beta \end{aligned} \quad (2.64)$$

It is well known that equality constraints usually obstruct

nonlinear optimization techniques from finding optimum feasible solutions. Therefore, a permissible deviation percentage is used, δ , to be decreased at the final optimization steps, $[\delta(0.1 \rightarrow 0.5)]$.

$$\phi_{35} = \delta - \left| \bar{U} - \frac{2}{1 - \beta_b^2} \int_b^1 u_2(\beta) \cdot \beta \cdot d\beta \right| \geq 0.0 \quad (2.65)$$

$$\phi_{36} = \delta - \left| \bar{U} - \frac{2}{1 - \beta_b^2} \int_b^1 u_3(\beta) \cdot \beta \cdot d\beta \right| \geq 0.0 \quad (2.66)$$

Having briefly explained the problem, its design variables, constraints and objective function, it is necessary to discuss the problem of integer and discrete design variables. The number of rotor and straightener blades, N_R , and N_S , have to be integer. Also motor horsepower, HP, is assumed to be available in a discrete form with a 0.25 HP step size. The number of revolution per minute, RPM, is also assumed to be discrete with a step size of ten revolutions per minute.

2.4 Results

In this section, a series of trade-off curves (surfaces) are displayed for both the shrink fitted cylinders

design problem and that of the ducted axial flow fan. A three dimensional trade-off surface is used in the following representation. It is plotted in the form of contours. A bicubic spline two-dimensional interpolator subroutine IBCIEU [28] is used to perform a two-dimensional interpolation to a given matrix of a set of optimum points. A general plotting subroutine is then employed to draw the generated surface in a convenient way. See Appendix F for illustration.

2.4.1 Shrink Fitted Cylinders TOC's

Even though the problem of two cylinders fitted together and subjected to an internal pressure is mathematically well defined, it is represented here to help in explaining the advantages a designer might gain by using trade-off technique.

It is clear that a minimum weight design will have maximum shear stresses in both the inner and outer parts. In addition, this shear stress should be the shear stress at the elastic limit, if full advantage of the material is to be realized. With this condition as the criterion, maximum shear stress for both the inner and outer shells are equated in order to solve for the optimum design condition; it can be found that

$$(R_1)_{\text{optimum}} = \sqrt{R_0 R_2} \quad (2.71)$$

$$(\Delta)_{\text{optimum}} = P_0 (R_1)_{\text{optimum}} / E \quad (2.72)$$

$$(P_f)_{\text{optimum}} = P_0 (R_2 - R_0) / 2 (R_2 + R_0) \quad (2.72)$$

$$(P_0)_{\text{maximum}} = \frac{S_y}{FS} \frac{R_2 - R_0}{R_2} \quad (2.74)$$

For a cylinder that is not prestressed

$$(P_0)_{\text{maximum}} = \frac{S_y}{4FS} \left\{ (R_2^2 - R_0^2) / R_2^2 \right\} \quad (2.75)$$

It is worthwhile to examine the feasibility of the hard specifications stated in section (2.2.1.a) in conjunction with the previous optimum design equations. It is obvious from equation (2.75) that a single cylinder can not withstand the applied internal pressure of 13,000 psi, since the maximum feasible internal pressure has to be less than 5000 psi to avoid an infinite outer radius. On the other hand, for the specified material and factor of safety and by using the maximum specified outer radius, ($R_0 = 5$ in.), the maximum applied internal pressure that two shrink fitted cylinders could carry is 16,000 psi, equation (2.74). However, for the specified internal pressure, an outer radius of 14.3 inch will be required. In this case, the intermediate radius will be 8.45 inch with 0.00366 inch interference. However, an intermediate interference of 0.0018 inch is specified as a maximum possible limit. Therefore, for this hypothetical assume problem an over-constrained infeasible design has been attempted.

Two two-dimensional trade-off surfaces, shown in Figures 2.9 and 2.10, give a clear picture for the bounds of feasibility for different values of the maximum intermediate interference, D_{Max} . The graphs also show the variation in the cylinders' cross sectional area, which is proportional to its weight, for different specified internal pressure. By increasing D_{Max} to .002 inch a feasible optimum design could be found with a total cross sectional area of 891.7 square inch and an outer radius of 17.57 inch Point "A" Figures 2.9 and 2.10. However, it is also worth observing that a decrease of 7.7% in the specified internal pressure to 12000 psi will lead to a dramatic decrease in the cylinders cross sectional area of 44% to 497.7 square inch, point "B" Figures 2.9 and 2.10.

Thus, a trade-off curve (surface) is a way of displaying to the designer a set of designs that are optimum in some sense. In order to select the optimum design, a "criterion" is needed that ranks the possible alternative combinations from the trade-off curve. But even without a criterion, the designer can certainly improve any design that does not fall on the trade-off curve. For example, if P_0 equals 11,000 psi, with a maximum interference of .002 inch and the designer chooses the inner and outer radii to be 5 and 13.5 inch, respectively with an area of 4.94

square inch, point "C" Figure 2.9 and 2.10. A better optimum design could be located using Figure 2.9, or 2.10 with an overall cross sectional area of 331.7 square inch, point "D".

A more complex optimization function could utilize value or utility concepts and permit the incorporation of additional design characteristics. No attempt will be made here to review the complete literature on value and utility theory. Siddall [11] has fully discussed the use of value curves in engineering decision-making, and the creation of value curves relating to design outcomes. Value curves are a way to measure the degree of fulfilment of needs, goals and objectives. An optimum design represents the highest level of value (satisfaction) obtainable from all of the designs defined by the trade-off curve (surface, hypersurface), and hence would be the "best" design. For an illustration, consider trade-off curve number three, Figure 2.10, where the specified internal pressure equals 12000 psi. We assume that a value curve has been established for weight, in which the value decreases as the weight increases. We assume, in addition, a value curve for interference, in which value is also inversely proportioned to interference because of higher temperatures required, greater assembly forces, and possible metallurgical problems. The trade-off decision can be made by combining the value curves with the trade-off curve, as shown in Figure 2.11, where the optimum design is at point B.

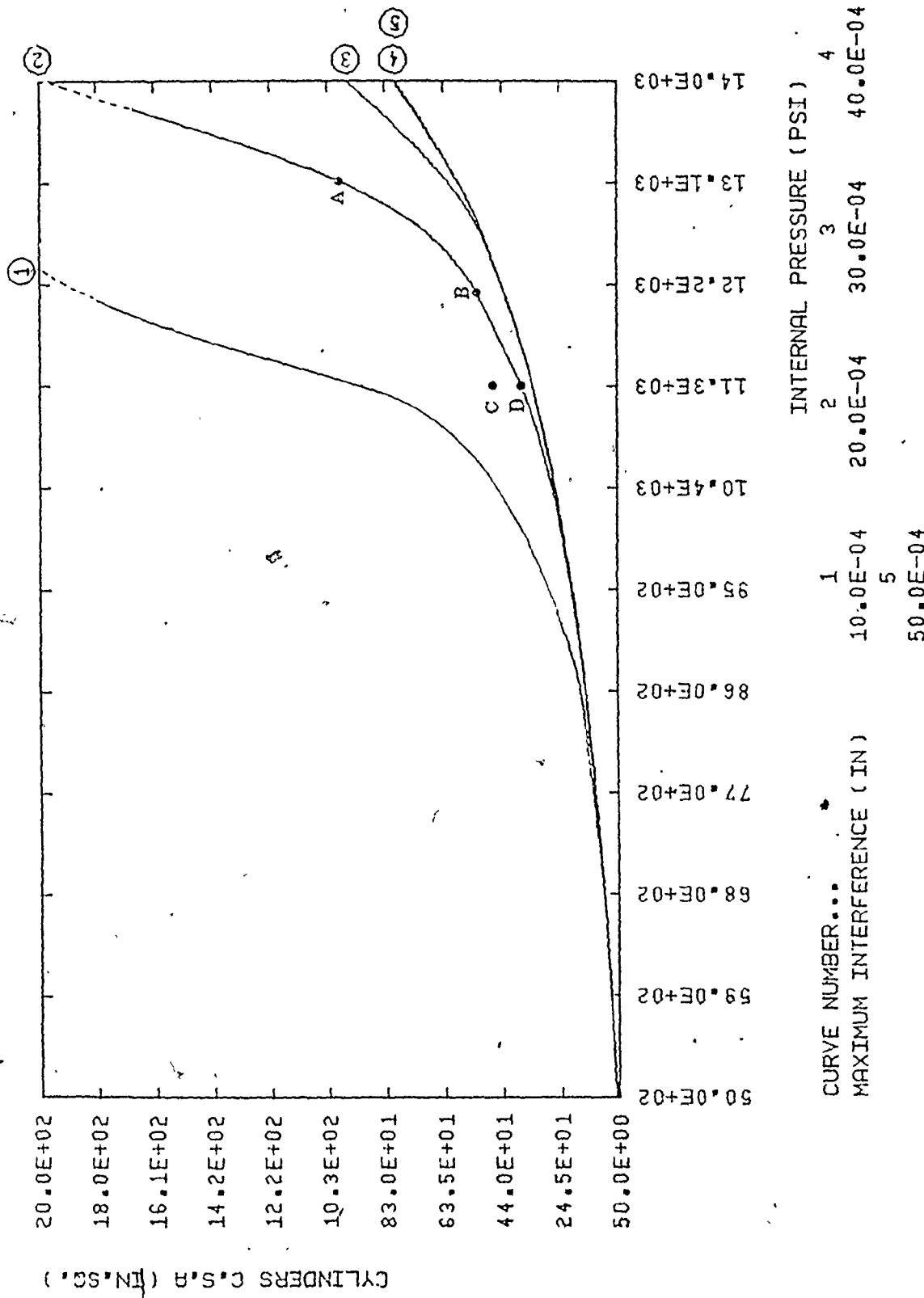


Figure. 2.9. Trade-off Surface.

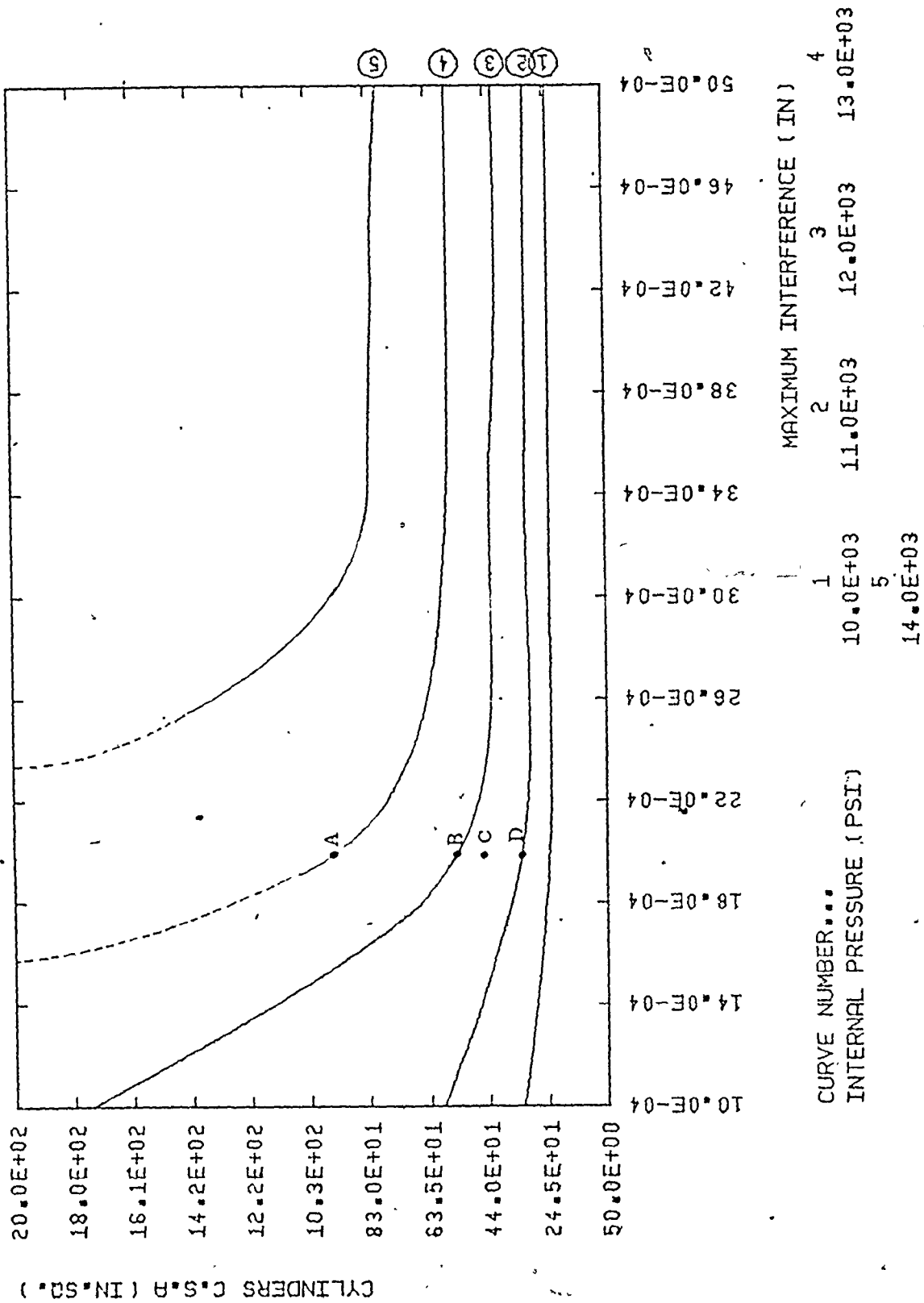


Figure 2.10. Trade-off surface.

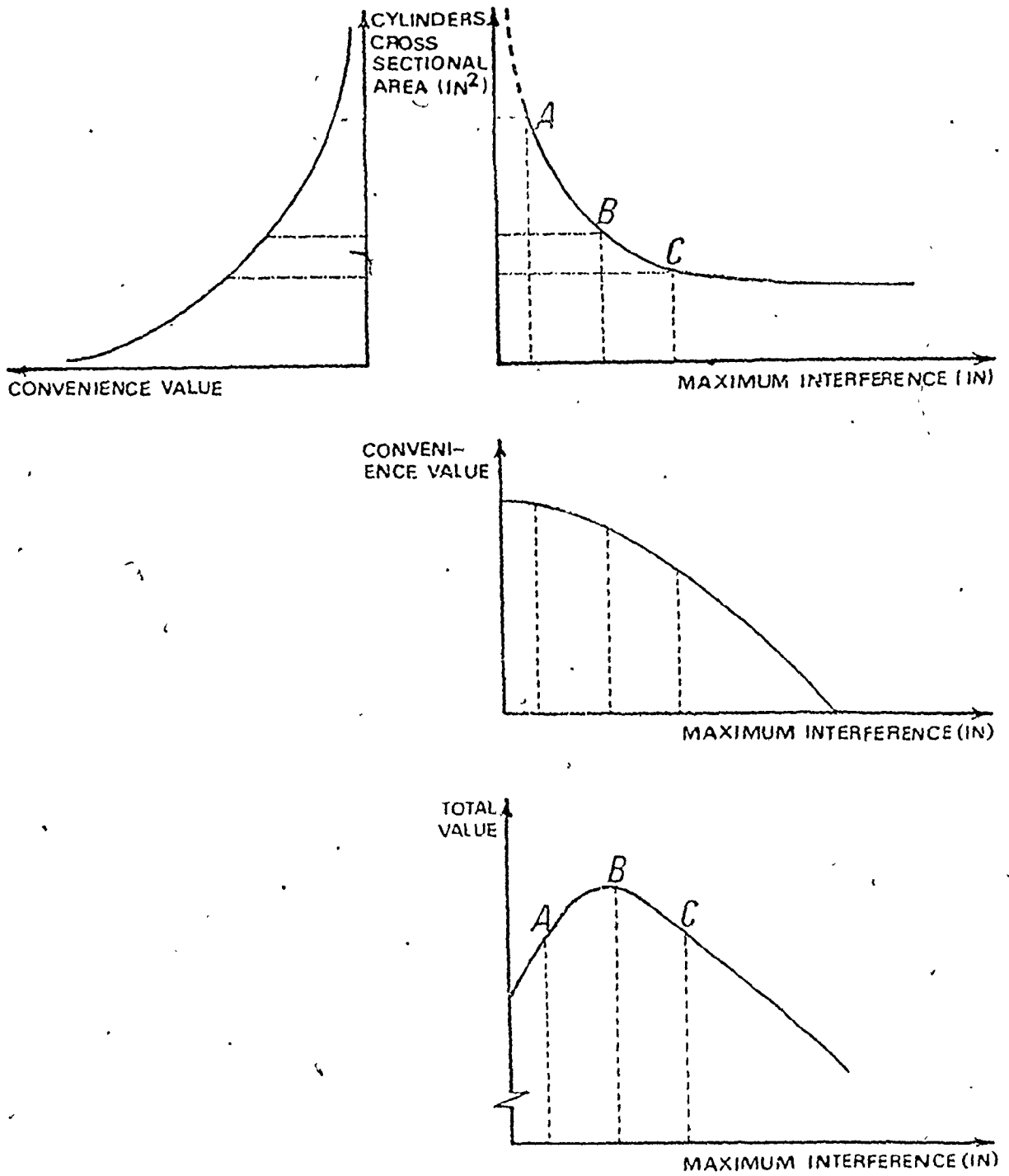


Figure 2.11. Associating Value Curves with Shrink Fitted Cylinders Trade-off Curves.

Value curves are particularly useful for optimal decision-making when there are more than two design characteristics.

The trade-off surface shown in Figures 2.9 and 2.10 have the same typical shape when the subjected internal pressure is maximized for a set of specifications for minimum cross sectional area and maximum interference. The identical surface was also generated by minimizing the intermediate interference for a specified cross sectional area and internal pressure.

Additional surfaces are shown through Figures 2.12 to 2.20. A similar analysis as that previously discussed could have been carried out leading to a better insight into the design and the relative importance of its input specifications and performance.

The maximum specified interference, D_{Max} , leads to generate type A trade-off curves, as shown in Figures 2.10 and 2.12. In addition, the minimum cylinder thickness, T_H , generates type A trade-off curves as shown in Figure 2.16. On the other hand, material yield strength, S_y , or design factor of safety, FS , give type B trade-off curves shown in Figure 2.20. Specified assembly inner radius, R_0 , affects the shape of the objective function, and so generates type B trade-off curves, shown in Figures 2.13 and 2.15. Finally, applied internal pressure, P_0 , produces also type B trade-off curves as indicated in Figures 2.9, 2.14, 2.18 and 2.19.

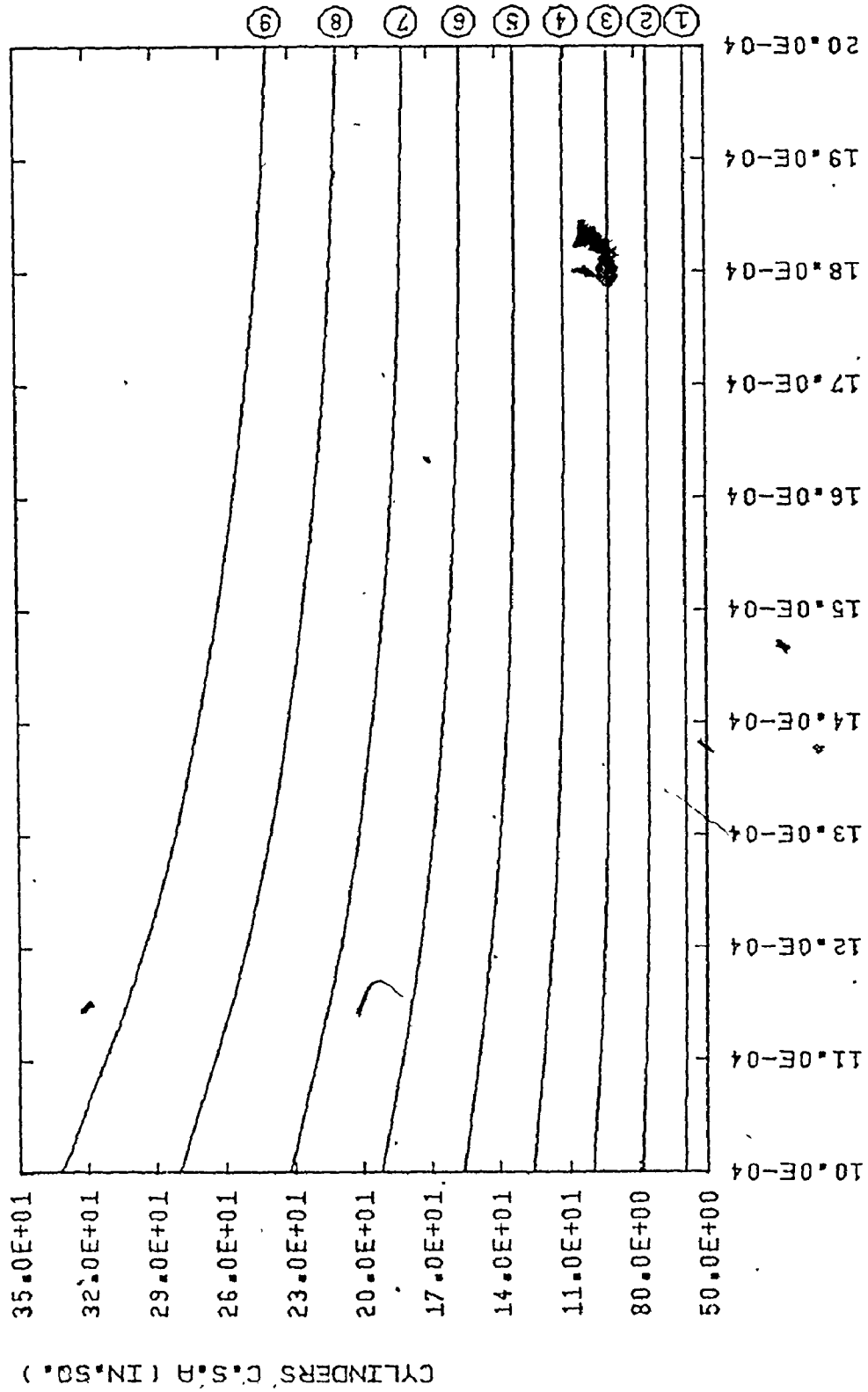
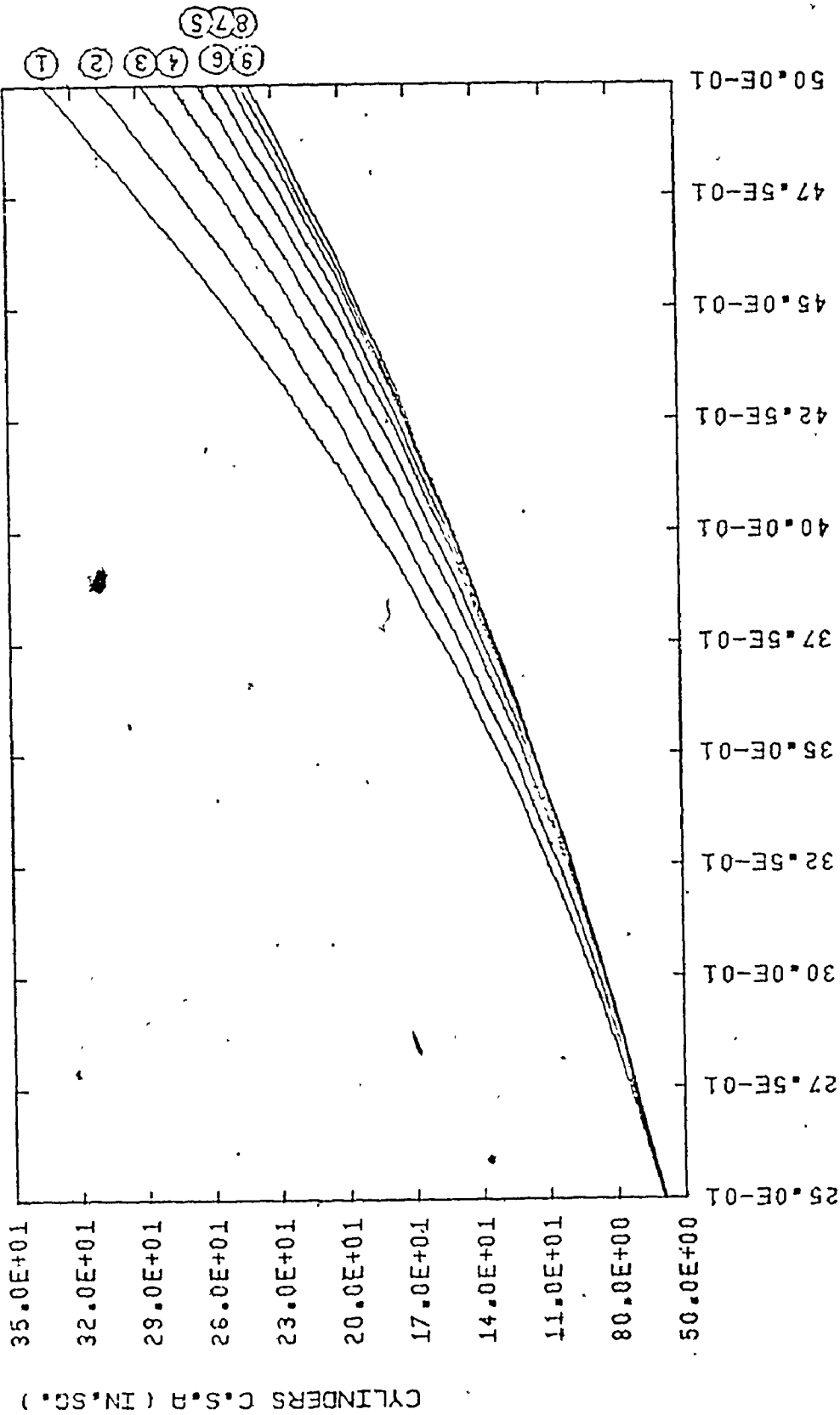


Figure 2.12.



CURVE NUMBER...	MAXIMUM INTERFERENCE (IN)	SPECIFIED INNER RADIUS (IN)
1	10.0E-04	40.0E-01
2	11.3E-04	42.5E-01
3	12.5E-04	45.0E-01
4	13.8E-04	47.5E-01
5	15.0E-04	50.0E-01
6	16.3E-04	42.5E-01
7	17.5E-04	45.0E-01
8	18.8E-04	47.5E-01
9	20.0E-04	50.0E-01

Figure 2.13.

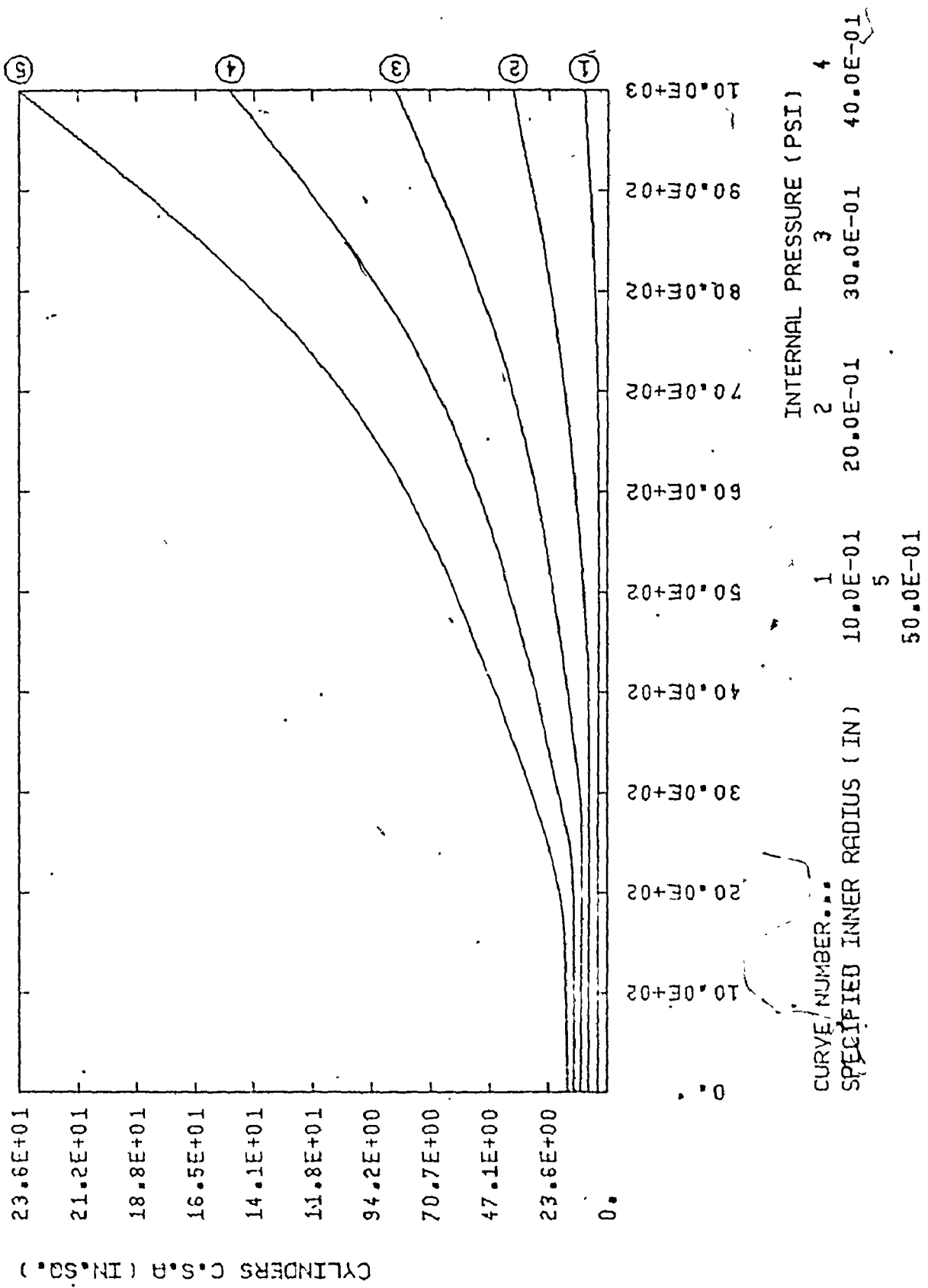


Figure 2.14.

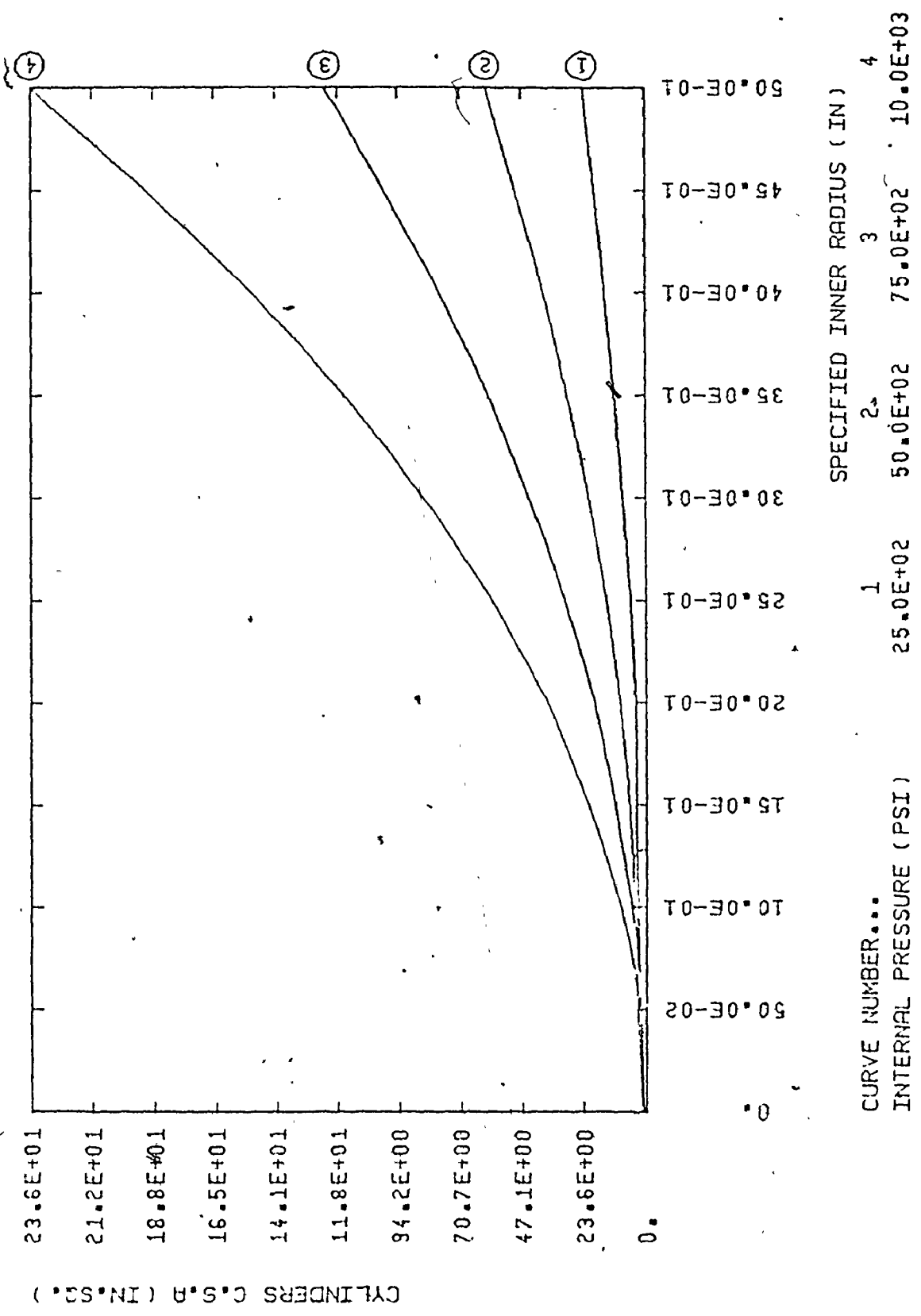


Figure 2.15.

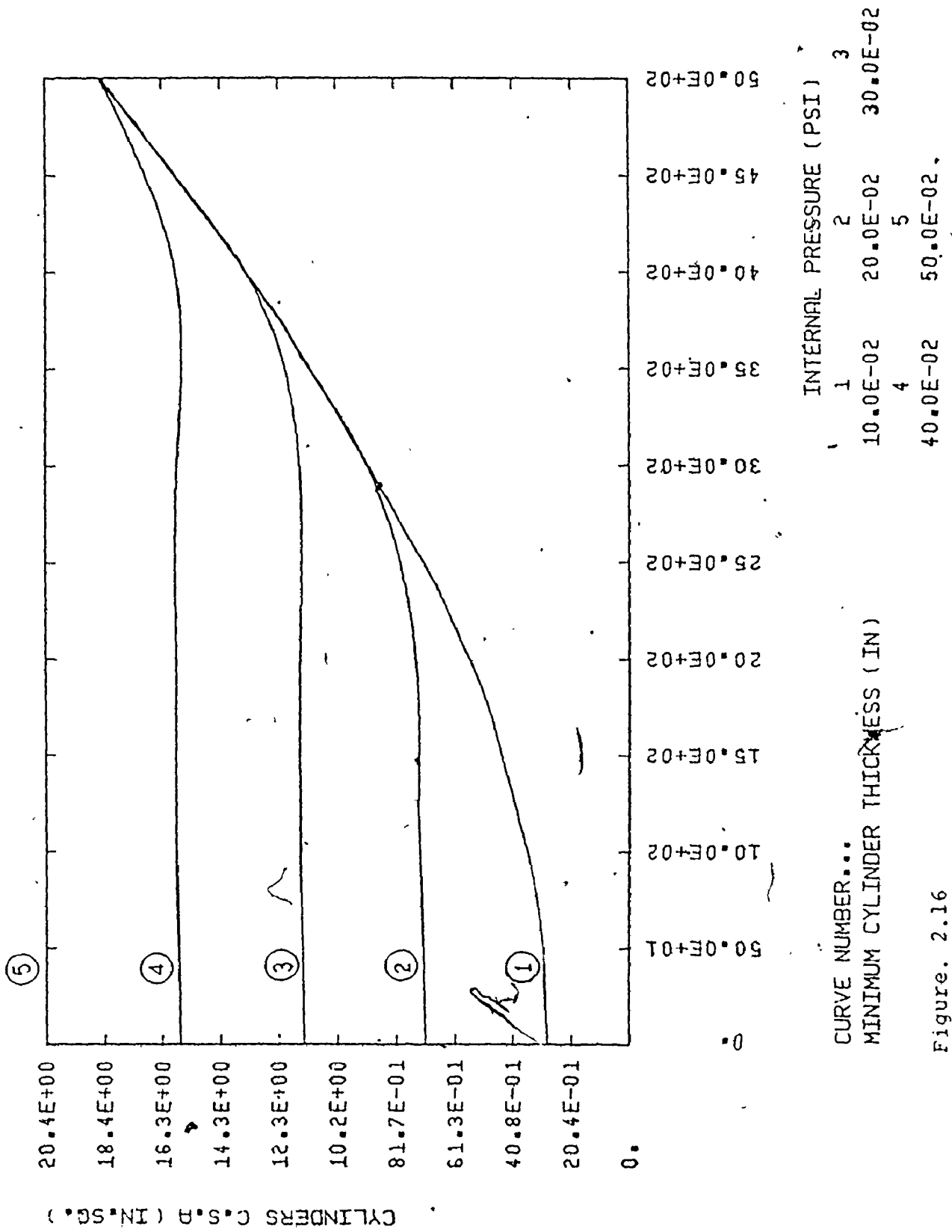
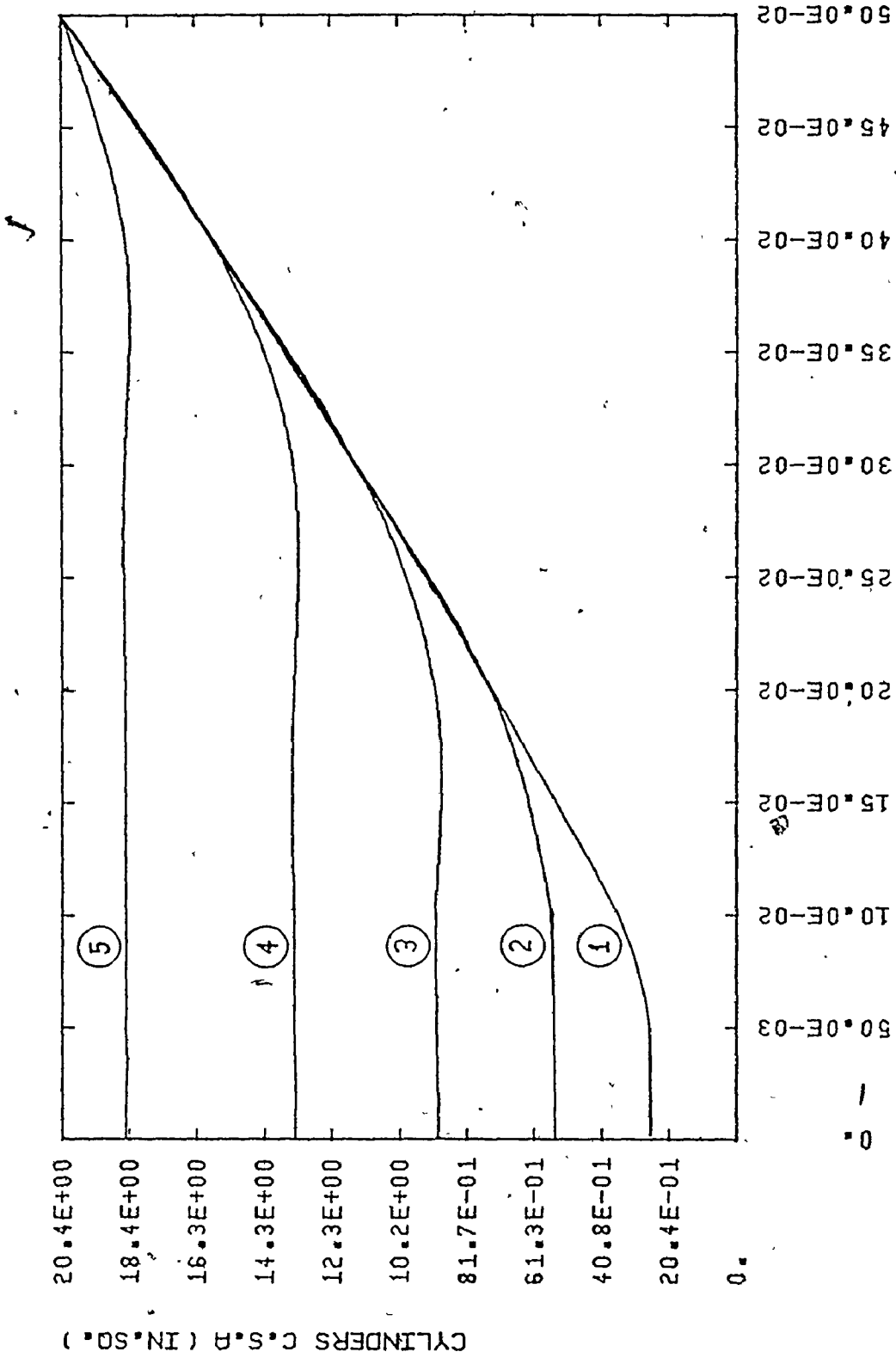


Figure. 2.16



CURVE NUMBER...
 INTERNAL PRESSURE (PSI)
 MINIMUM CYLINDER THICKNESS (IN)

Figure 2.17.

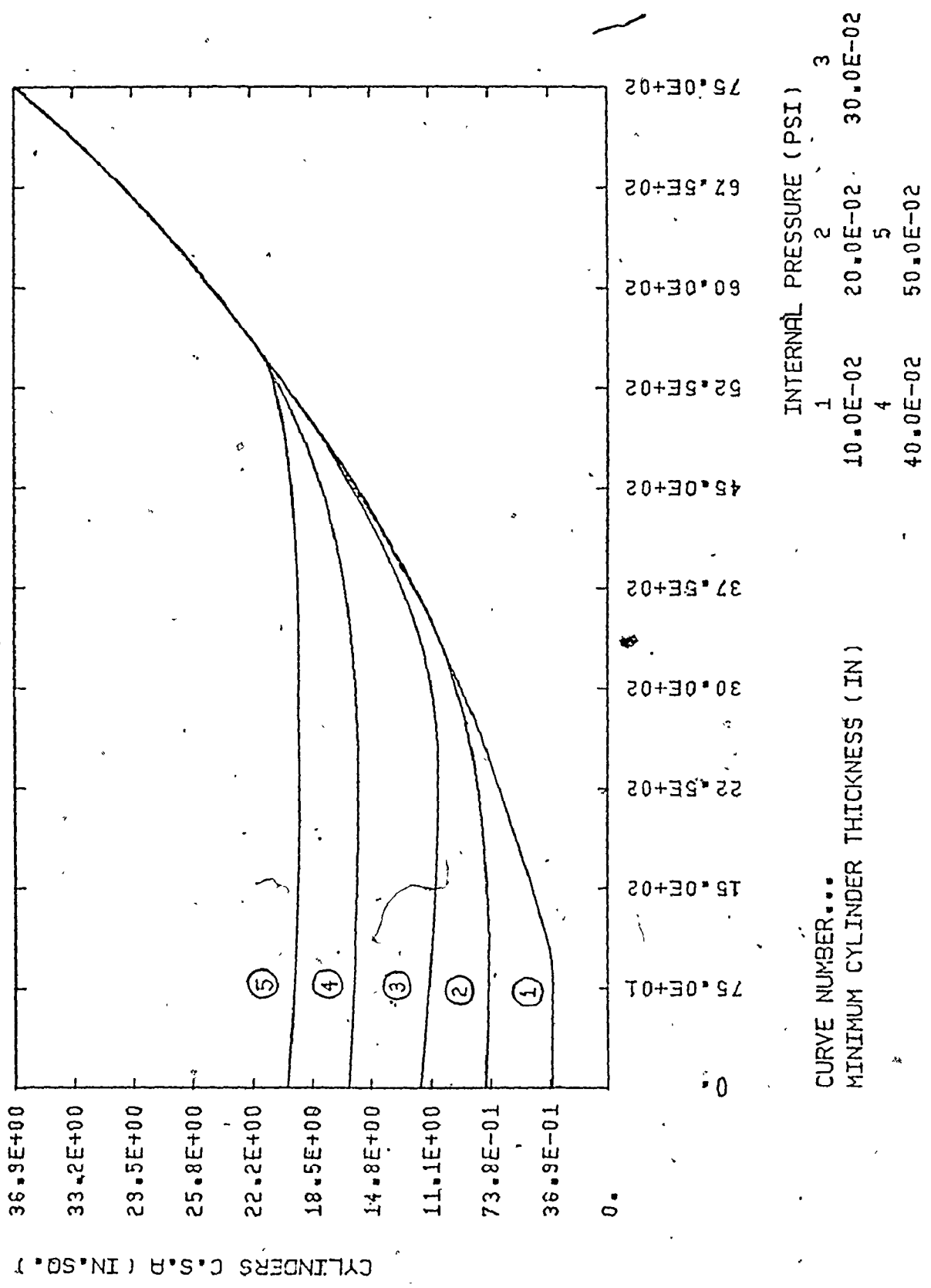
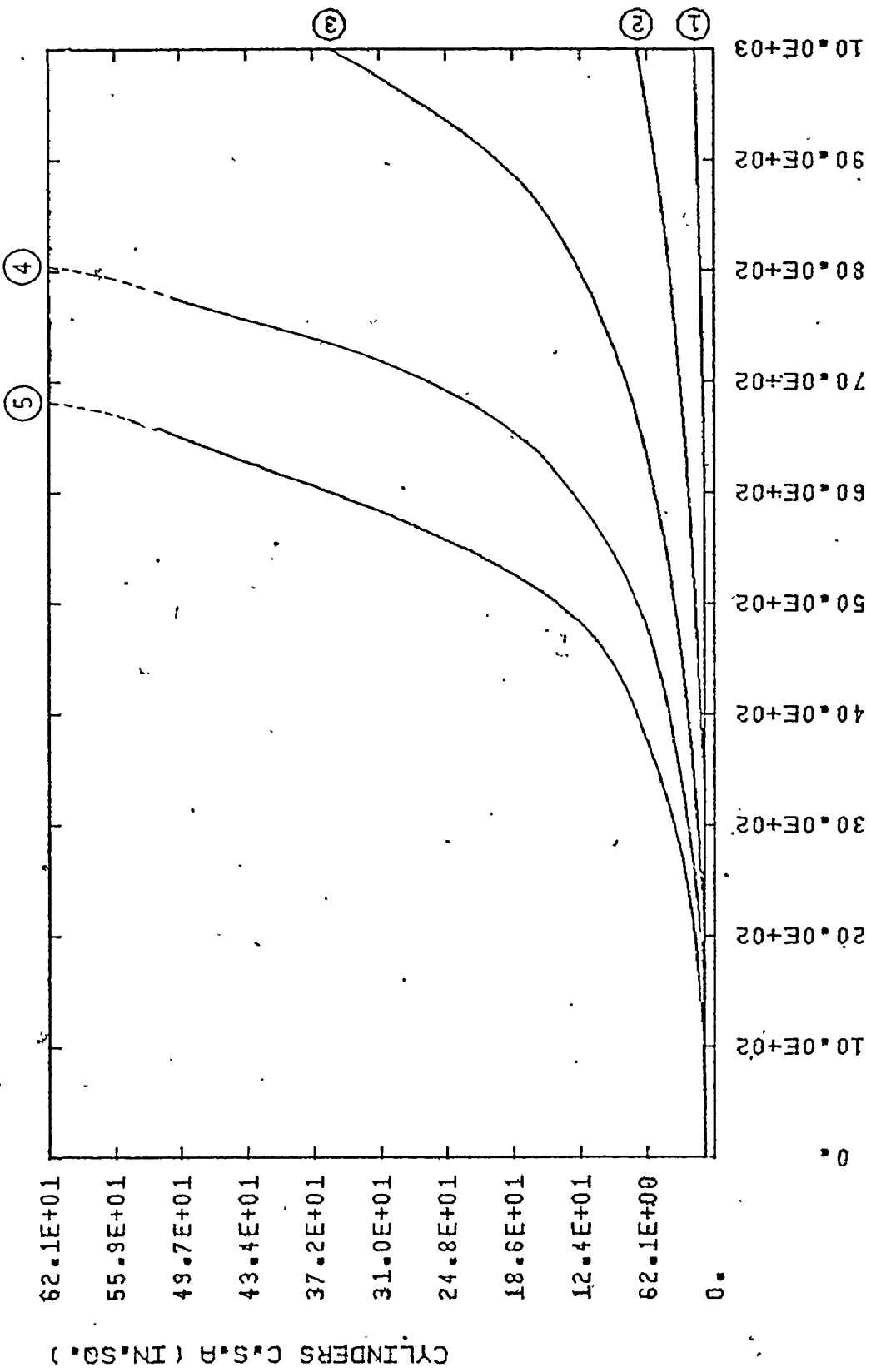


Figure 2.18.



CURVE NUMBER... 1 2 3 4 5
 FACTOR OF SAFETY 10.0E-01 20.0E-01 30.0E-01 40.0E-01 50.0E-01

Figure 2.19.

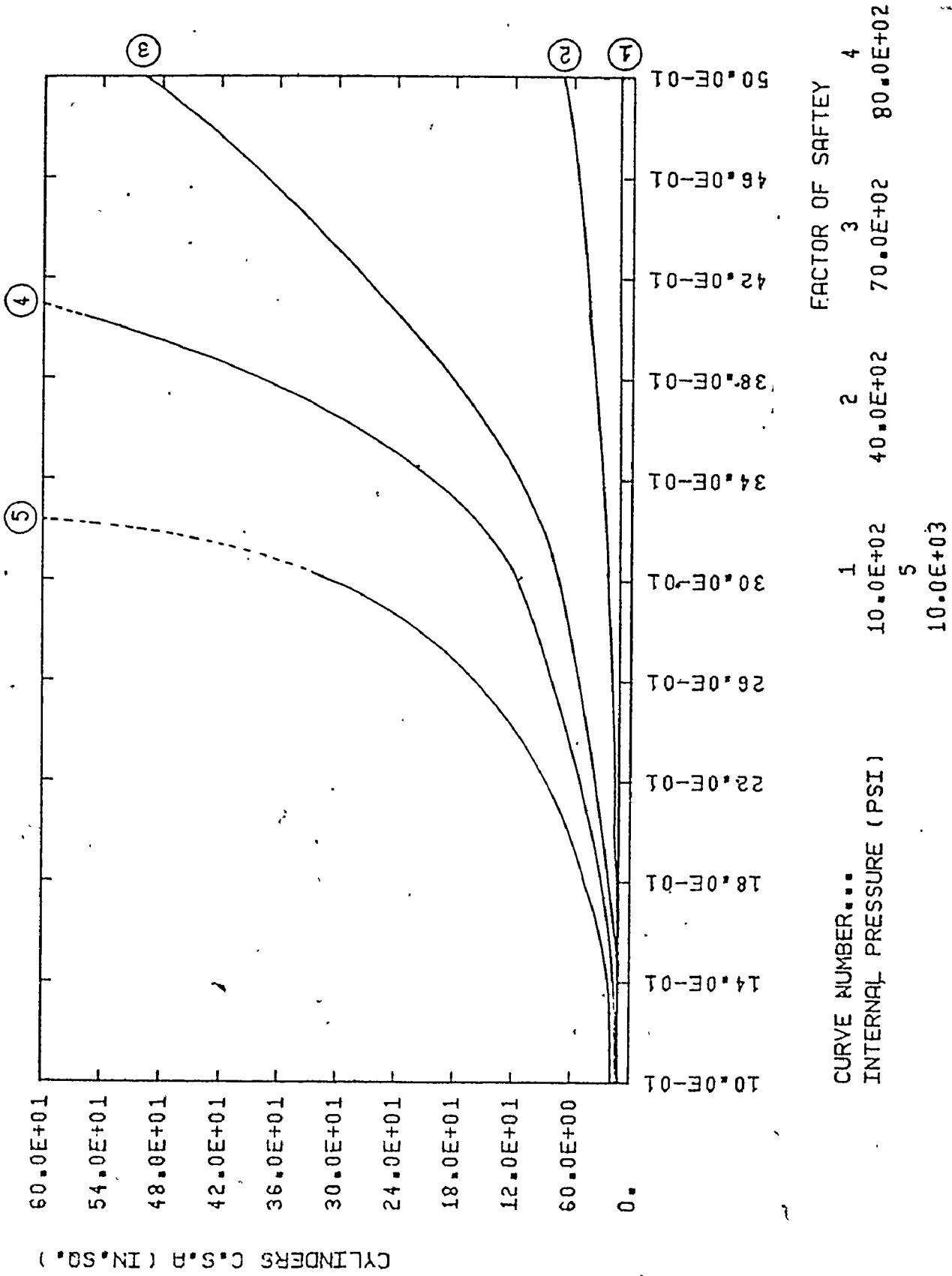


Figure 2.20.

2.4.2 Axial Flow Fan TOC's

The optimum configuration of a rotor with a straightener fan unit, Section 2.32 and Appendix B, will be considered here based on the previously listed specifications. The design details of the optimum rotor and straightener blades are listed in Table 2.1. Figures 2.21 to 2.32 show trade-off surfaces generated by relaxing the hard specifications of the axial flow fan design problem. Insight into the design could have been gained by carrying out a similar analysis, as previously discussed. Figures 2.21 to 2.26 are Type-B trade-off surfaces while the rest are type-A.

2.5 Conclusions

Trade-off curves (surfaces) are shown to be a very useful tool in analytical decision-making, and give particular insight into the problem of specifications, [11]. In short, the usefulness of the trade-off curves becomes a matter of the designer's ingenuity and ability to recognize what particular characteristics of the trade-off curve he is looking for and how to use them to solve his problem. The trade-off curve displays to the designer almost all of the possible compromises that need to be considered if he gives up hard specifications for soft ones. The approach of using trade-off curves to obtain the "best" design ever is interactive and requires that the designer has a good understanding or "feel" for the

problem, which he might codify using value curves. The number and complexity of the regions bounded by these trade-off curves grows rapidly as the number of the design input specifications increases.

Trade-off curves have been proposed as a tool for making the trade-off decision. They do give considerable discernment into the design problem on hand, and the importance of specifications with their relative effect on the objective criterion. Trade-off curves may be used also to provide a feasible start and revelation of an over constrained formulation. The smooth trend of the trade-off curves gives confidence that convergence has been achieved to at least a local optimum. More than that, they might be of use to detect a global optimum over local ones, as shown in Figure 2.6. Last but not the least, trade-off curves (surfaces) can be used in decomposition to optimize large compound systems, as the next chapter explains.

Table 2.1 Axial Flow Fan Optimum Design

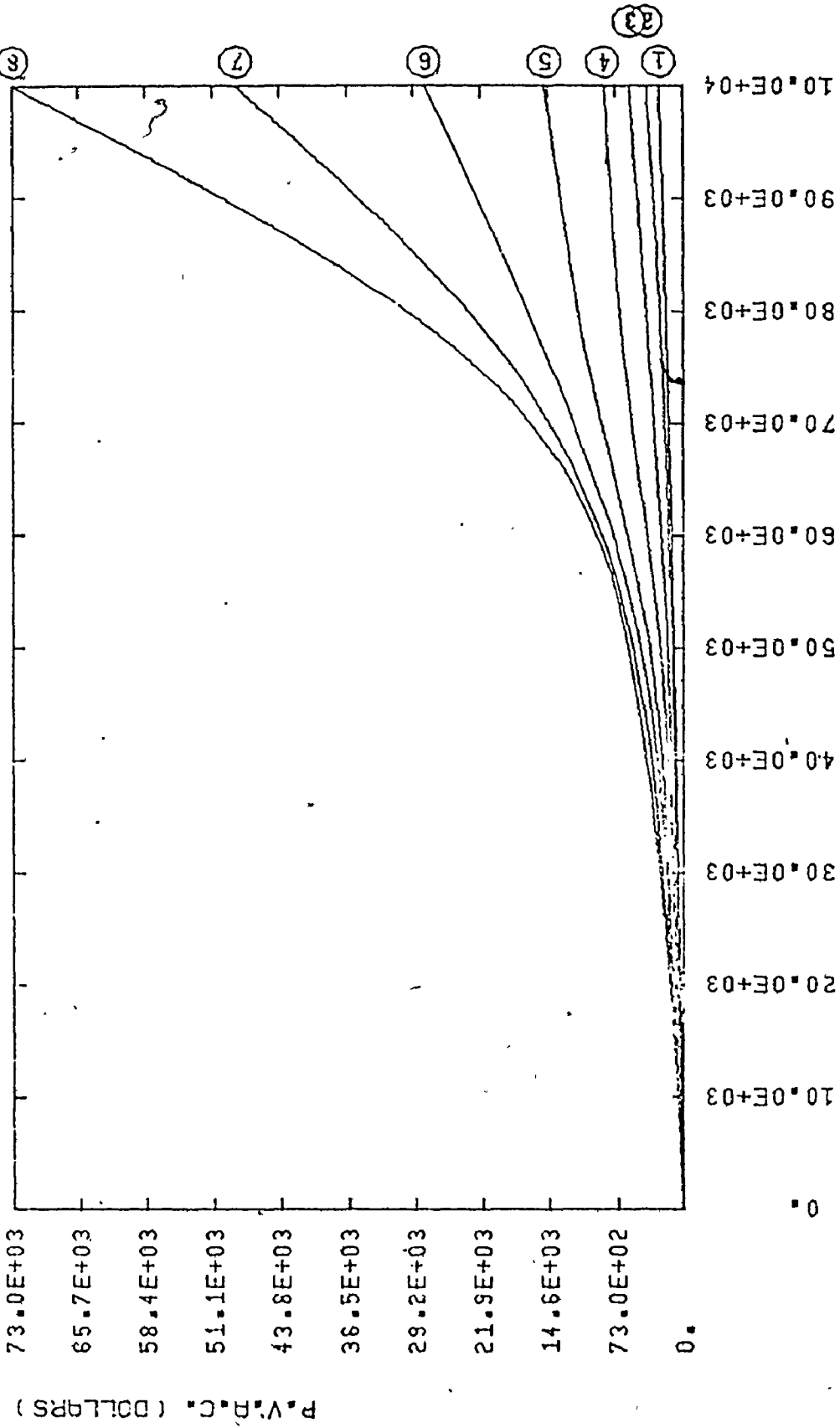
R	=	8.59 in.,	r_b	=	5.89 in.,
t_R	=	0.06 in.,	t_S	=	0.07 in.,
N_R	=	29	N_S	=	31
RPM	=	2030 rpm,	HP	=	10.75 hp,
η	=	77%	ΔH	=	5.8 in.water,
P.V.A.C.	=	325 dollars	\bar{u}	=	116.0 ft/sec,

r in.	5.89	6.43	6.97	7.51	8.05	8.59
u_2 ft/sec	139.3	140.6	142.3	144.2	146.3	148.7
u_3 ft/sec	116.0	123.7	130.8	137.6	144.1	150.3
ϕ_R^0	66.2	63.1	60.2	57.6	55.2	52.9
ϕ_S^0	72.3	71.8	71.2	70.7	70.1	69.5
C_{LR}	1.13	1.38	1.51	1.63	1.72	1.80
C_{LS}	1.11	1.14	1.18	1.21	1.24	1.26
σ_R	1.26	1.18	1.11	1.05	1.00	0.96
σ_S	1.04	0.99	0.94	0.89	0.84	0.79
C_R	1.61	1.64	1.68	1.71	1.74	1.79

C_S in.	1.80	1.61	1.43	1.25	1.09	0.94
θ_R †	61.5	58.3	55.7	53.4	50.8	47.9
θ_S	59.0	56.9	55.0	53.2	51.2	50.1
R	7.3	13.4	16.0	19.7	22.9	24.8
S	14.5	13.6	12.8	11.9	11.2	10.4

† See Figures B.4 and B.5

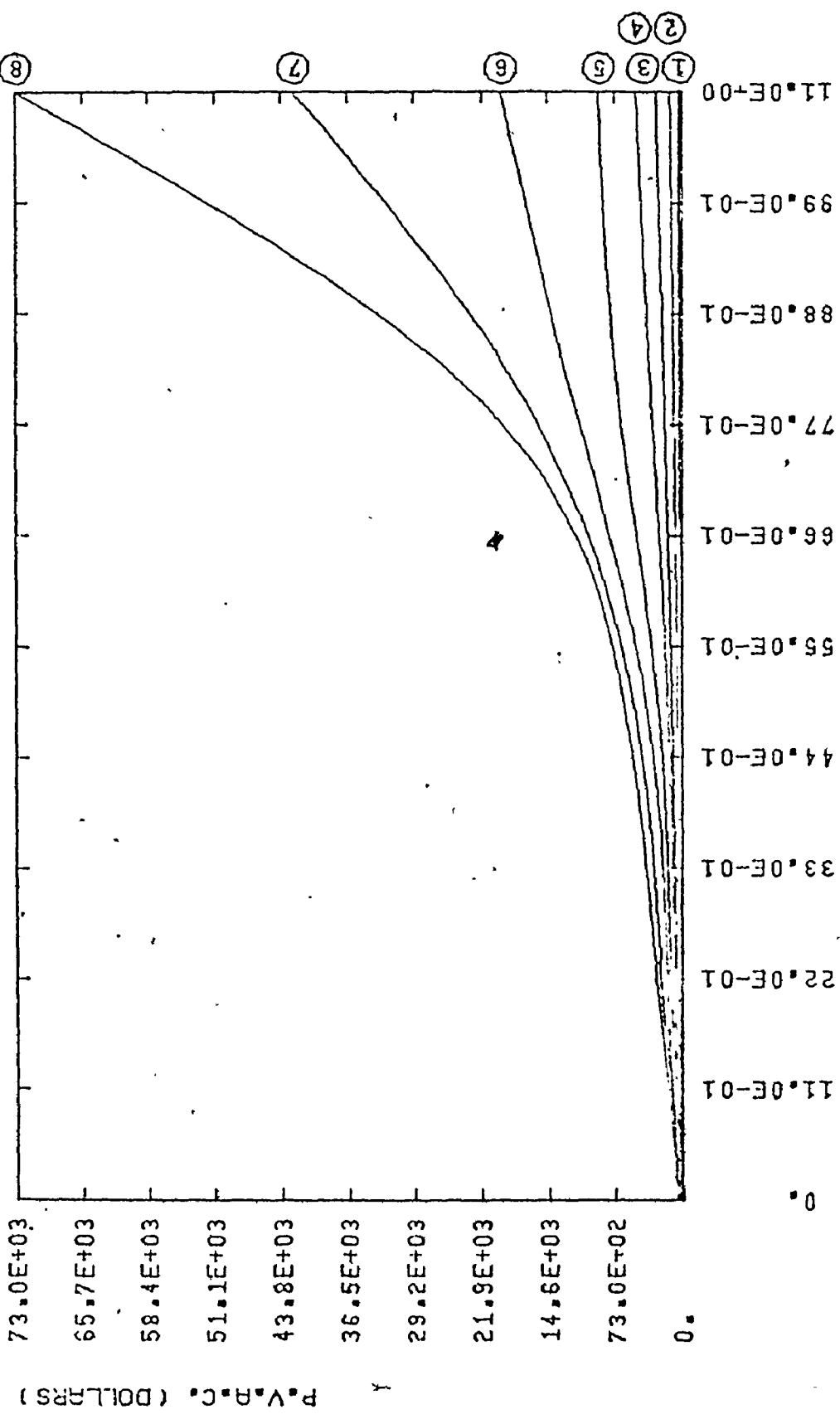
2 5



P.V.P.R.C. (DOLLARS)

CURVE NUMBER...	HEAD RISE (IN. WATER)	VOLUME FLOW RATE (CFM)
1	20.0E-01	32.9E-01
2	32.9E-01	45.7E-01
3	45.7E-01	58.6E-01
4	58.6E-01	71.4E-01
5	71.4E-01	84.3E-01
6	84.3E-01	97.1E-01
7	97.1E-01	11.0E+00
8	11.0E+00	

Figure 2.21.



CURVE NUMBER...	VOLUME FLOW RATE (CFM)	HEAD RISE (IN. WATER)
1	50.0E+02	73.0E+03
2	18.8E+03	65.7E+03
3	32.1E+03	58.4E+03
4	45.7E+03	51.1E+03
5	59.3E+03	43.8E+03
6	72.9E+03	36.5E+03
7	86.4E+03	29.2E+03
8	10.0E+04	21.9E+03

Figure 2.22.

P.V.A.R.C. (DOLLARS)

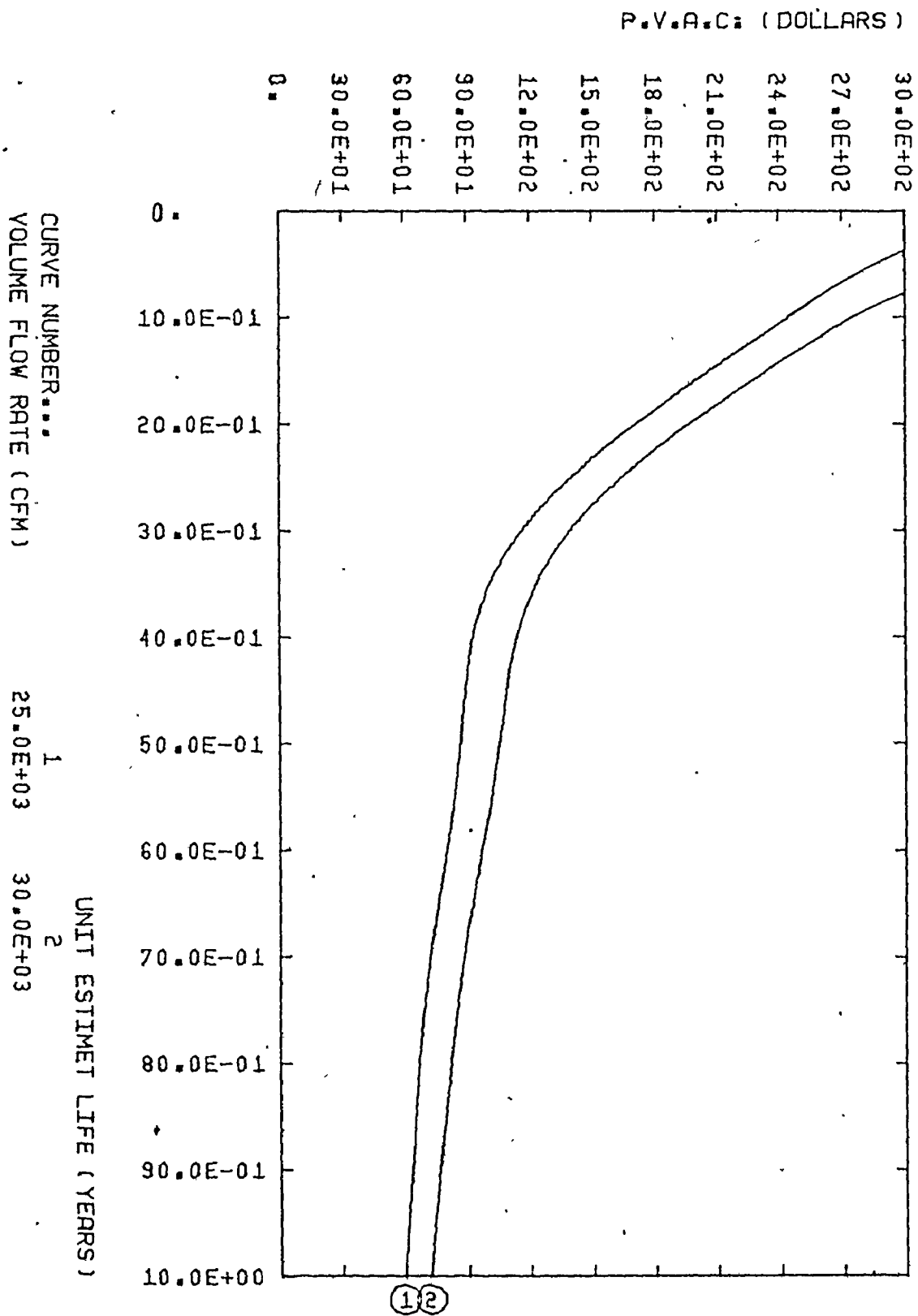
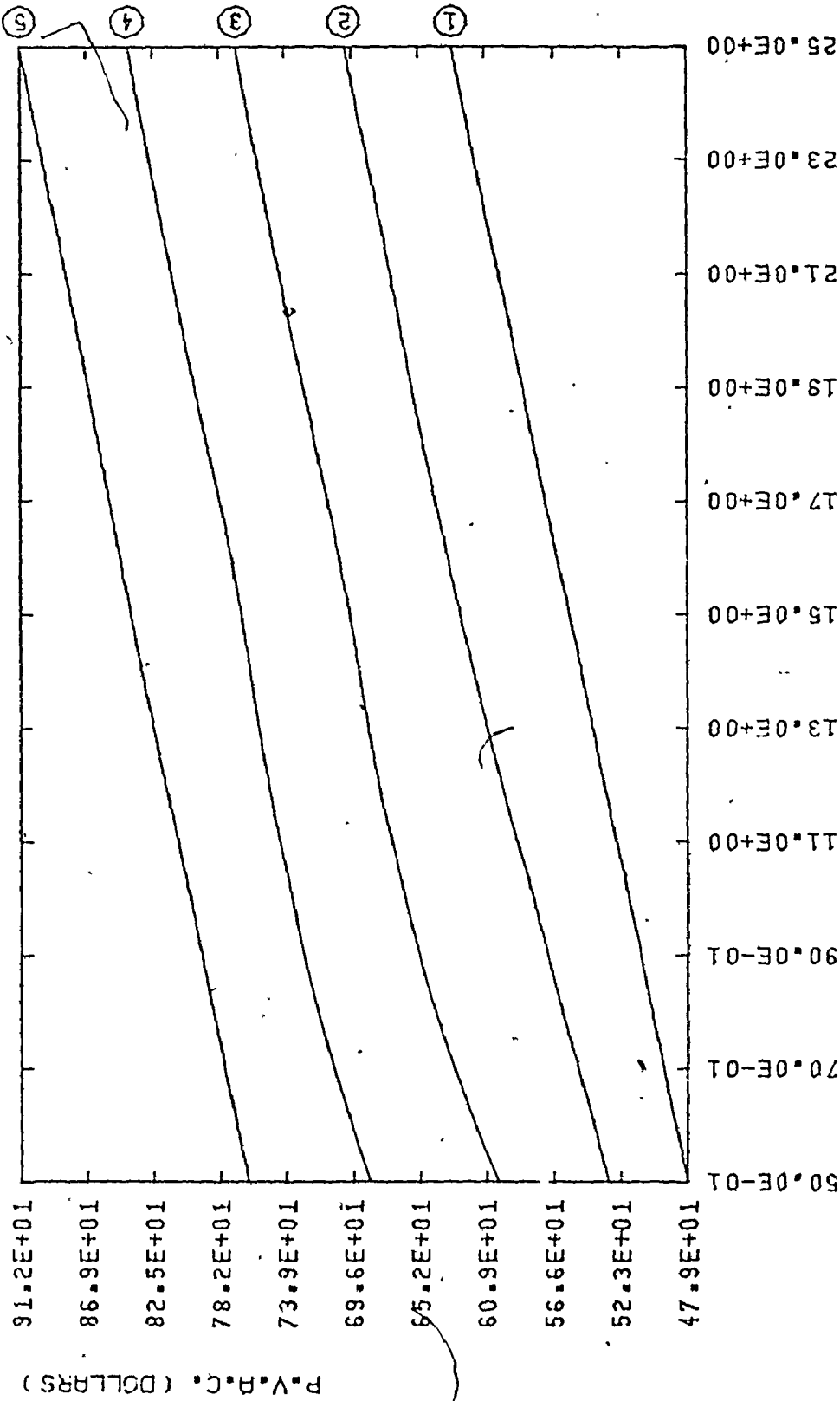


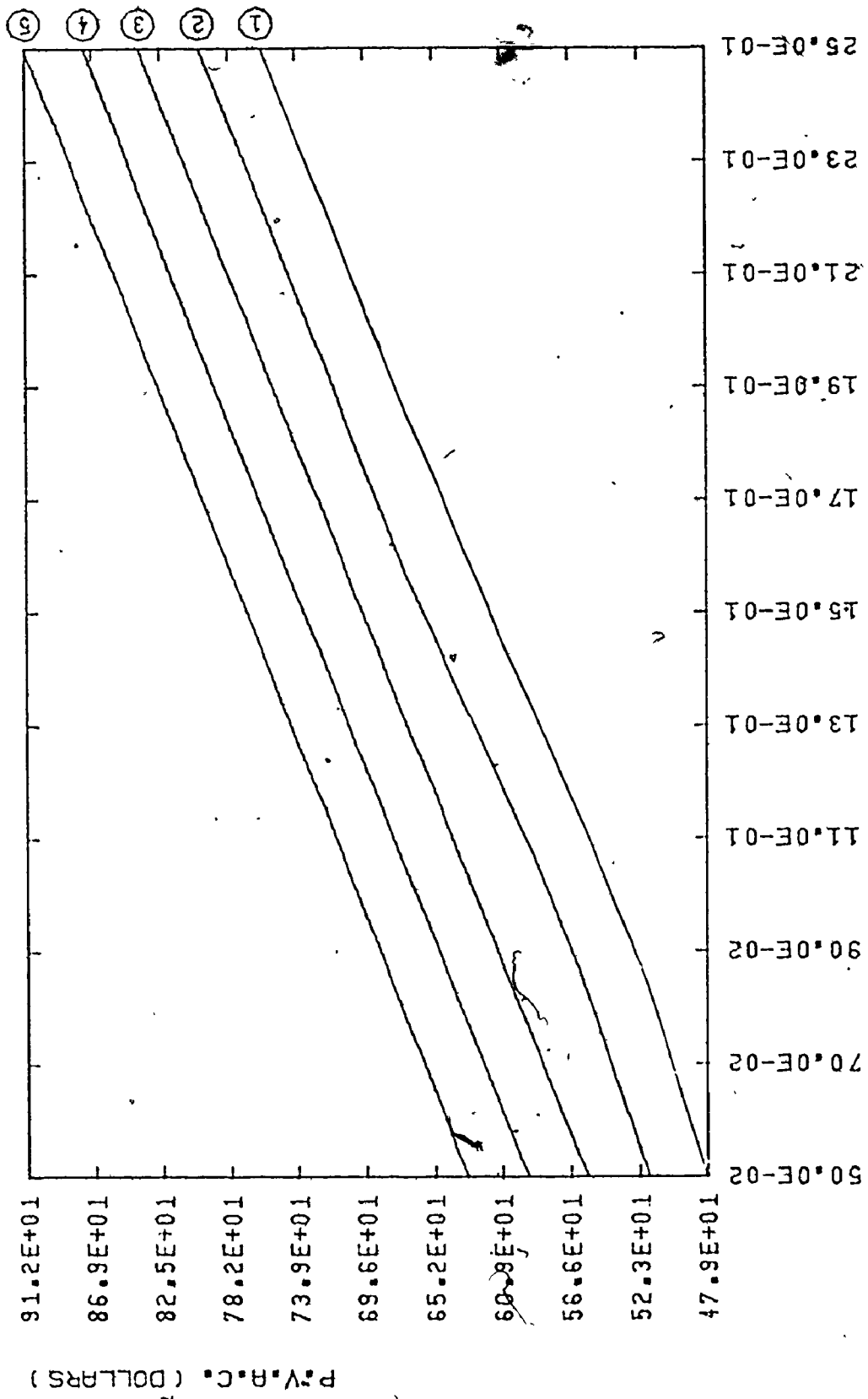
Figure 2.23.



CURVE NUMBER...
 1 50.0E-02 10.0E-01
 2 15.0E-01 20.0E-01
 3 25.0E-01
 4
 5

FIXED COST RATE PER FAN SHAFT VOLUME (\$/CU.IN)
 FIXED COST RATE PER BLADES VOLUME (\$/CU.IN)

Figure 2.24.



FIXED COST RATE PER BLADES VOLUME (\$/CU.IN)

CURVE NUMBER...

FIXED COST RATE PER FAN SHAFT VOLUME (\$/CU.IN)

1	50.0E-01	10.0E+00
2	10.0E-01	20.0E+00
3	15.0E+00	
4	20.0E+00	
5	25.0E+00	

Figure 2.25.

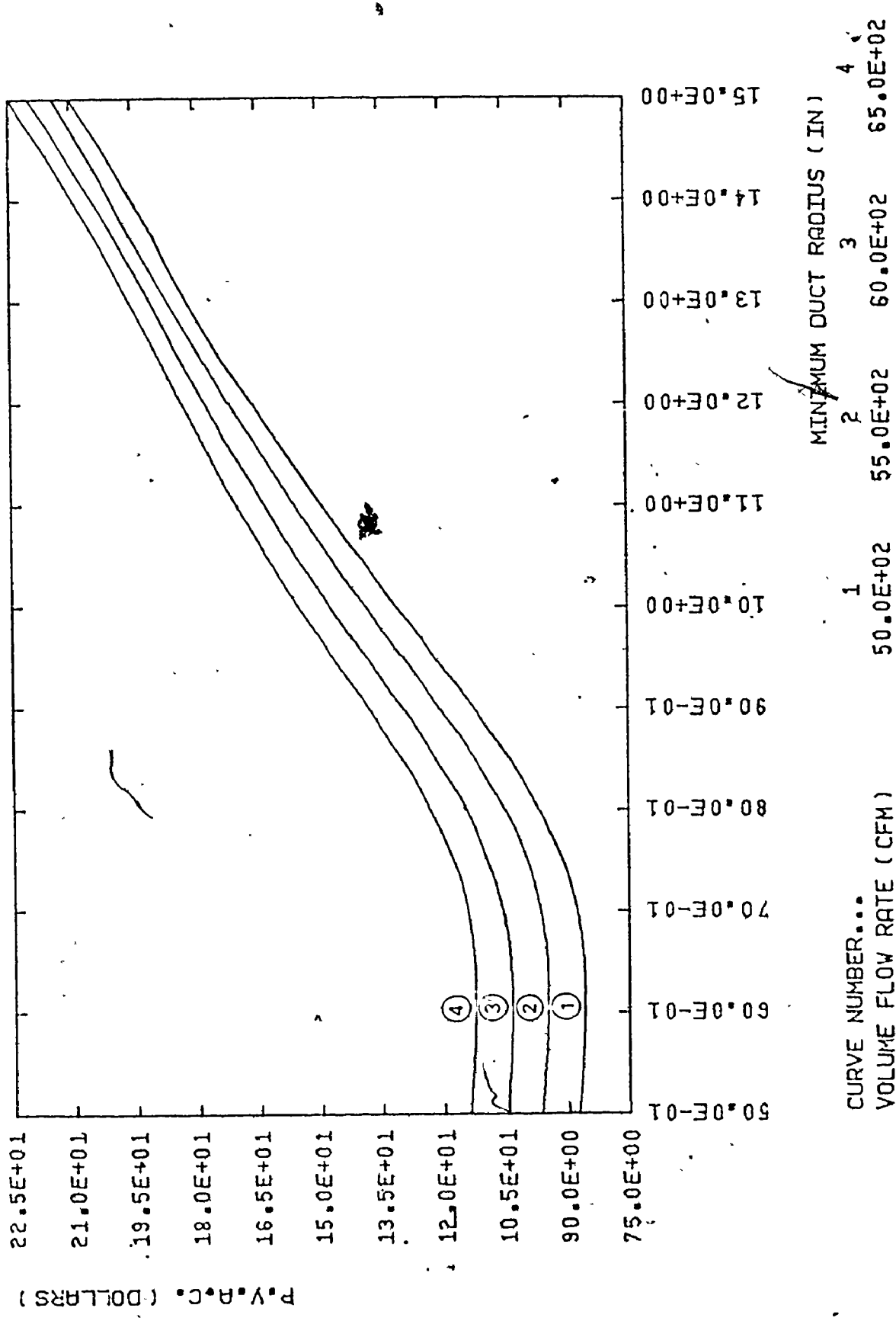
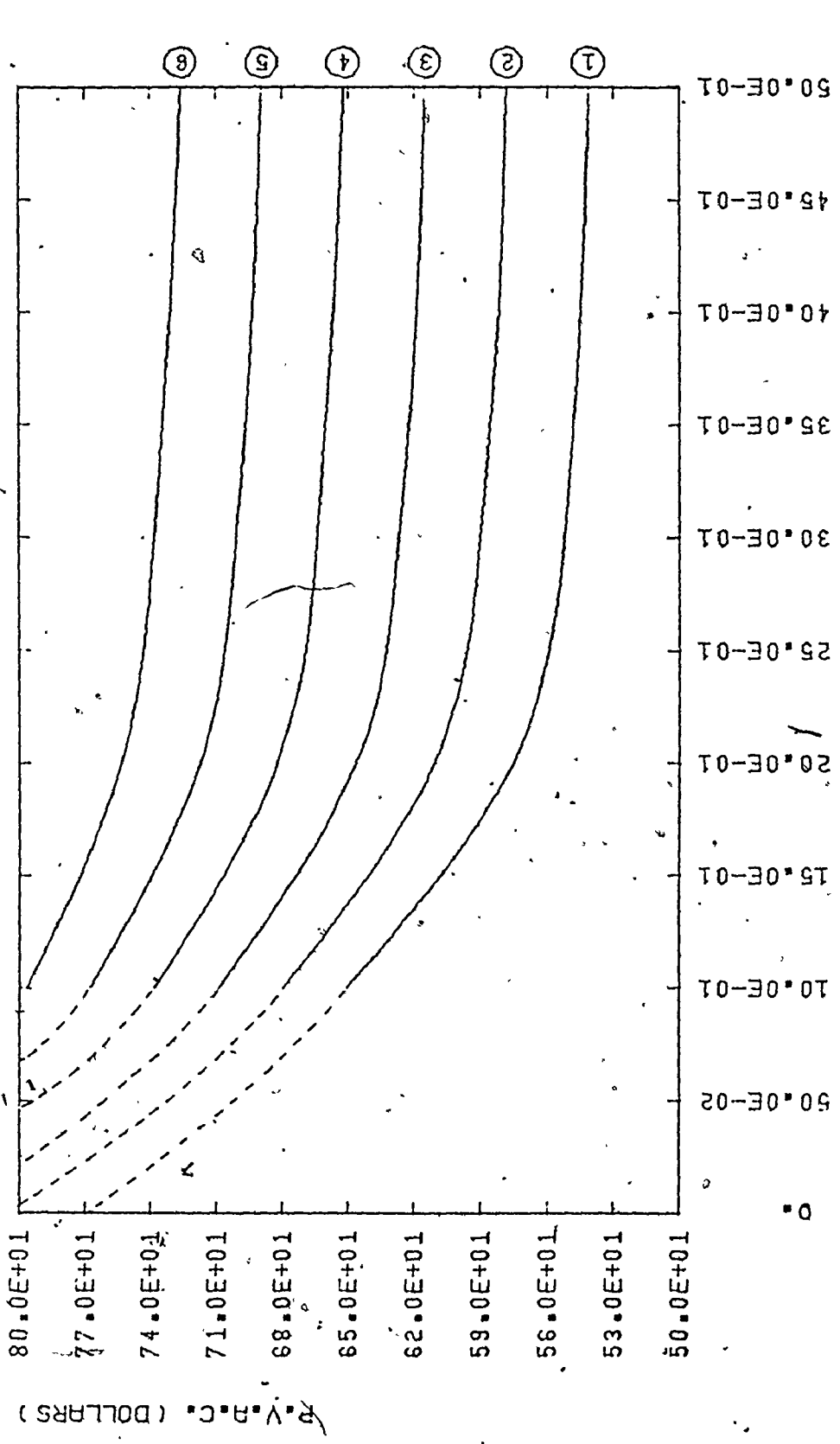


Figure 2.26.



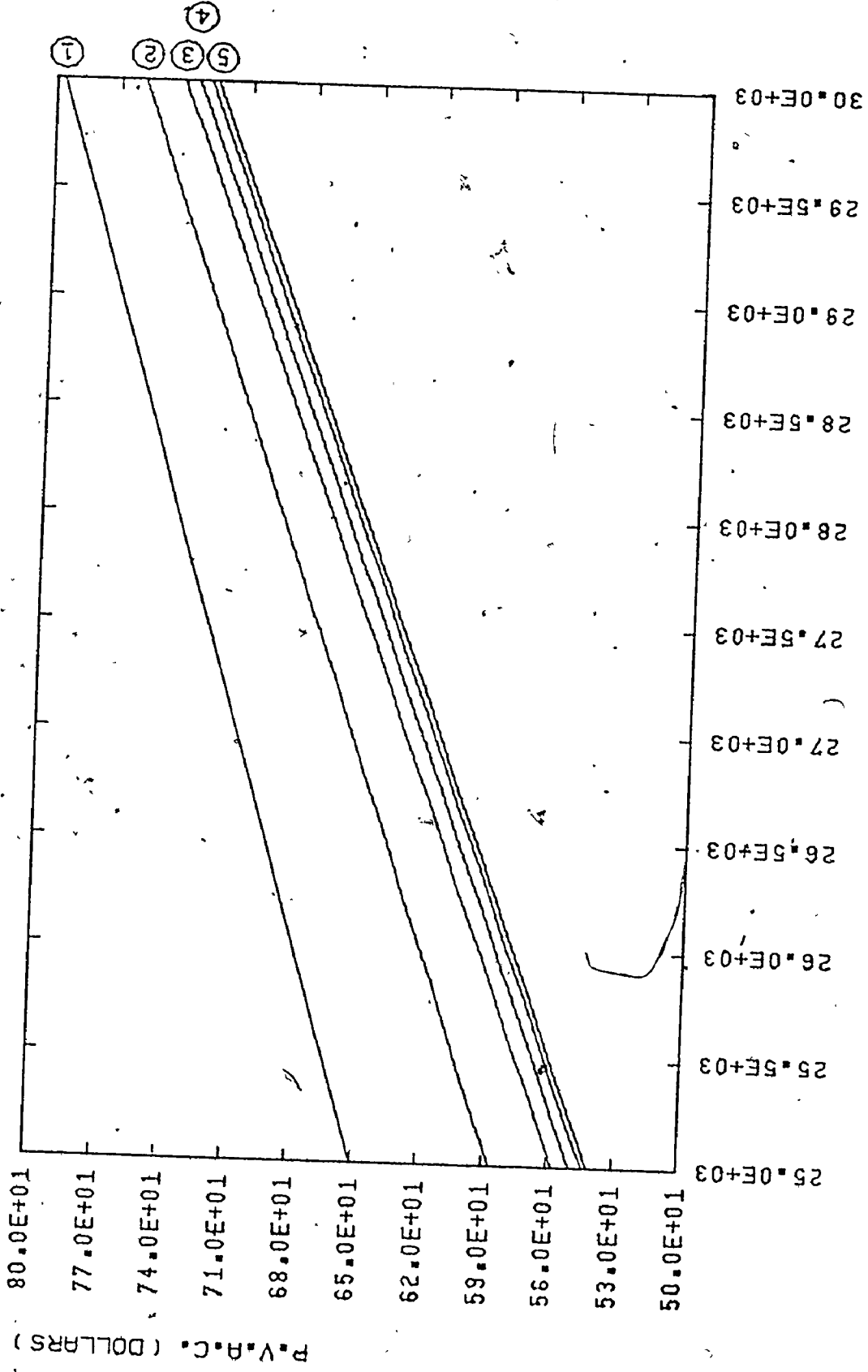
P.V.A.C. (DOLLARS)

MAXIMUM ROTOR ASPECT RATIO

CURVE NUMBER...
VOLUME FLOW RATE (CFM)

CURVE NUMBER	VOLUME FLOW RATE (CFM)
1	25.0E+03
2	26.0E+03
3	27.0E+03
4	28.0E+03
5	29.0E+03
6	30.0E+03

Figure 2.27.



CURVE NUMBER... 1 2 3 4 5 6
 ROTOR ASPECT RATIO 10.0E-01 18.0E-01 26.0E-01 34.0E-01 42.0E-01 50.0E-01
 VOLUME FLOW RATE (CFM) 25.0E+03 26.0E+03 27.0E+03 27.5E+03 28.0E+03 28.5E+03 29.0E+03 29.5E+03 30.0E+03

Figure. 2.28

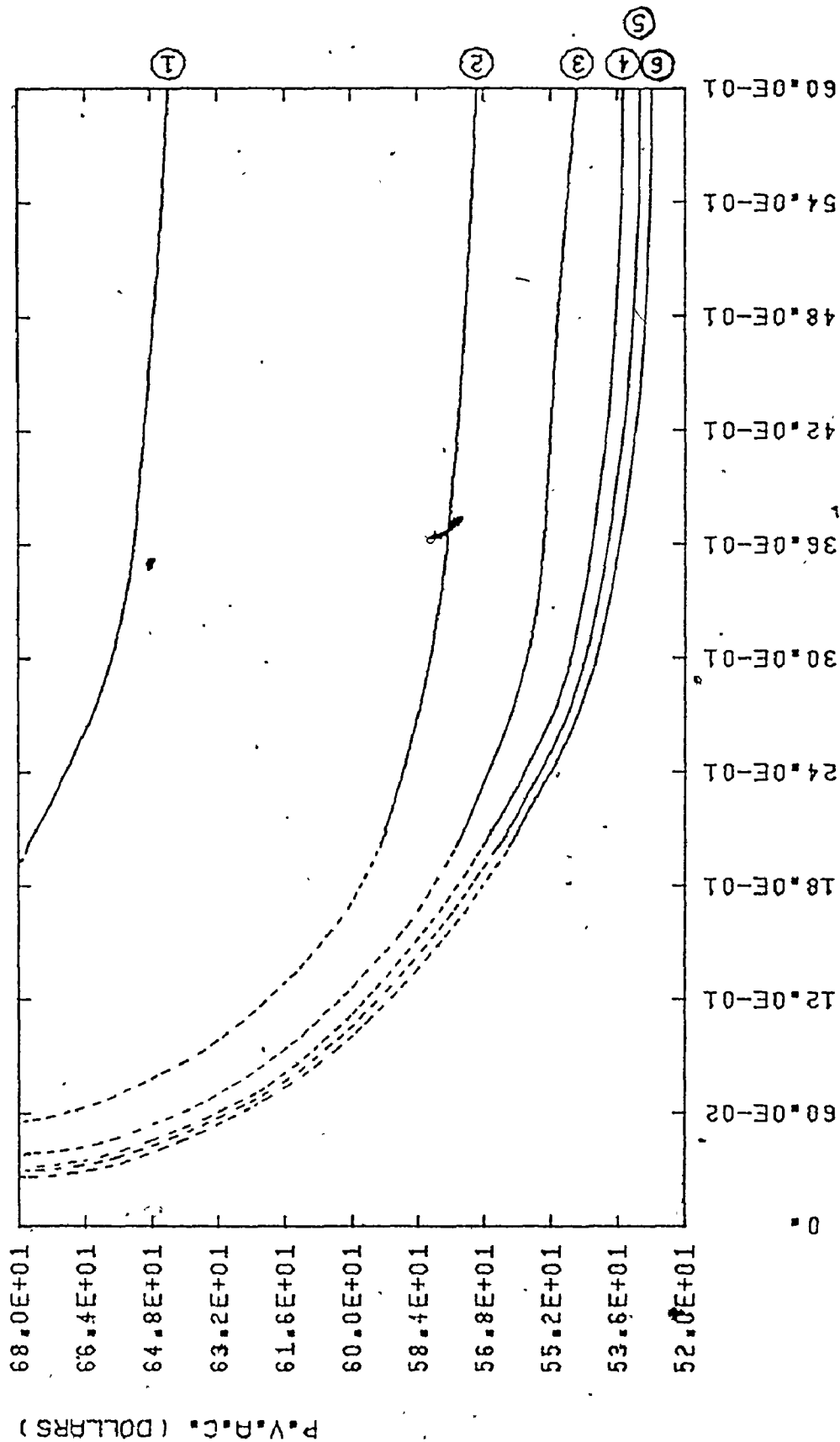
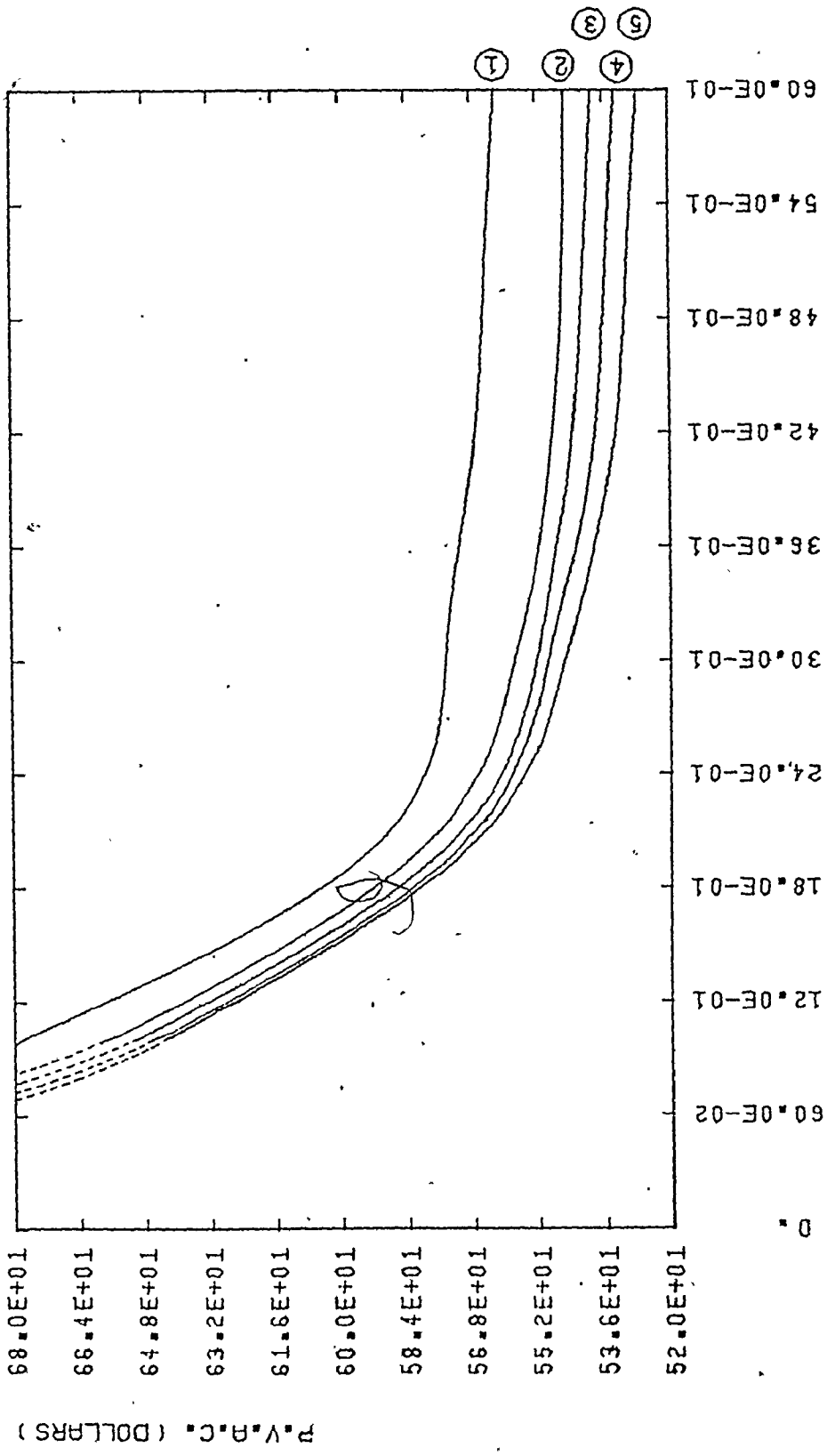
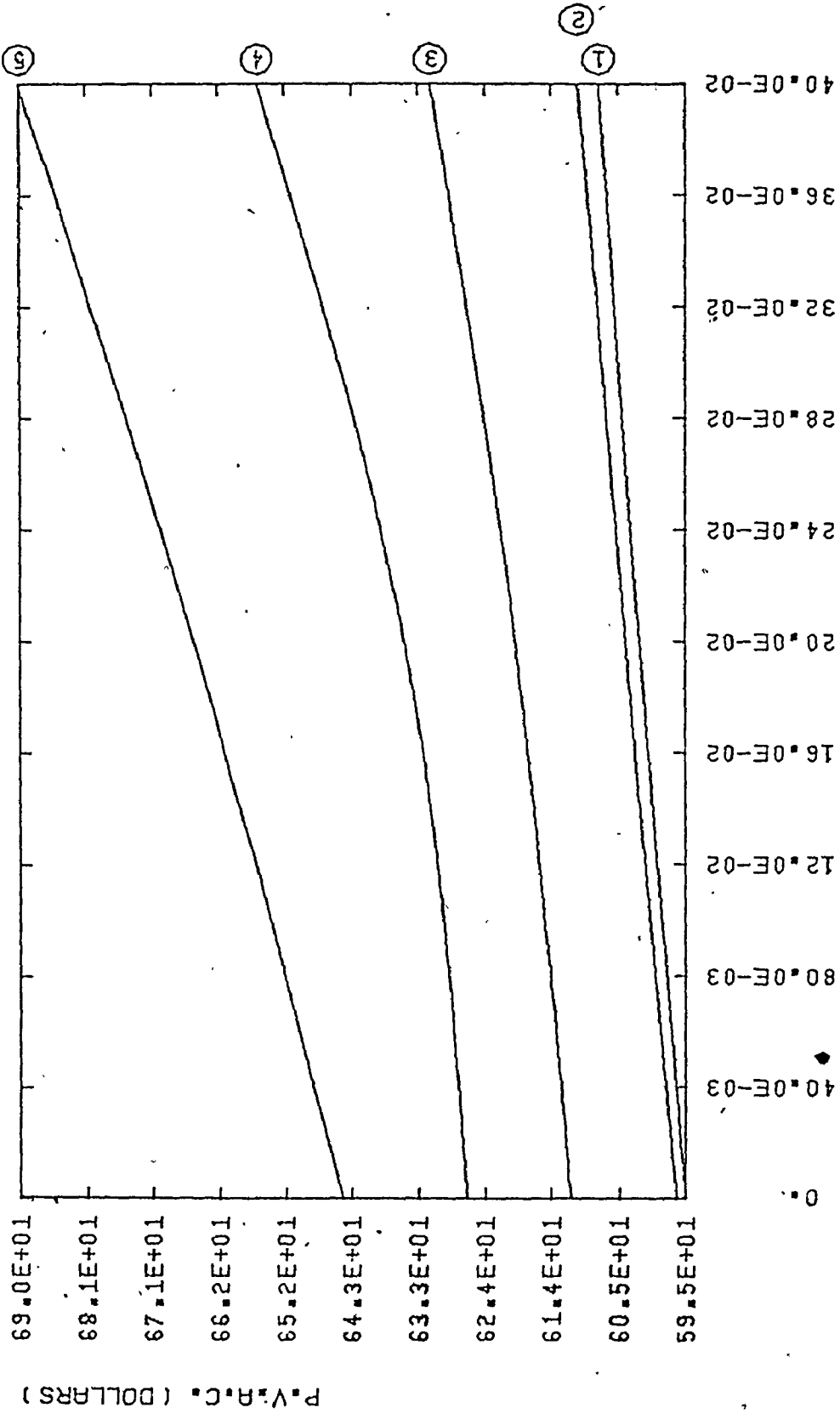


Figure. 2.29.



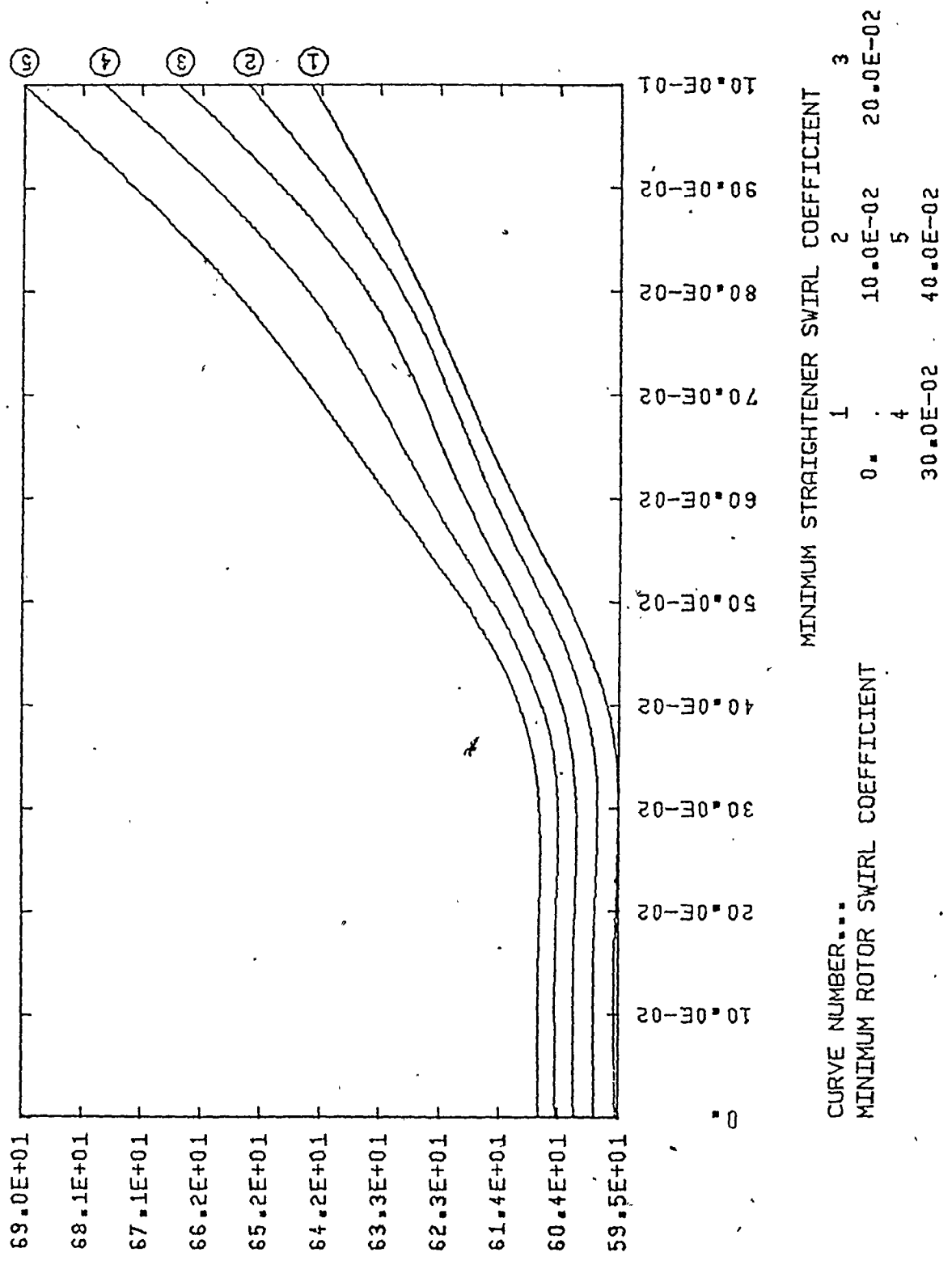
CURVE NUMBER...
 STRAIGHTENER ASPECT RATIO
 1 20.0E-01
 2 30.0E-01
 3 40.0E-01
 4 50.0E-01
 5 60.0E-01

Figure 2.30.



CURVE NUMBER... 1 2 3
 MINIMUM STRAIGHTENER SWIRL COEFFICIENT 20.0E-02 40.0E-02 60.0E-02
 MINIMUM ROTOR SWIRL COEFFICIENT 80.0E-02 10.0E-01

Figure 2.31.



P.V.R.C. (DOLLARS)

Figure 2.32.

CHAPTER 3
DECOMPOSITION

3.1 General

This chapter addresses the application of the decomposition of a large engineering system to the design process by using trade-off curves. As an area of research, the design optimization and solution procedures for nonlinear programming problems can perhaps be described as an area of considerable current investigation. This chapter relates the potential applications of the previously defined trade-off approach or concept to engineering design. The scope of computational testing is defined along with the application of the derived algorithm to an engineering design problem. The use of interaction or trade-off curves in decomposition was recently described by Siddall [3] as a way to establish implicitly the best system design specifications based on the concept that specifications are really junctions with other parts of the system of which the sub-system is a part.

Many decomposition algorithms presently exist in the literature. Lasdon [29] has made excellent surveys of existing algorithms. Most of these algorithms, however, apply to large linear programming although some have been extended to

handle certain nonlinear or integer programming problems. The fundamental issue remains that in almost all engineering design situations, nonlinear constraints are essential to the problem formulation. Several new approaches toward the solution of nonlinear programming problems have recently been developed and investigated. Among these are the Sequential Unconstrained Minimization Technique and the Flexible Tolerance Method [4]. Still, however, when the number of constraints and/or the number of design variables become large, the solution process is often difficult if possible at all. In this sense, Siddall suggested an algorithm in which a decomposition procedure would decompose such large nonlinear system into a collection of smaller sub-systems, in anticipation that this might lead to a simpler and more efficient solution technique where each sub-system is designed separately.

3.2 Approach

A decomposition algorithm can basically be described as a procedure which breaks down a large mathematical programming problem into a collection of smaller subproblems whose solution in a prescribed manner will generate the solution to the original mathematical programming problems, [29]. To facilitate the application of the proposed decomposition procedure, the original large system design problem should possess what is known as a "block angular structure". This structure

is defined by assuming initially that the original vector of N design variables \bar{X} , can be partitioned into a set of design variables \bar{X}_k , $k = 1, 2, \dots, K$. This partitioning is effected so that all the system constraints can be expressed as functions of only members of one set.

$$\phi_j(\bar{X}_k) \geq 0.0 \quad j=1, \dots, J_k \quad (3.1)$$

$$\psi_l(\bar{X}_k) = 0.0 \quad l=1, \dots, L_k \quad (3.2)$$

where, $\bar{X}_k = (x_1, x_2, \dots, x_{n_k})$ (3.3)

and $\sum_{k=1}^K n_k = N$ (3.4)

However, no coupling constraints among the partitioned system components of the different \bar{X}_k are assumed. An optimization criterion is applied of the form

$$U(\bar{X}_1, \bar{X}_2, \dots, \bar{X}_K) \rightarrow \text{Minimum} \quad (3.5)$$

The requirement that a block angular structure must exist before a decomposition procedure can be applied may appear to be rather stringent. Due to the nature of many engineering design problems, however, a large portion of these problems do possess or nearly possess such a structure. Once block angular structure has been demonstrated for a particular design optimization problem, then a decomposition procedure can

be applied. The resulting structure of the decomposition is displayed in Figure 3.1. As shown, the decomposition model consists of two basic types of subsystems, one master sub-system and $(K-1)$ minor subsystems. Each of the minor subsystems is governed by a set of input specifications, $y_{i,k}$, ($i=1,2,\dots,I_k$), where, I_k , is the number of input specifications for the particular subsystem, (k) . These specifications are quantities common to adjacent sub-systems. If the sub-systems are independently optimized, as is often done in practice, the specifications must be hard, i.e., rigidly established by engineering judgment. Decomposition permits the connecting specifications to automatically adjust to optimum values for the whole system. These specifications can, in this event, be considered "soft". A typical design optimization procedure can then be applied to each of the minor sub-systems, which has the following optimization criterion,

$$U_k(\bar{X}_k) \rightarrow \text{Minimum} \quad (3.6)$$

subjected to equality and inequality constraints shown in equations (3.1) and (3.2), and governed by a set of soft input specifications, $y_{i,k}$. By performing a series of optimizations for a range of values of the specifications, it is possible to define a "Type-B" trade-off hypersurface of order I_k . A linear or a non-linear equation could then be generated describing the best fitted trade-off hypersurface, where the optimization criterion is a dependent variable and the input specifications are independent variables, see Appendix E. The

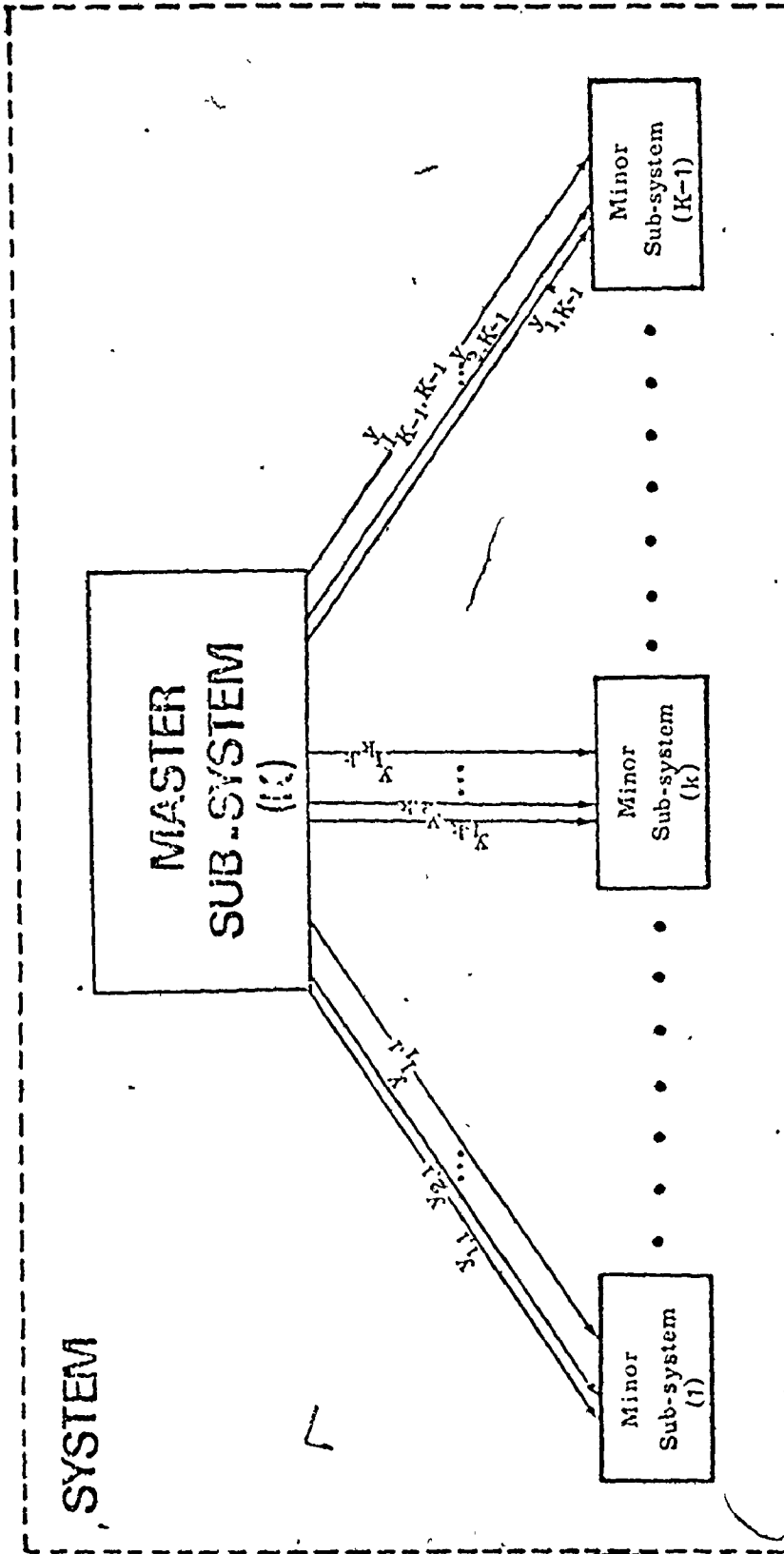


Figure 3.1. The Hierarchical Structure of a Decomposed System into a Multiple Sub-system.

fitted equation, $U_k(y_{i,k})$, must be obtained for all the minor subsystems. That is to say, (K-1) equations are now available to describe the relation between the master and the minor subsystems. It is obvious that, all the minor subsystems and also the master subsystem have optimization criteria that can be combined since all are a part of one overall system.

The role of the master subsystem is to coordinate the decisions of each of the (K-1) minor subsystems toward the solution of the original system. All the input soft specifications for all the minor subsystems have to be considered now as a part of the master subsystem design variables, \bar{X}_k . The master subsystem optimization function must now include the minor subsystem value contributions, and can be written as follows:

$$U_K(\bar{X}_k) + \sum_{k=1}^{K-1} U_k(y_{1,k}, y_{2,k}, \dots, y_{I_k,k}) \rightarrow \text{Minimum}$$

$$, k=1, 2, \dots, K-1 \quad (3.7)$$

subjected to

$$\phi_{j,k}(x_1, x_2, \dots, x_k) \geq 0, \quad j = 1, J_k \quad (3.8)$$

$$\psi_{l,k}(x_1, x_2, \dots, x_k) = 0, \quad l = 1, L_k \quad (3.9)$$

Having obtained the overall objective function value, Equation (3.7), and the master design variables vector, (\bar{X}_k) , the final optimum soft specifications for each of the minor sub-systems, which in turn are contained in (\bar{X}_k) , can be determined. A set of design optimization runs might be necessary to determine the final optimum exact design variables for each of the minor

sub-systems subjected to the pre-determined best system design specifications.

The generalized model proposed in this section should be viewed as a vehicle for extensive computational testing to prove its convergency and feasibility. It should be noted, however, that the trade-off hyper-surfaces should be represented by an empirical equation with a moderate variance from the actual global feasible design states describing all the practical feasible specifications ranges for each of the minor sub-system. The optimum status finally obtained from optimizing the master sub-system might logically represent the overall system feasible optimum design. Even though the convergence to an optimum solution for the original mathematical system representation will be extremely difficult, if not impossible to analytically ascertain.

3.3 Example - Heat exchanger and fan system

3.3.1 Definition of Problem

In the steel industry, steel ingots must be heated to an even temperature in the soaking pits before being rolled flat. This process takes about 8 to 10 hours. When completed, the ingots are conveyed to the roughing mill, where they are reduced in thickness in preparation for hot rolling. In this sense, a soaking pit is a furnace which reheats steel ingots up to about 2400⁰F prior to rolling them into slabs. It is usually fired by a mixture of by-product gases; coke oven gas

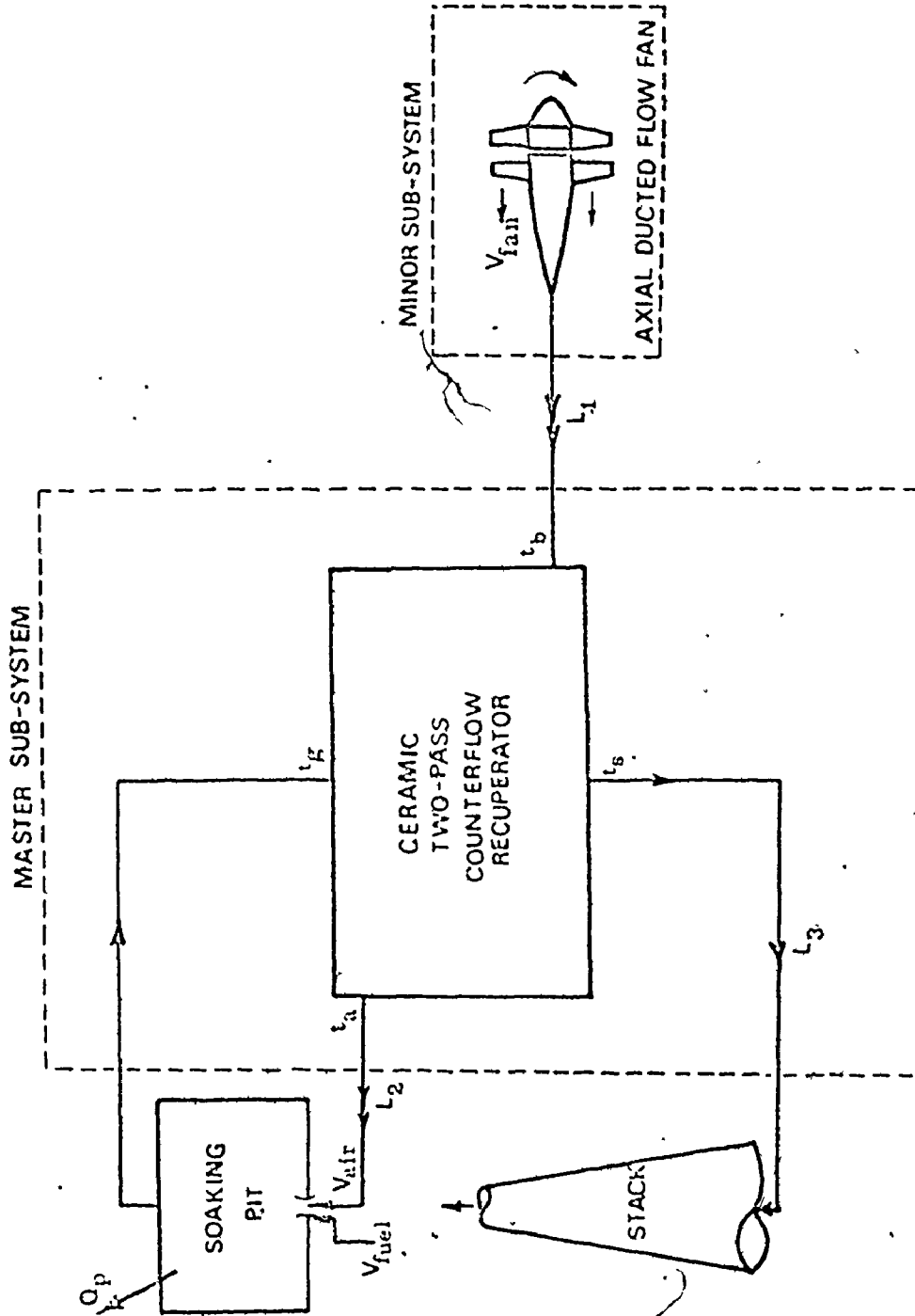


Figure 3.2. Decomposed recuperator and Fan System.

(COG), and blast furnace gas (BFG). The heat in the exhaust gases can be recovered by preheating the intake air in order to reduce fuel consumption, and consequentially decrease the unit running cost. A ceramic recuperator has been proposed for this.

The system, which is to be optimally designed, consists of a counter flow two pass ceramic recuperator, an axial flow fan, and duct work. The soaking pit and the stack are assumed to be already designed and operate with predetermined specifications, although they could also be treated as minor subsystems. The axial flow fan will be considered as a minor sub-system, while the recuperator and the duct work will be treated as the master sub-system. The connecting specifications between master and minor subsystems will be preheated air volume flow rate, Q , (cfm), and the total fan head rise, H , (in. of water).

In waste heat recuperators the hot gases flow inside a tube bank. The cold intake air flows around the outside of the tubes, heating the air and cooling the exhaust gases. The recuperators mainly depend on heat transfer by convection. The flow of the hot gases relative to the cool air is chosen to be counter-flow, which optimizes the log mean temperature difference and the heat transfer area. See Appendix C.

The design of the minor sub-system was demonstrated in Chapter 2. The type-B trade-off surface generated by the

two minor sub-system governed specifications is shown in Figures 2.24 and 2.25, while the surface fitted expression for $U_1(Q,H)$ is developed in Appendix E.

The following hard specifications are set for the system design, and in particular the master sub-system design.

Stack height	$(H_{sta}) = 135$ ft.
Stack mean inside diameter.....	$(D_{sta}) = 31.5$ in.
Roughness height of the duct work tubes	$\epsilon_D = 15 \times 10^{-5}$ ft.
Roughness height of the recuperator tubes.....	$\epsilon_R = 5 \times 10^{-3}$ ft.
Ambiant average temperature.....	$t_{amb} = 68^\circ\text{F}$.
Ambiant average pressure.....	$P_{amb} = 14.7$ psi
Duct work lengths.....	$L_1, L_2, \& L_3 = 50, 41 \& 53$ ft.
Percentage volumetric gases leakage.....	$l = 10\%$
Recuperator tubes thermal conductivity.....	$k_w = \text{Appendix D}$
Maximum adiabatic flame temperature	$AFT_{max} = 3500^\circ\text{F}$
Maximum recuperator width.....	$W_{max} = 7.75$ ft.
Maximum recuperator side length.....	$B_{max} = 7.75$ ft.
Maximum recuperator height length.....	$L_{max} = 6.67$ ft.
Minimum recuperator tube relative thickness.....	$t_{min} = 5\%$
Minimum recuperator number of tubes per row or column.....	$N_{min} \geq 3$

Minimum recuperator tube
spacing ratio..... $A_{\min} = 1.1$

Specified average hot gases
temperature..... $t_{\text{Gas}} = 2350^{\circ}\text{F}$

Minimum heat flux per pit..... $Q_{\text{sp}}^* = 6.5 \times 10^5$
Btu/min

3.3.2 Formulation for Optimization of Master Sub-System

The configuration of the heat exchanger is illustrated in Figure 3.3. The design variables of the master sub-system are:

V_{air} = Preheated air volume flow rate, cubic ft. per min.
 H = Fan total head rise, inch water
 W = Recuperator width, ft.
 B = Recuperator side length, ft.
 L_{I} = First pass recuperator height, ft.
 L_{II} = Second pass recuperator height, ft.
 d_0 = Recuperator tube outside diameter, ft.
 d_1 = Recuperator tube inside diameter, ft.
 A = Recuperator tube spacing ratio
 d_{D} = Mean duct work inside diameter, ft.
 x_{fuel} = Volumetric Coke Oven Gas ratio to total fuel
gas mixture

The optimization criterion is to minimize the system present value average cost, Appendix A. It is the sum of the master sub-system, recuperator and duct work, present value average cost, and the minor sub-system, axial flow fan, present value

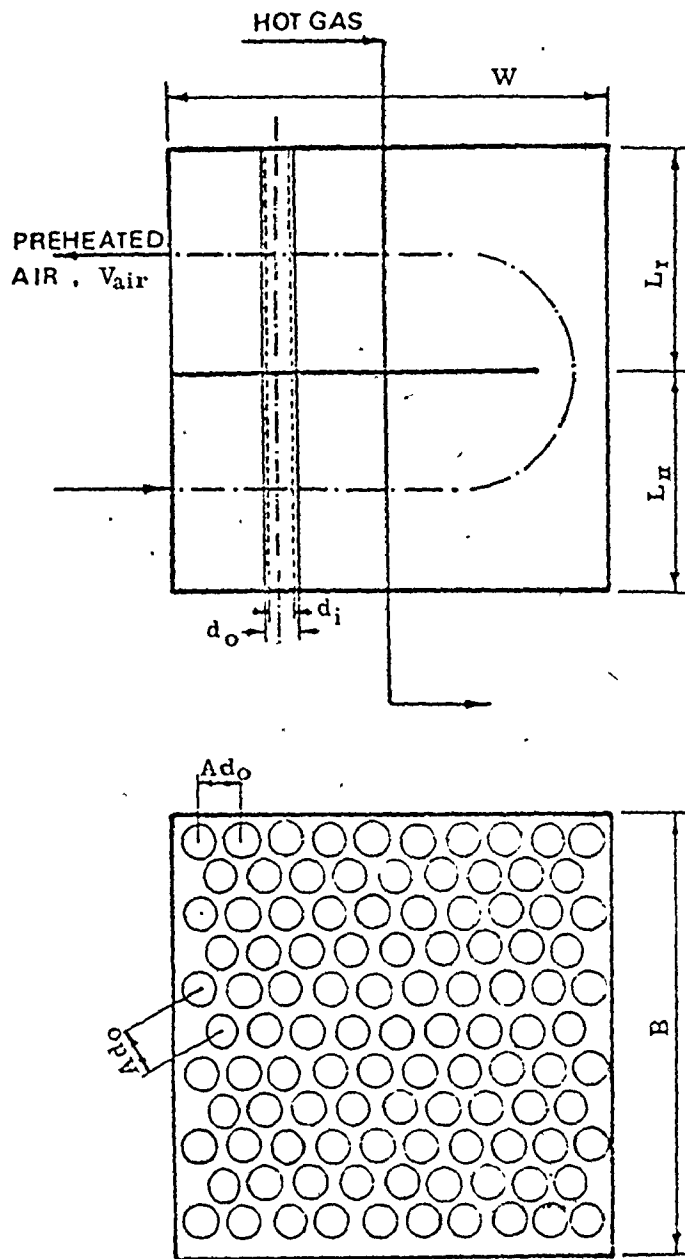


Figure 3.3. Two-Pass Counterflow Recuperator.

average cost, $U_1(H, Q)$.

$$U = \text{P.V.A.C.} \left| \begin{array}{c} \text{Master} \\ \text{Minor} \end{array} \right. + \text{P.V.A.C.} \left| \begin{array}{c} \text{Master} \\ \text{Minor} \end{array} \right. + \text{Minimum} \quad (3.10)$$

The following input specifications must be stated first before determining P.V.A.C. $\left| \begin{array}{c} \text{Master} \\ \text{Minor} \end{array} \right.$ for the recuperator and the duct work.

Recuperator estimated life	g_R	=	3 years
Ducts estimated life	g_D	=	10 years
Unit estimated tax life	y	=	12 years
Estimated interest rate	i	=	9.25%
Estimated interest rate with risk	i_m	=	12%
Estimated tax rate	t	=	50%

The initial recuperator fixed cost, I_{FR} , can be considered as a function of total tube surface, [16 & 32],

$$\text{Total tube surface} = N_T / 2 \cdot (d_I + d_Q) \cdot (L_I + L_{II}) \quad (3.11)$$

where, N_T is the total number of tubes as given in equation (C-8). Then,

$$I_{FR} = 57,000 (\text{Total tube surface}/1076)^{0.71} \quad (3.12)$$

Equation (3.12) is based on the information that the cost ratio of Aluminum tubes to clay or Ceramic tubes is 2.75: 16.34 dollars/ft.² On the other hand, initial fixed cost of the duct work, I_{FD} , can be estimated as a function of the mean duct

diameter, d_D , per unit length as follows

$$I_{F_D} = 4.0 (L_4 + L_5 + L_6) \cdot (d_D/42)^{0.807} \quad (3.13)$$

The running cost or the annual gross expense, P^* , is the unit maintenance and fuel cost. It is assumed that the maintenance cost is a direct proportion of the fuel running cost. Therefore

$$-P^* = T.E. (V_{COG} \cdot C_{COG} + V_{BFG} \cdot C_{BFG}) (1+M) \quad (3.14)$$

in which

T = Total operating working minutes = $365 \times 60 \times 24$ min/year

E = Average unit efficiency = 50%

M = Percentage running cost increase due to maintenance = 5%

V_{COG} , V_{BFG} = Coke oven gas and blast furnace gas volume flow rate (cfm), respectively. They are functions of x_{fuel} and V_{air} as shown in Equations D-49 and D-50.

C_{COG}^\dagger = Rate of coke oven gas estimated cost per gas volume = 0.586×10^{-3} dollars/ft³

C_{BFG} = Rate of blast furnace gas estimated cost per gas volume = 0.109×10^{-3} dollars/ft³.

Employing the previous specifications and equations (3-11 through 3.14) in the present value average cost expression

[†] C_{COG} and C_{BFG} are based on the estimated natural gas cost of 0.004 \$/kw hr. Hence, the ratio of COG and BFG calorific values to that of the natural gas are 500:1000 and 93:1000 (BTU/cf), respectively. Therefore, COG and BFG costs would have the same relative ratios.

described in Appendix A, the present value average cost for both the recuperator and the duct work could be evaluated to form the master sub-system optimization criterion. Adding to that the empirical equation, which represents the fan present value average cost, the whole system optimization criterion will be formed as indicated in Equation (3.10). The fan present value average cost is a function of the joining specifications, H , and Q , as shown in the trade-off surface Figure 2.21.

The master sub-system set of constraints can be divided into two sections, direct constraints on design variables and state variables constraints. The recuperator width, side, and height length are limited by the maximum available space.

$$\phi_1 = W_{\max} - W \geq 0.0 \quad (3.15)$$

$$\phi_2 = B_{\max} - B \geq 0.0 \quad (3.16)$$

$$\phi_3 = L_{\max} - (L_I + L_{II}) \geq 0.0 \quad (3.17)$$

Width and side lengths have also to be constrained by a minimum limit values which depending on the minimum practical number of tubes, N_{\min} .

$$\phi_4 = W - d_0 A N_{\min} \geq 0.0 \quad (3.18)$$

$$\phi_5 = B - d_0 A N_{\min} \geq 0.0 \quad (3.19)$$

Recuperator tube thickness must be positive and greater than a minimum practical relative thickness to tube diameter, t_{\min} .

$$\phi_6 = (d_0 - d_i) / d_0 \frac{t_{\min}}{t_{\min}} \geq 0.0 \quad (3.20)$$

The recuperator tube spacing ratio has to be positive and greater than a minimum limit, A_{\min} .

$$\phi_7 = A - A_{\min} \quad (3.21)$$

The volumetric Coke Oven Gas ratio to total fuel gas mixture must be less than one.

$$\phi_8 = 1.0 - x_{\text{fuel}} \quad (3.22)$$

By using the preceding specifications and design variables as an input vector for the design procedures of the two-pass overall-counterflow recuperator described in Appendix C, the preheated air outlet temperature, t_{air} , and the hot gases outlet temperature to the stack, t_{st} , can be determined. Total pressure drop across the system ΔP_{Total} can be evaluated as follows:

$$\Delta P_{\text{Total}} = \Delta P_{\text{rec}} + \Delta P_{\text{duct}} + \Delta P_{\text{noz}} - \Delta P_{\text{st}} \quad (3.23)$$

where, ΔP_{rec} is the total pressure drop inside the ceramic recuperator as described in detail in Appendix C. ΔP_{duct} is the sum of the pressure drops in the duct connecting the fan with the recuperator, ΔP_{D_1} in the duct connecting the recuperator with the soaking pit, ΔP_{D_2} in the preheated

air line, and ΔP_{D_3} in the duct between the recuperator and the stack. They can be evaluated as following:

$$\Delta P_{D_1} = f_t \frac{L_i}{d_D} \frac{(4V_i/\pi d_D^2)^2}{2(32.22)} \rho_i, \quad (i=1,2,3) \quad (3.24)$$

where, f_t is the ducts friction factor. It is given in Appendix D, Section 4. V_1 , V_2 , and V_3 are the fan, preheated air and stack volume flow rates. Fan and stack volume flow rates are computed in Appendix D, Section 9. ρ_1 and ρ_2 are the air density at the ambient and preheated air temperatures, respectively. While ρ_3 is the hot product of combustion gas density at inlet stack temperature. The head loss in the soaking pit preheated air nozzle, ΔP_{noz} , could be evaluated as follows

$$\Delta P_{noz} = K_{noz} \frac{(4 V_{air}/\pi d_D^2)^2}{2(32.22)} \quad (3.25)$$

where, K_{noz} is the nozzle head loss coefficient, taken as 1/2, and ρ is the preheated air density. ΔP_{st} is the natural draft of the stack as described in Appendix D, Section 10.

The following constraints are related to state variables. The preheated air temperature, t_{air} , has to be greater than the inlet air ambient temperature, t_{amb} .

$$\phi_9 = t_{air} - t_{amb} \geq 0.0 \quad (3.26)$$

The hot gas outlet temperature, t_{st} , must be less than the hot gas inlet temperature, t_{gas} , and greater than a minimum specified limit, t_{min} , to prevent condensation.

$$\phi_{10} = t_{gas} - t_{st} \geq 0.0 \quad (3.27)$$

$$\phi_{11} = t_{st} - t_{min} \geq 0.0 \quad (3.28)$$

The hot gas temperature drop must exceed the air temperature rise.

$$\phi_{12} = 1 - (t_{air} - t_{amb}) / (t_{gas} - t_{st}) \quad (3.29)$$

The axial flow fan head rise, H must be greater than the total pressure drop across the system, ΔP_{total} .

$$\phi_{13} = 5.204 H - \Delta P_{total} \geq 0.0 \quad (3.30)$$

The total heat flux into the soaking pit, Q_{sp} , generated from the heating value of the mixed fuel, COG and BFG and from the recuperated air must exceed the minimum specified heat flux, Q_{sp}^* .

$$\phi_{14} = Q_{sp} - Q_{sp}^* \geq 0.0 \quad (3.31)$$

where Q_{sp} = total heat into soaking pit
 = heating value of mixed fuel + heat from preheated air.

$$= (V_{\text{COG}}[CV_{\text{COG}}] + V_{\text{BFG}}[CV_{\text{BFG}}]) + (t_{\text{air}} - t_{\text{amb}}) C_{p_{\text{air}}} \rho \cdot V_{\text{air}} \quad (3.32)$$

V_{COG} and V_{BFG} are the coke oven gas and blast furnace gas volume flow rates as computed in Equation D-49 and D-50. CV_{COG} and CV_{BFG} are the calorific values for both COG and BFG [500 and 93 (BTU/scf)]. $C_{p_{\text{air}}}$ is the air specific heat, equation D-13.

Finally the adiabatic flame temperature AFT cannot exceed a specified maximum temperature, $AFT|_{\text{max}}$, otherwise the radiant heat transfer would increase beyond the limit imposed by the steel ingot surface temperature gradient, and the ingots would melt.

$$\phi_{15} = AFT|_{\text{max}} - AFT \geq 0.0 \quad (3.33)$$

$$\text{where, } AFT = t_{\text{amb}} + Q_{\text{sp}} / [(C_{p^{\circ}} V)_{\text{COG}} + (C_{p^{\circ}} V)_{\text{BFG}}] \quad (3.34)$$

The design procedure for determining the pressure drop and the outlet temperatures of the working gases is an iterative process and requires long computation time. Therefore, during the search, for optimum the recuperator design procedure will not be carried out if one or more of the direct design variable constraints ($\phi_1, \phi_2, \dots, \phi_8$) are violated.

3.4 Results

For the previously described decomposed system, and by using 'OPTISEP' optimization subroutines package [27], the ensuing optimum system design was found.

W	=	Recuperator width	=	7.60 ft
B	=	Recuperator side length	=	7.37 ft
L _I	=	Recuperator first pass height	=	2.97 ft
L _{II}	=	Recuperator second pass height	=	2.98 ft
d _o	=	Recuperator tube outside diameter	=	0.3966 ft
d _i	=	Recuperator tube inside diameter	=	0.3491 ft
A	=	Recuperator tube spacing ratio	=	1:213
d _D	=	Mean ducts inside diameter	=	0.844 ft
V _{air}	=	Q = Preheated air volume flow rate	=	4773 cfm
V _{Fan}	=	Fan air volume flow rate	=	7275 cfm
V _{COG}	=	Coke Oven Gas volume flow rate	=	345 cfm
V _{BFG}	=	Blast Furnace Gas volume flow rate	=	3764 cfm
V _{st}	=	Hot gases passing through the stack volume flow rate	=	9412 cfm

V_{POC}	=	Product of combustion volume flow rate	=	8168 cfm
t_{Air}^+	=	Preheated air temperature	=	1328 ⁰ F
t_{st}	=	Hot gases outlet temperature	=	828 ⁰ F
N_T	=	Total number of the recuperator tubes	=	421 tubes (15 x 15)
H	=	Fan total head rise	=	5.8 in. water
(P.V.A.C.) _T	=	Total system present value average cost	=	10.5x10 ⁴ dollars.
AFT _g	=	Adiabatic flame temperature	=	3290 ⁰ F
LMT	=	Recuperator logarithmic mean temperature	=	884.5 ⁰ F

After determining the master subsystem optimum design variables, the optimum ducted axial flow fan design can be precisely determined. A design point for the fan corresponding to the final solution for the master sub-system will not exist at this stage, any discrete variables are also properly discretized. The fan optimum design for 5.8 in. water head rise and 4773 cfm air volume flow rate is given in Chapter 2. It should be emphasized here that these specification values, being the two sub-systems together, are optimum choices

First pass hot gases outlet temperature = 1627⁰F
 First pass air inlet temperature = 652⁰F

for the specifications, any deviation from these will yield a more expensive combined system.

The example of this thesis could be extended to obtain trade-off curves and surfaces for the whole system by relaxing its hard specifications, (minimum soaking pit's heat input, hot gases' stack specifications, duct work lengths, fuel properties, and so on). The relative effect of the system specifications on the objective criterion could then be detected and examined to gain more insight and understanding of the larger system design.

3.5 Conclusions

The following conclusions may be drawn concerning the proposed new decomposition algorithm.

1. The generalized model proposed through the implementation of the described algorithm is believed to be a simple, powerful, fast and efficient way of handling many of the large system problems that the design engineer must face, which either were impossible to solve or needed tedious, long, and complicated mathematical computation.
2. The overall large system, which is to be optimally designed, must be in a form that can be decomposed into a master sub-system and a set of minor sub-systems as described in Figure 3.1.

3. One or more of the minor sub-systems could be selected from a catalog of commercial equipment. In this event it may be possible to develop trade-off curves from information provided by the manufacturers--such as cost versus power for an electric motor. Consequently, the overall system optimum design could still be found by following the prescribed decomposition algorithm.
4. The decomposed overall large system might be governed or constrained by already existing components (the soaking pit furnace, the stack). They can be treated as applied input specifications (hard or soft).
5. A trade-off curve is the locus of all the optimum design points for a given configuration, i.e. each point on a trade-off curve, surface, or hypersurface is an optimum point. If we assume that the fitted empirical equation represents the trade-off surface with a reasonable variance (within the sub-system accuracy range), then the optimization of the master sub-system, in which all the empirical trade-off expressions are combined with the master sub-system optimization criteria, will converge into a limiting optimum solution. It should be noted however, that this limiting solution cannot be guaranteed to be the optimal global solution to the original system. This implies that convergence to a true optimum solution for the original system before decomposition, will be extremely difficult, if not impossible to analytically

ascertain.

6. The non-linear empirical equation, which fits the trade-off surface, must cover all of the feasible ranges of the specifications being varied. However, it might happen during the optimization process of the master sub-system that one of the joint specifications, (master sub-system design variables), is assigned values outside the range of the empirical trade-off equations. Therefore it may be desirable to include a large positive number as a final point at the end of the range of the trade-off curve. This is equivalent to an additional set of direct constraints on the joint specifications.
7. No coupling constraints among the partitioned system components (sub-systems) are assumed. Thus, the two-pass counterflow recuperator could not be partitioned into two sub-systems of one pass each, since due to the nature of the problem, there will be constraints governing both sub-systems and also their joint specifications (intermediate temperatures, design configuration, flow rates).
8. Although it was mentioned earlier that all the minor sub-systems and the master sub-system must have the same optimization criterion, this presents no particular problem when maximum overall system "value" is used as an

optimization criterion [1].

9. The block angular structure described in Figure 3.1 is not engraved in stone. In an extreme case we might have to decompose a system into several block-angular structures governed by a major master sub-system.

CHAPTER 4DISCUSSION and RECOMMENDATION4.1 Evaluations and Conclusions

This thesis provides a technique for analyzing and decomposing the optimum design problem of large systems. The term decomposing, is used here to mean an algorithm which partitions the design variables of a problem into two or more sub-sets. The partitioning to be used is, for the problems considered here, determined in an obvious way by the problem structure. Some definite structure is almost always found in truly large problems, since they commonly arise from a linking of independent minor sub-systems, in either time or space, by a set of design specifications, with a master sub-system which governs all the joint specifications. By developing specialized solution algorithm to take advantage of this structure, significant gains in computational efficiency and reductions in computer memory requirements may be achieved. The technique produces a way of displaying graphically and numerically the trade offs between each minor sub-system design objective and the sub-system joint design specifications. The resulting trade-off curves, surface or hypersurface of each of the system minor sub-systems must be combined with the system master sub-system optimum design which in turn leads to

the whole system optimum design.

This thesis also demonstrates the relative ease with which the trade-off curves can be determined and their values as a design tool in ways other than their use in a decomposed system. A new contribution has been achieved by the author in developing a nonlinear multi-variable fitting model to represent a trade-off hypersurface, discussed in Appendix E. Trade-off curves have been categorized into two types, Type A and Type B, based on the effect of relaxing the design's specification over the design's objective. One of the major advantages of trade-off curves is the insight that they provide to the designer; insight into the overall design problem, insight into improvements which can be gained by relaxing a hard specifications, and insight into the feasible bounds of the problem.

To illustrate the shape, potential and advantages of the trade-off surfaces, two design problems were investigated, a high pressure vessel with multiple walls and an axial ducted flow fan. In both cases, further insight into the selection of an optimum design was gained. Application of trade-off curves to decomposition is illustrated by a numerical design example of two pass counterflow ceramic recuperator.

In order to optimize the combined sub-systems their optimization criteria must be the same. In the event that they have different objectives, or multiple objectives, value

theory could be used to set up a single combined and common optimization criterion.

4.2 Future Research

There are several possibilities for future research. The overall effectiveness of the decomposition method described above, using a trade-off technique, lies in being able to generate sets of optimum points for different combinations of the relaxed specifications, and in creating an empirical formula to represent the trade-off hypersurface quickly, simply and with reasonable accuracy. Therefore, there is a need to develop a package which is capable of handling multi-dimensional trade-off surfaces. In the area of applications, work is needed to investigate ways of using the decomposed angular block system for problems with many minor sub-systems with different objectives. Work is also needed in the development of procedures which will determine quantitatively with the help of computer, graphical value curves associated with each of the objectives.

REFERENCES

1. Siddall, J.N., Analytical Decision-Making in Engineering Design, Prentice-Hall, 1972.
2. Fox, R.L., Optimization Methods For Engineering Design, Addison-Wesley, 1971.
3. Siddall, J.N., "An Orderly Approach to Design Decisions", ASME Paper No. 76-DE-12.
4. Bayoumi, S.E., "Mechanics of Deformable Solids", Part II, Faculty of Engineering, Cairo University, 1971.
5. Daniel, C., and Wood, F.S., Fitting Equations to Data, Wiley-Inter-science, 1971.
6. Woods, D.R., Financial Decision Making in the Process Industry, Prentice-Hall, 1975.
7. Bartel, D.L., and Marks, R.W., "The Optimum Design of Mechanical Systems With Competing Design Objectives", ASME, Paper No. 73-DET-11.
8. Faupel, J.H., Engineering Design, John Wiley and Sons, 1964.
9. Wallis, R.A., Axial Flow Fans Design and Practice, George Newnes, 1961.
10. Buffa, S.E., Modern Production Management, John Wiley and Sons, 1969.

11. Siddall, J.N., "Special Notes For Theory of Design", McMaster University, 1974.
12. Conte, S.D., and Boor, C., Elementary Numerical Analysis, McGraw Hill, 1972.
13. Dokainish, M.A. and Mansour, W.M., "On the Design of Air-Cooled Radial Turbine Blades", Symposium on Applications of Solid Mechanics, University of Waterloo, June 1972.
14. Carter, A.D. and Cohen, E.M. "Preliminary investigation into the three dimensional flow through a cascade of aerofoils", Aero. Res. Council, 1946.
- 15.. Woods, D.R. and Anderson, S.J., "Evaluation of capital cost data: Drives", The Canadian Journal of Chemical Engineering, vol. 53, August, 1975.
16. Woods, D.R., "Use of Cost Correlation Data", Department of Chemical Engineering, McMaster University, Hamilton, 1975.
17. Giedt, W.H., Principles of Engineering Heat Transfer, Van Nostrand East West Press, 1961.
18. Mikheyev, M., Fundamentals of Heat Transfer, Peace Publishers, Moscow.
19. Bird, R.B., Stewart, W.E., and Lightfoot, E.N., Transport Phenomena, John Wiley and Sons, 1960.
20. Sucec, J., Heat Transfer, Simon and Schuster, 1975.
21. Streeter, V.L., and Wylie, E.B., Fluid Mechanics, McGraw-Hill, 1964.

22. Van Wylen, G.J., and Sonntag, R.E., Fundamentals of Classical Thermodynamics, John Wiley and Sons, 1973.
23. Kays, W.M., and London, A.L. Compact Heat Exchangers, McGraw-Hill, 1964.
24. Latto, B., and Innes, S., Energy Conservation in Soaking Pits, McMaster report No. ME-76-FM-R19, 1976.
25. Wood, D.J., "An Explicit Friction Factor Relationship", Civ. Eng., Dec. 1966, pp. 60, 61.
26. Eckert, E.R.G., and Drake, R.M., Analysis of Heat and Mass Transfer, McGraw Hill, 1972.
27. Siddall, J.N., 'OPTISEP' Designers' Optimization Sub-routines, Part 1 and 2, Faculty of Engineering, McMaster University, Canada, 1974.
28. Holman, J.P., Heat Transfer, McGraw-Hill, 1963.
29. Landron, L.S., "Optimization Theory for Large Systems", The Macmillan Company, N.Y. 1970.
30. Himmelblau, D.M., "Process Analysis by Statistical Methods", John Wiley and Sons, Inc., 1970.
31. Woods, D.R., Anderson, S.J., and Norman, S.L., "Evaluation of Capital Cost Data: Heat Exchangers", Department of Chemical Engineering, McMaster University, December 1975.
32. Perry's J.H., Chemical Engineers' Handbook, McGraw Hill, Chemical Engineering Series; 1969.

A P P E N D I C E S

7

APPENDIX "A"
COST OR PROFIT AS AN
OPTIMIZATION CRITERION

Optimization criteria are, strictly speaking, based on design characteristics which contribute to the philosophical value (as opposed to monetary value) of the device or system. In some situations, the criterion may be a rather complex combination of purely monetary values, or design characteristics that may be all measured in dollars or other monetary units. A typical example is when we wish to minimize capital cost, and also minimize running cost, where each occurs at different times, [6, 10 & 11].

A.1 Time Value of Assets: Depreciation

Fixed assets can increase or decrease in value as time progresses. Four different methods are commonly used to represent the rate of depreciation. These are straight line declining balance, sinking fund and sum of the year's digits as shown in Figure A.1. However, according to the tax regulations concerning depreciation in Canada the double declining balance method must be used, [6].

We must begin by defining the following quantities.

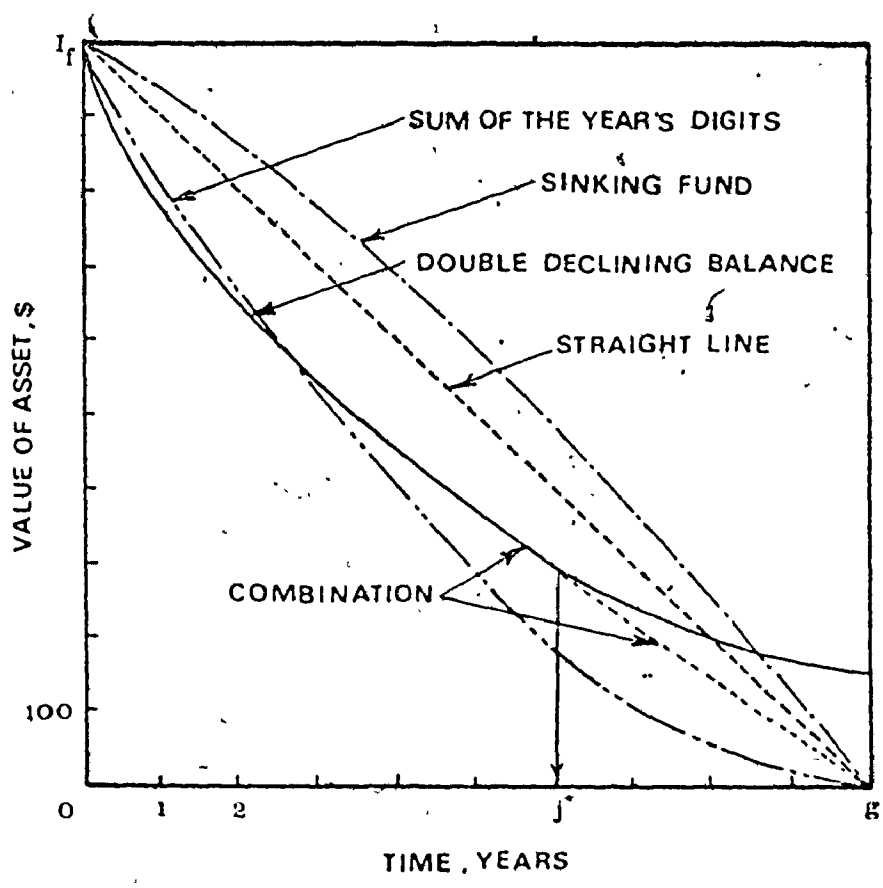


Figure A.1: Changes in Asset Value With Time for Different Methods of Depreciation.

D_j = annual amount of depreciation in the j^{th} year, dollars.

I_F = initial fixed capital investment in the asset, dollars.

e_j = book rate depreciation in the j^{th} year

V_S = scrap value, dollars.

g = economic, design or book life of the asset, years

i = interest rate per period with no risk.

We can now write.

$$D_j = e_j I_F \quad (\text{A.1})$$

$$e_j = \frac{2}{g} \left(1 - \frac{2}{g}\right)^{j-1}, \quad j = 1, 2, \dots, (j^* - 1) \quad (\text{A.2})$$

where,

$$j^* = (2g + \cos(\pi/g) + 7)/4 \quad (\text{A.3})$$

and,

$$e_j = \left(1 - \frac{2}{g}\right)^{J^* - 1} / (g - j^* + 1), \quad j = j^*, J^*, \dots, g \quad (\text{A.4})$$

This approach is applicable when $V_S = 0$. To force the scrap value to zero at the end of the g^{th} year, straight line depreciation (equation A.4) is used in the latter years with the economic life starting from J^* year, while the double declining balance method (equation A.2) is used during the first years until $(J^* - 1)$.

A.2 Present Value Average Cost

In reality, the annual sales and running costs are not constant, and the variations can be represented on a cash position diagram (Figure A.2). The principle is that each element of the diagram is replaced by its present value so that the complete diagram is the net sum of the present values of the elements, [6].

We must define the following quantities first:

$d_j I_F$ = annual depreciation for taxation purpose based on rate d in the j^{th} year, dollars.

t = annual tax rate to be applied to the annual gross profits with the allowable annual depreciation, $d_j I_F$.

P = annual net profit after tax plus book depreciation $e I_F$, dollars.

P^* = annual gross profit before tax plus book depreciation $e I_F$, dollars.

i_m = interest rate with risk.

y = tax life, years. (usually greater than g)

The present value cost can be expressed as follows

$$\begin{aligned}
 P.V. &= \text{net return} - \text{capital expenditure} + \text{terminal recovery.} \\
 &= \sum_{k=1}^{k=g} \frac{P^*(1-t)}{(1+i)^k} + \sum_{k=1}^{k=y} \frac{d_k I_F t}{(1+i)^k} - I_F + (P.W.F.) \\
 &\quad (i_m - i) I_F + (P.S.F.) (1-t) V_S \qquad (A.5)
 \end{aligned}$$

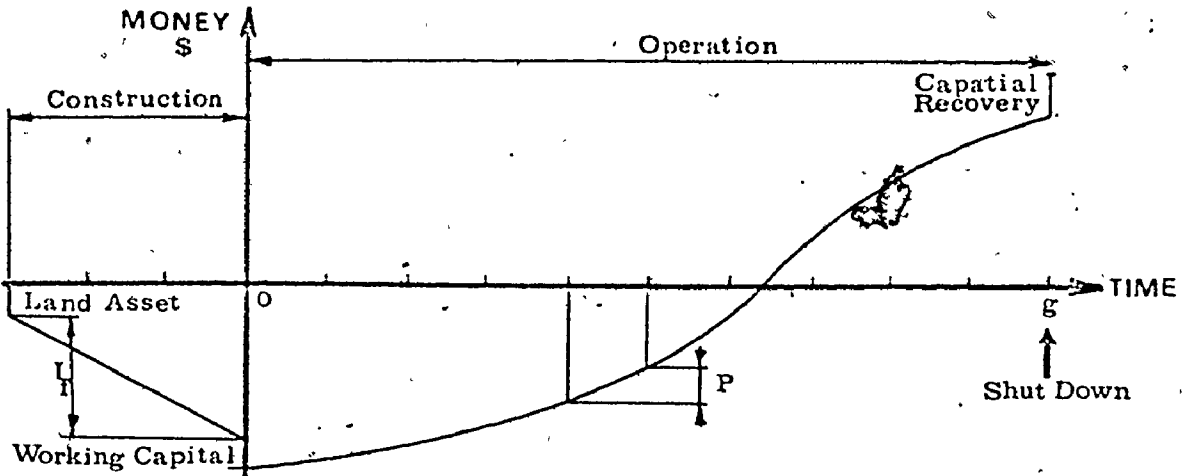


Figure A.2. Cash Position Diagram.

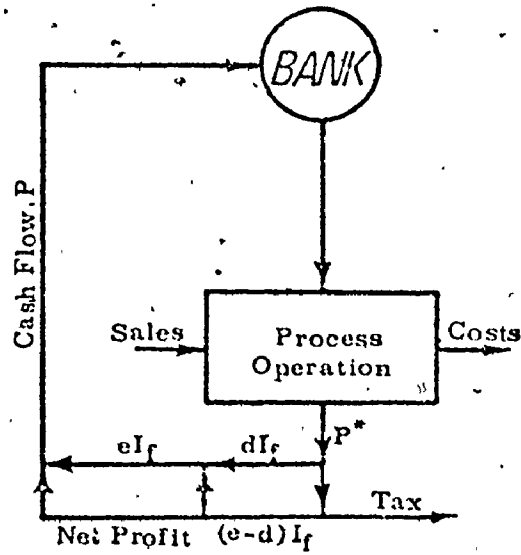


Figure A.3. Cash Flow Diagram.

Where, P.W.F. is the present worth factor

$$= ((1+i)^g - 1) / i(1+i)^g \quad (A.6)$$

and P.S.F is the single payment of P.W.F.

$$= 1 / ((1+i)^g) \quad (A.7)$$

Therefore, Present Value Average Cost

$$= P.V.A.C. = P.V. / g \quad (A.8)$$

An instantaneous cash flow diagram for a single project shows the net passage of dollars into or out of a system as a result of operations, Figure (A.3).

By this way we can combine different monetary values, which occur at different times (I_p and P^*) for different systems by combining their P.V.A.C. This might be considered as an optimization criteria for a maximum profit or minimum cost objective design problems.

APPENDIX "B"
DESIGN PROCEDURES
FOR AN
AXIAL FLOW DUCT FAN

There are two principle methods of designing for ducted acial flow fans, "free vortex flow" and "arbitrary vortex flow" [9]. The following design steps will use the arbitrary vortex flow approach, where simplifying assumptions based on experimental evidence are employed. Figure (B.1) shows the components of the ducted fan unit in question.

The following procedures predict a given fan performance when the following quantities are input.

Q ,	air volume flow rate, ft^3/min .
H ,	unit total head rise, in. of water.
R & r_b ,	duct and boss radii, respectively, in.
RPM,	motor revolutions per minute
N_R & N_S ,	number of rotor and straightener blades respectively.
r_{uR} & r_{uS} ,	radial position at which axial velocity $u(r)$ equals mean axial velocity \bar{u} for the rotor and straightener blades, respectively, in.
t_R & t_S ,	maximum rotor and straightener blades thickness at the boss radius, respectively, in.

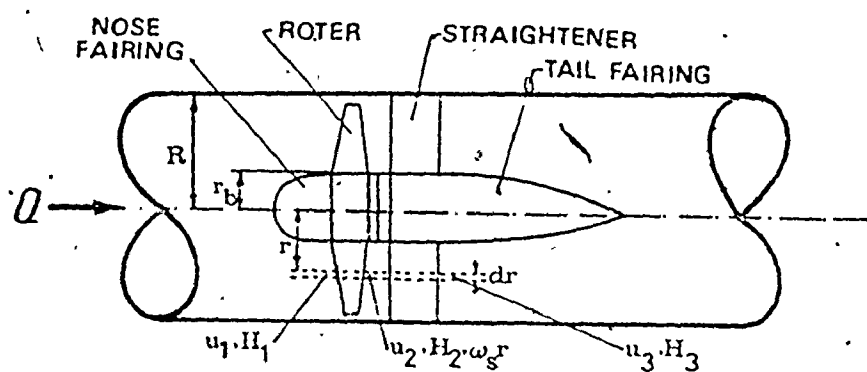


Figure B.1. Components of Ducted Fan Unit.

Employing the previous specifications and data with the following design procedures the chord, span, radius of curvature and camber angle for both the rotor and straightner blades can be computed, leading to a full definition of the blades section at any radial position. It is also possible to determine the lift, drag and centrifugal forces at any radial section to estimate the combined stresses. The total unit efficiency and therefore the specified motor horsepower are finally computed.

Design Procedure and Assumptions:

(1) We assume that the total head rise and the axial velocity component (u) remain constant along the blade length.

$$\text{Mean axial velocity, } \bar{u} = 144 \times Q / \{60 \times \pi (R^2 - r_b^2)\} \text{ ft/sec} \quad (\text{B.1})$$

$$\text{Rotor rotational speed, } \Omega = 2\pi \text{RPM} / 60 \text{ rad/sec} \quad (\text{B.2})$$

Let, Dimensionless radial position,

$$\beta = r/R, \quad r_b \leq r \leq R \quad (\text{B.3})$$

$$\beta_b \leq \beta \leq 1$$

$$\text{Mean Flow coefficient, } \bar{A} = 12 \times \bar{u} / \Omega R \quad (\text{B.4})$$

(2) The overall unit efficiency (η_T) must have an assumed value between (0.65 - 0.95) in order to be readjusted by fixed point iteration [12], when the actual efficiency (η_T^*) is found at step number (13) below.

The non dimensional mean total head rise is given by

$$K_{th} = 5.204 \times \Delta H / (0.5 \rho \bar{u}^2 \eta_T) \quad (B.5)$$

(3) Radial equilibrium is assumed to be established very quickly downstream of each blade row. The velocity heads associated with the small radial flows have been ignored as being of second order magnitude. Bernoulli's equation is applied before and after the fan rotor, where the axial velocity component is a variable in both the radial and axial directions. Since the flow parameters at station r_{uR} are known in detail, this radial position is chosen as an integration limit. Defining first the following non-dimensional quantities

Mean total swirl coefficient for the rotor

$$\bar{\epsilon} = \frac{\omega r_{\bar{u}}}{\bar{u}} = \frac{K_{th} \bar{\lambda}}{2\beta \bar{u}} \quad (B.6)$$

Preliminary flow coefficient

$$\bar{\lambda}(\beta) = \frac{\bar{\lambda}}{\beta} \quad (B.7)$$

where $\beta_{\bar{u}} = r_{\bar{u}}/R$, $\beta = r/R$

However, the swirl coefficient and the flow coefficient are both assumed to be linear function of r . As a preliminary design step it is more convenient to use \bar{u} since the distributions of the axial velocity at the different sections are

initially unknown. A bar is then placed over the coefficients to denote that the mean velocity has been used. Therefore, the axial velocity component at any radial section in the fan annulus at section 2 and 3, as shown in Figure B.1., can be determined approximately by

$$u_2(\beta) = \bar{u} \sqrt{1 + 2\bar{\epsilon}^2} \left\{ \frac{1}{\bar{\epsilon} \bar{\lambda}(\beta)} - \frac{1}{\bar{\epsilon} \bar{\lambda}(\beta \bar{u})} - \ln \beta + \ln \beta \bar{u} \right\} \quad (\text{B.8})$$

$$u_3(\beta) = \bar{u} \sqrt{1 + 2\bar{\epsilon}^2} \left\{ \frac{1}{\bar{\lambda}(\beta)} - \frac{1}{\bar{\lambda}(\beta \bar{u})} \right\} \quad (\text{B.9})$$

(4) The rotor and straightener blades are divided into m radial strips. For each, the radial velocities $u_2(\beta)$ and $u_3(\beta)$ are assumed to be constant along the blade's span.

(5) Flow and swirl coefficients can be approximated by better values, after knowing the velocity distribution in both rotor and straightener, as follows:

$$\lambda_R(\beta) = \frac{u_2(\beta)}{2\bar{u}} + .5 \frac{\bar{\lambda}}{\beta} \quad (\text{B.10})$$

$$\lambda_S(\beta) = \left(\frac{u_2(\beta) + u_3(\beta)}{2\bar{u}} \right) \frac{\bar{\lambda}}{\beta} \quad (\text{B.11})$$

$$\epsilon_R(\beta) = 2\bar{u} \bar{\epsilon} / (u_2(\beta) + \bar{u}) \quad (\text{B.12})$$

$$\epsilon_S(\beta) = 2\bar{u} \bar{\epsilon} / (\bar{u}_2(\beta) + u_3(\beta)) \quad (B.13)$$

(6) The angle which relative velocity (w_r) makes with plane of rotation for the rotor blade at different radii, as shown in figure (B.2), can be easily calculated from: <

$$\phi_R(\beta) = \tan^{-1}[\lambda_R(\beta) / (1 - .5\epsilon_R(\beta) \lambda_R(\beta))] \quad (B.14)$$

For the straightener blade

$$\phi_S(\beta) = \tan^{-1}[2./\epsilon_S(\beta)] \quad (B.15)$$

(7) The optimum lift coefficient can be obtained from use of the Howell relationship [14] as follows for rotor blades

$$C_{L_R}^*(\beta) = 2 \left[\left\{ 1 + \left(\frac{1 - \epsilon_R(\beta) \lambda_R(\beta)}{\lambda_R(\beta)} \right)^2 \right\} / \left\{ 1 + \frac{1}{\lambda_R^2(\beta)} \right\} \right]^{1.375} \quad (B.16)$$

The optimum lift coefficient based on experimental data [9] can be written approximately for straightener blades as follows:

$$\begin{aligned} C_{L_S}^*(\beta) &= 1.43 \epsilon_S(\beta) \quad \text{for } \epsilon_S(\beta) \leq 0.5 \\ &= 2.18 - 1.43 \epsilon_S(\beta) \quad \text{for } \epsilon_S(\beta) < 0.5 \end{aligned} \quad (B.17)$$

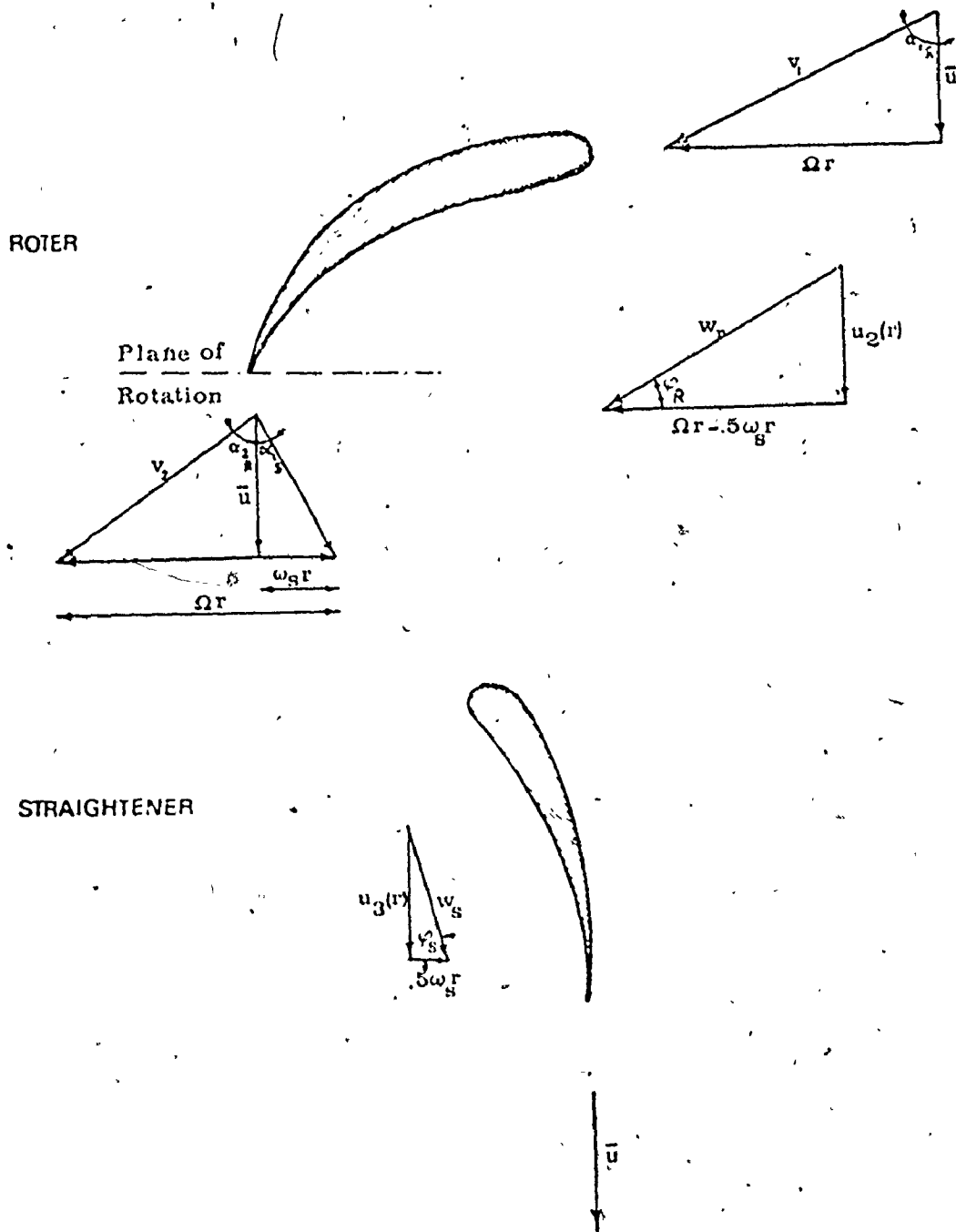


Figure B.2. Velocity Vectors for Rotor and Straightener Blade Element.

(8) The solidity $\sigma(\beta)$ at any radial station can be derived from momentum considerations. Ignoring the drag term, $(\sigma(\beta)C_D \cot \phi(\beta))$ which is usually small, we can write rotor and straightener solidity terms as follows

$$\sigma_R(\beta) = [2\epsilon_R(\beta) \cdot \sin \phi_R(\beta)] / C_{L_R}^*(\beta) \quad (B.18)$$

$$\begin{aligned} 1/\sigma_S(\beta) &= [2\epsilon_S(\beta) \cdot \sin \phi_S(\beta)] / C_{L_S}^*(\beta), \text{ for } \epsilon_S(\beta) > .5 \\ &= 1.5, \text{ for } \epsilon_S(\beta) \leq .5 \end{aligned} \quad (B.19)$$

(9) Hence, solidity is the chord[†] length by the span^{**} length at any radial section.

Therefore, the chord lengths of the rotor and straightener are:

$$C_R(\beta) = \sigma_R(\beta) \frac{2\pi R\beta}{N_R} \quad (B.20)$$

$$C_S(\beta) = \sigma_S(\beta) \frac{2\pi R\beta}{N_S} \quad (B.21)$$

(10) From the force vector diagram, Figure B.3, the lift L_R , for rotor blade element may be expressed at any radial section as follows:

†Chord: is the length of the straight line which joins the extreme leading and trailing edges of the airfoil in a streamwise direction.

**Span: is the length of the airfoil in a direction perpendicular to the chord line.

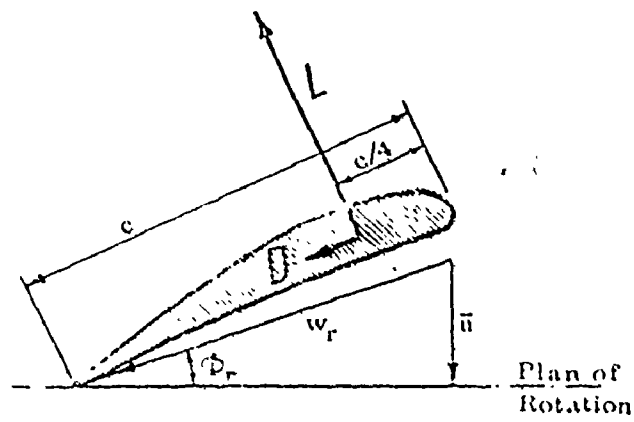


Figure B.3. Force Vector Diagram for Rotor Blade Element.

$$L_R(\beta) = C_{L_R}^*(\beta) \frac{\rho}{2} C_R(\beta) \left(\frac{u_2(\beta)}{\sin\phi_R(\beta)} \right)^2 \frac{d_r}{144} \quad (\text{Lb})$$

(B.22)

where, d_r , is the strip thickness and, ρ , is the air density.

The straightener lift force is given by

$$L_S(\beta) = C_{L_S}^*(\beta) \frac{\rho}{2} C_S(\beta) \left(\frac{u_3(\beta)}{\sin\phi_S(\beta)} \right)^2 \frac{d_r}{144} \quad (\text{Lb}) \quad (\text{B.23})$$

(11) Consideration can now be given to the blade element. However, it is apparent that no single design method can cover the entire range of ducted axial flow fans. Multi-plane interference prevents the use of the "isolated aerofoil design method", for solidities much above unity, while the "cascade design method" cannot be used for solidities much less than 2/3. The problem which arises, therefore, is the fixing of a nominal boundary between the two methods. Detailed experiments [14] on a fan designed by the isolated airfoil method showed appreciable discrepancies for boss ratio greater than 0.5. The cascade method is preferable for values of greater than 0.8, otherwise ϕ_r may exceed 40° and loss of lift may result. The above recommendations apply to a specific blade element. When the rotor as a whole is considered, modifications may be necessary. A combination of the above two methods, especially with a moderate boss ratio of 0.5, is also

possible. Rotors designed entirely by the cascade method tend to be high pressure rise fans with large boss ratios. The main variables involved in determining the blade shape are given in Figure B.4. After developing the circular arc type camber line, it is subsequently clothed with a symmetrical aerofoil section whose chord line is bent around the camber line [9]. Figure B.5 gives the important details of the main parameters involved in designing a circular arc camber straightener airfoil using the cascade method which is preferable for the straightener design when the value of ϵ_s exceeds 0.4. Lastly, the detailed design of both rotor and straightener blades can be considered as a final step in the whole design procedure where the specific optimum specifications were determined.

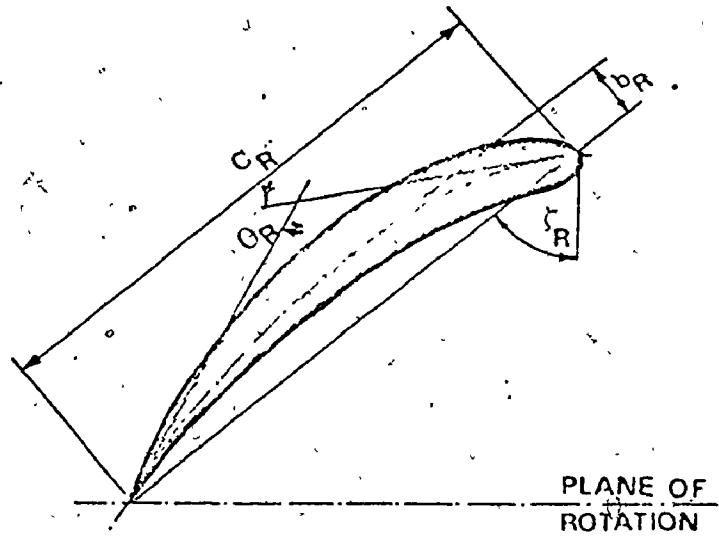
(12) Steps (4) to (11) have to be evaluated for each radial position along blade length, i.e. $(m+1)$ times.

(13) Overall fan unit efficiency can now be calculated as follows

$$\eta_T^* = 1 - \frac{K_R}{K_{th}} + \frac{K_S}{K_{th}} + \frac{K_D}{K_{th}} \quad (B.24)$$

where,

$$\frac{K_R}{K_{th}} = \text{mean combined rotor loss coefficient.}$$



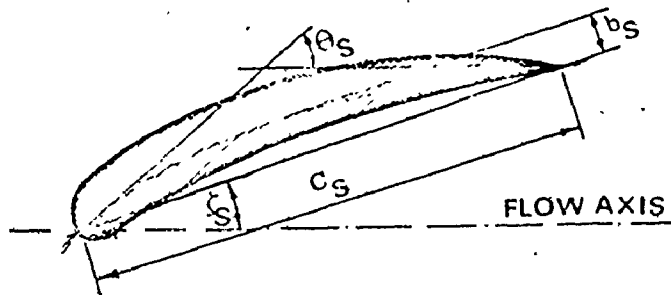
$$\theta = \frac{\tan^{-1}\left\{\frac{1}{\lambda_R}\right\} - \tan^{-1}\left\{\frac{1 - \epsilon_R \lambda_R}{\lambda_R}\right\}}{1 - 0.26\sqrt{1/\sigma_R}}$$

$$b_R = \frac{C_R}{2} \tan\left(\frac{\theta_R}{4}\right)$$

$$\zeta_R = \text{Stagger Angle} = \tan^{-1}\left(\frac{1}{\lambda_R}\right) - \frac{\theta}{2}$$

$$\text{Radius of Curvature} = \frac{C_R}{2 \sin\left(\frac{\theta_R}{2}\right)}$$

Figure B.4. Geometric Details of Rotor Blade Element, Cascade Method.



$$\theta_s = \frac{\tan^{-1} \epsilon_s}{1 - 0.26 \sqrt{1/\sigma_s}}$$

$$b_s = \frac{c_s}{2} \tan \frac{\theta_s}{4}$$

$$\zeta_s = \tan^{-1} \epsilon_s - \frac{\theta_s}{2}$$

$$\text{Radius of Curvature} = \frac{c_s}{2 \sin \left(\frac{\theta_s}{2} \right)}$$

Figure B.5. Geometric Details of Straightener Blade Element, Cascade Method.

$$\frac{K_S}{K_{th}} = \text{mean combined straightener, loss coefficient.}$$

$$\frac{K_D}{K_{th}} = \text{diffusion loss coefficient.}$$

$$\frac{K_R}{K_{th}} = \text{profile + secondary + annulus drag loss, co- efficiencies}$$

$$= \frac{K_{RP}}{K_{th}} + \frac{K_{RS}}{K_{th}} + \frac{K_{RA}}{K_{th}} \quad (\text{B.25})$$

$$\frac{K_{RP}}{K_{th}} = \sum_{i=1}^{m+1} \frac{0.016 \lambda_R(\beta)}{(m+1) C_{LR}(\beta) \sin^2 \phi_R(\beta)} \quad (\text{B.26})$$

$$\frac{K_{RS}}{K_{th}} = \sum_{i=1}^{m+1} \frac{0.018 C_{LR}(\beta) \lambda_R(\beta)}{(m+1) \sin^2 \phi_R(\beta)} \quad (\text{B.27})$$

$$\frac{K_{RA}}{K_{th}} = 0.03 \quad (\text{B.28})$$

$$\frac{K_S}{K_{th}} = \sum_{i=1}^{m+1} \frac{\lambda_S(\beta) [0.025 C_{LS}^2(\beta) + 0.022]}{(m+1) \sin^2 \phi_S(\beta) C_{LS}^*(\beta)} \quad (\text{B.30})$$

$$\frac{K_D}{K_{th}} = \frac{\beta_b^2 (2 - \beta_b^2)}{K_{th}} (1 - \eta_D) \quad (\text{B.31})$$

where η_D = diffuser efficiency
assumed 0.8.

$$(14) \text{ Consumed horsepower} = \frac{5.204 Q \Delta H}{33000 \eta_T^*} \quad (\text{HP})$$

(B.32)

$$\text{Motor power} = \frac{1.343 \text{ HP}}{\eta_m \eta_b} \quad (\text{B.33})$$

where, η_m and η_b are the motor and bearing efficiency, and are assumed to have a value of 0.9.

(15) The rotating shaft cross sectional area has to withstand torque and thrust subjected to it. The shaft applied principal stress $\bar{\sigma}_{sh}$, is calculated as follows assuming that the shaft radius equals the unit boss radius.

$$\bar{\sigma}_{sh} = \frac{\sigma_x}{2} + \sqrt{\left\{\frac{\sigma_x}{2}\right\}^2 + \tau_{xy}^2} \quad \text{psi} \quad (\text{B.34})$$

where, σ_y is neglected.

$$\sigma_x = \text{thrust} / \pi r_b^2 \quad \text{psi} \quad (\text{B.35})$$

$$\tau_{xy} = 12 r_b \times \text{torque} / \text{polar moment of inertia} \quad \text{psi} \quad (\text{B.36})$$

$$I_0 = \text{polar moment of inertia} = 0.5 \pi r_b^4 \quad \text{in.}^4 \quad (\text{B.37})$$

$$\text{Thrust} = T_c \frac{\rho}{2} \bar{u}^2 \frac{R^2}{144} \quad \text{lb.} \quad (\text{B.38})$$

$$T_c = \text{thrust coefficient} = K_{th} \eta_R^* (1 - \beta_b^2) + \frac{K_{th} \bar{V}}{2} \ln(\beta_b)$$

(B.39)

from, (B:25) η_R^* = rotor efficiency = $(1 - K_R/K_{th})$ (B.40)

$$\text{Torque} = Q_c \frac{\rho}{2} \bar{u}^2 \pi \frac{R}{12}^3 \quad (\text{lb.ft}) \quad (\text{B.41})$$

$$Q_c = \text{torque coefficient} = K_{th}^{-1} (1 - x_b^2) \quad (\text{B.42})$$

Substitutions from (B-35, 36....,42) to (B-34) yields the principal stress.

(16) The maximum rotor blades thickness at its root must be big enough to withstand centrifugal, lift and drag forces. Tensile stress due to the centrifugal effect constitutes the major stress component in rotor blades. Bending moments due to aerodynamic load increase the tensile stresses by a small but significant amount. However, shear stresses and torsional moments are negligible. Blades are assumed to have a triangle cross section with a uniform height for all the radial positions, as shown in Figure (B.6). The tensile stress due to centrifugal force, $\bar{\sigma}_{1R}$ can be calculated as follows:

$$\bar{\sigma}_{1R} = \frac{\Omega^2 \rho_m R^2}{(12)^4 g_0 C_R(\beta)_b} \int_1^{B_b} \beta C_R(\beta) d\beta \quad (\text{PSI}) \quad (\text{B.43})$$

where, ρ_m is the blade's material density, lb/ft^3
 g_0 is the acceleration of gravity, ft/sec^2

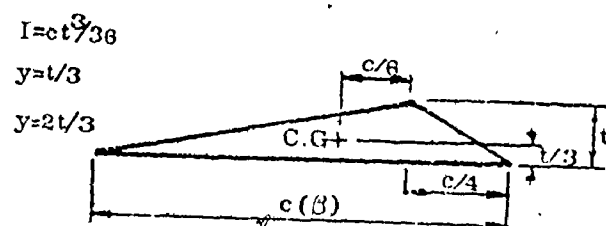


Figure B.6. Assumed Blades Cross Section for Stresses Calculations.

Bending stress due to the lifting force, $\bar{\sigma}_{2R}$, can be computed as follows

$$\bar{\sigma}_{2R}^+ = \frac{My^+}{I} = \frac{12 R}{t_R^2} \sum_{\beta=\beta_b}^{\beta=1} L_R(\beta) \cdot (\beta - \beta_b) / C_R(\beta) \text{ psi} \quad (\text{B.44})$$

$$\bar{\sigma}_{2R}^- = \frac{My^-}{I} = \frac{24 R}{t_R^2} \sum_{\beta=\beta_b}^{\beta=1} L_R(\beta) \cdot (\beta - \beta_b) / C_R(\beta) \text{ psi} \quad (\text{B.45})$$

Hence, the drag force is neglected; the lifting force is concentrated at C/4; and the torsional effect is neglected. Therefore, applied design stress, $\bar{\sigma}_R$, is the maximum between $(\bar{\sigma}_{1R} + \bar{\sigma}_{2R}^+)$ and $(\bar{\sigma}_{1R} - \bar{\sigma}_{2R}^-)$.

(17) The straightener blades, following the previous assumptions, have bending stress due to lifting force as the only active stress, (compression).

$$\bar{\sigma}_S = \frac{24 R}{t_S^2} \sum_{\beta=\beta_b}^{\beta=1} L_S(\beta) (\beta - \beta_b) / C_S(\beta) \text{ (PSI)} \quad (\text{B.46})$$

To summarize, ducted axial flow fan design using the arbitrary vortex flow approach with the isolated airfoil method for blades design was employed to determine the unit efficiency and the required operating power. Furthermore, detailed blades cross sections, at different radial positions were also clearly specified for the input configurations. Finally, the stresses

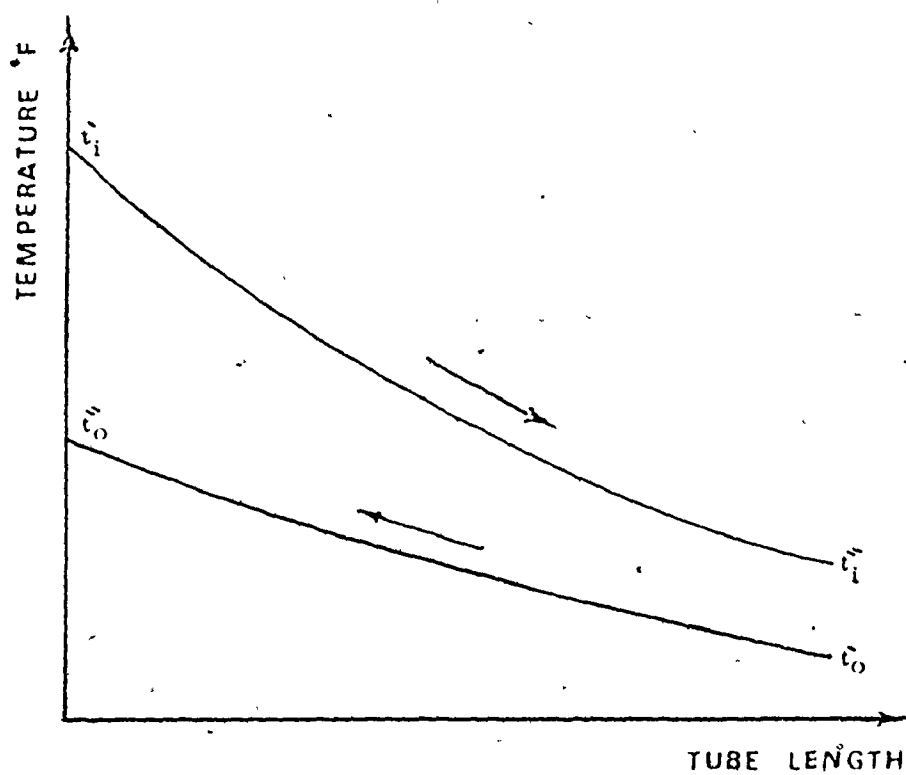
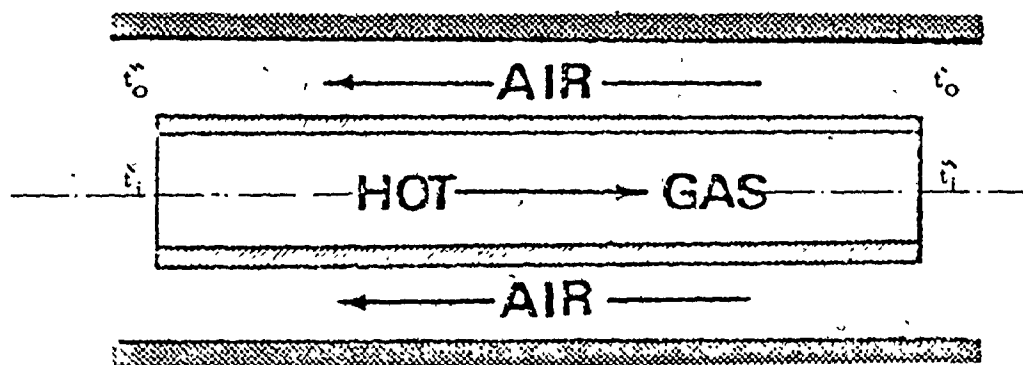
were determined to ensure the feasibility and safety of an assumed material.

APPENDIX C
DESIGN PROCEDURES
OF A
MULTIPASS COUNTERFLOW RECUPERATOR

A recuperator is a gas flow heat exchanger, using a shell and tube configuration. When both gases flow past the heating surface in opposite direction and parallel to each other, the configuration is called "counterflow", [Figure C.1.]

The design of a new apparatus is aimed at determining the operating conditions, pressure drop, and outlet temperatures of the working gases, where the heating surface is known. For illustration, the two-pass overall-counterflow exchanger is shown in Figure (C.2) will be considered. The following input specifications are assumed to be known.

First pass height length	, L_I	ft
Second pass height length	, L_{II}	ft
Unit width	, W	ft
Unit side length	, B	ft
Tube outside diameter	, d_o	ft
Tube inside diameter	, d_i	ft
Hot gases inlet temperature,	t_{i_I}	$^{\circ}F$



. Figure C.1. Variation in Gases Temperature in Counterflow Recuperator.

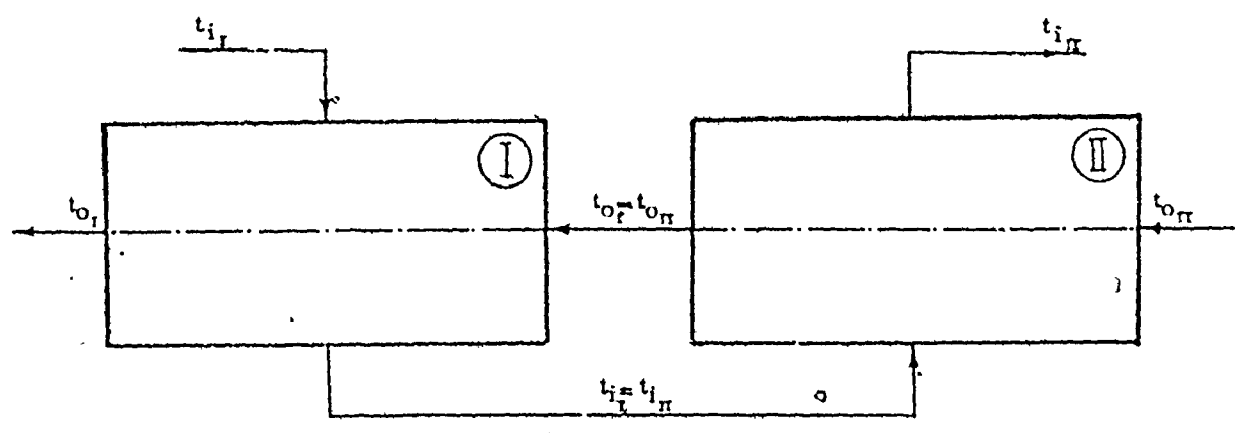
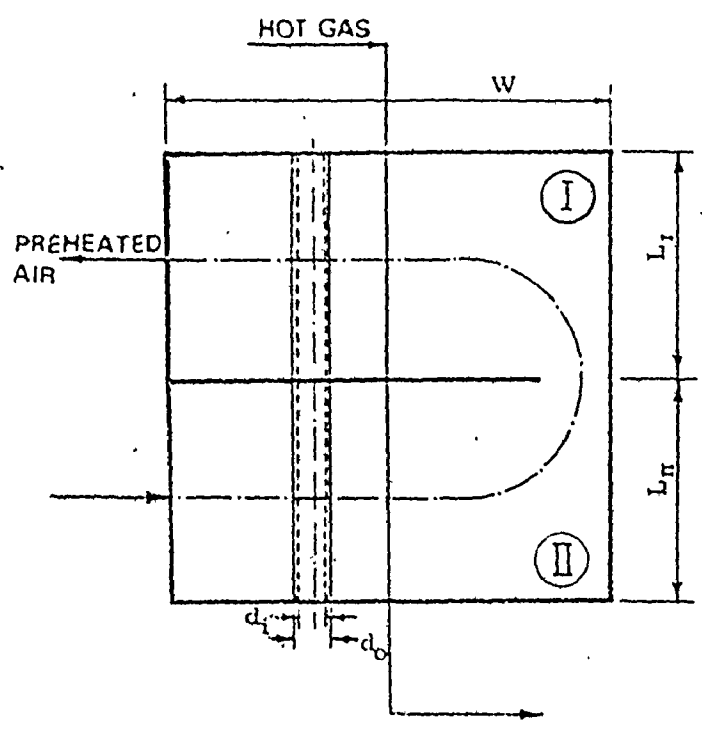


Figure C.2. Two-Pass Overall-Counterflow Exchanger.

Cold air inlet temperature	, $t_{0_{II}}$	$^{\circ}F$
Tube spacing ratio	, A	
Mean duct work inside diameter	, d_D	ft
Preheated air volume flow rate	, V_{air}	cfm
Hot gas volume flow rate	, V_g	cfm

C.1 Calculating the Outlet Temperature of Working Gases:

Details of the derivation of the final equations are omitted when literature references are provided. Major emphasis is placed on the principles and the conceptual ideas employed.

Here and below the subscript (i) indicates the values pertain to the hot gas passing inside the recuperator tubes, and the subscript (0) to the cold gas. The superscript (^) indicates the inlet temperature and the superscript (^) the outlet temperature of the working gases. The top pass heat exchanger will be described by the subscript (I) where the bottom one by (II).

The heat transfer equation which combines the convective and conductive mechanisms can be represented as follows, [17, 18, 19, 20, 22, 23, 26].

$$\text{Heat flux} = q = \text{LMT} / \left[\frac{1}{h_i A_i} + \frac{d_o - d_i}{2K_M A_m} + \frac{1}{h_o A_o} \right] \text{ [BTU/hr]} \quad (\text{C-1})$$

where LMT is known as the logarithmic mean temperature difference. It has the following expression for a counter flow arrangement, Figure C.1.

$$\text{LMT} = \frac{(t_i - t_o) - (t_i' - t_o')}{\ln \frac{t_i - t_o'}{t_i' - t_o}} \quad (\text{C-2})$$

$$A_i = \pi L d_i N_T \quad (\text{C-3})$$

$$A_o = \pi L d_o N_T \quad (\text{C-4})$$

$$A_m = (A_o - A_i) / \ln(A_o/A_i) \quad (\text{C-5})$$

in which N_T is the total number of tubes. Knowing the overall recuperator dimension (B, W & L), N_T could be counted for symmetrical staggered tube banks as follows, [Figure C.3].

$$\begin{aligned} N_B &= \text{number of tube rows in flow direction} \\ &= [(B - d_o) / (A d_o)] + 1 \end{aligned} \quad (\text{C-6})$$

$$\begin{aligned} N_W &= \text{number of tube columns in flow direction} \\ &= [(W - d_o) / (A d_o)] + 1 \end{aligned} \quad (\text{C-7})$$

$$N_T = [(N_B N_W)] + [(N_B - 1) (N_W - 1)] \quad (\text{C-8})$$

The quantities h_i and h_o are the inside and outside tubes surface coefficients of heat transfer. For tubes having a sharp-edged-entrance with a Reynolds number, based on diameter,

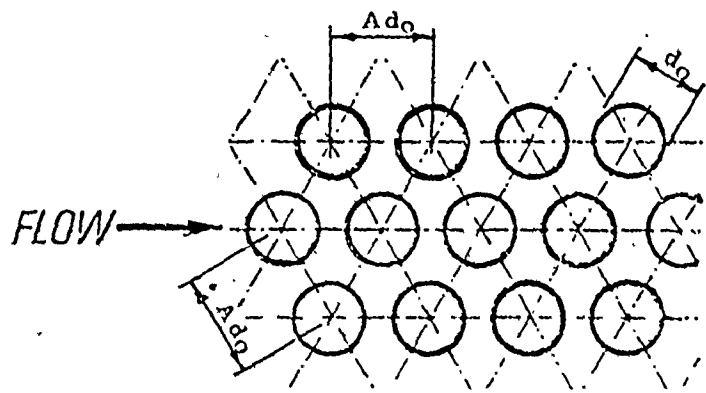


Figure C.3 Staggered Tube Banks.

greater than 10^4 , McAdams (Reference [20], page 420) recommends the use of the following equation

$$h_i = \frac{0.023 N_{Pra}^{1/3} k_a}{d_i} N_{Rw}^{0.8} \left(\frac{\mu_a}{\mu_w} \right)^{0.14} \left[1 + \left(\frac{d_i}{L} \right)^{0.7} \right] \quad \text{BTU/hr ft}^2 \text{ } ^\circ\text{F} \quad (\text{C-9})$$

where, subscript (a) stands for the average bulk mean temperature, $t_B = (t_{i1} + t_{i2})/2$, and the subscript (w) stands for the average wall temperature, $t_w = (t_{o1} + t_{o2})/2$. On the other hand, the outside tube surface coefficient of heat transfer, h_o , can be approximately evaluated using Grimson's formula, (Reference [20], page 432), as follows

$$h_o = 1.13 C_1 N_{Prf}^{1/3} C_2 N_{Rf} k_f C_3/d_o \dots \text{BTU/hr ft}^2 \text{ } ^\circ\text{F} \quad (\text{C-10})$$

where C_1 and C_2 are constants for various tube spacing ratio, A. They are listed in Table C.1. For banks less than ten rows deep a correction factor, C_3 , has to be introduced. It presented in Table C.2 Subscript (f), stands for average film temperature, $t_f = (t_B + t_w)/2$.

Other variables are defined as follows.

$$\begin{aligned} \mu &= \text{viscosity coefficient } \text{lb}_m/\text{hr}^2 \text{ ft} \\ N_{Pr} &= \text{Prandtl number } (\mu C_p/k) \\ k &= \text{gas thermal conductivity } \text{BTU/hr ft } ^\circ\text{F} \\ C_p &= \text{specific heat at constant pressure } \text{BTU/lb}_m \text{ } ^\circ\text{F} \end{aligned} \quad (\text{C-11})$$

TABLE C.1. CONSTANTS C_1 AND C_2 FOR USE IN EQUATION (C-3) FOR TUBE BLANKS

SPACING, A	C_1	C_2
1.00 < A < 1.25	0.518	0.556
1.25 < A < 1.50	0.460	0.562
1.50 < A < 2.00	0.482	0.556
2.00 < A < 3.00	0.421	0.574

TABLE C.2. CONSTANT C_3 FOR USE IN EQUATION (C-3) FOR TUBE BLANKS

NUMBER OF ROWS	4	5	6	7	8	9	<10
C_3	0.88	0.92	0.94	0.97	0.93	0.99	1.0

$$\begin{aligned}
 N_R &= \text{Reynolds number } (d_i G / \mu) \\
 G &= \text{flow stream mass velocity } (4.0 V_g \rho / 60 d_i^2) \\
 &\quad \text{lb}_m / \text{hr ft}^2 \quad \quad \quad (C-12)
 \end{aligned}$$

Values of μ , C_p and N_{Pr} as a function of temperature for both cold air and hot exhaust gases are given in detail in Appendix D, Sections 1, 2 and 3. k could be estimated from the value of N_{Pr} using equation (C-11).

The quantity K_M occurring in equation (C-1) is the recuperator tube thermal conductivity in $[\text{BTU} / \text{hr ft}^0 \text{F}]$, and it also is a function of mean tube surface temperature. The value of K_M for a semi-silicon carbide tube is given at Appendix D, Section 4.

Two additional expressions may be written for the heat transfer rate, q , based on energy-balance considerations:

$$q = V_g C_{p_i} \rho_i (t_i - t_i') / 60 \quad \text{BTU/hr} \quad (C-13)$$

$$q = V_{\text{air}} C_{p_0} \rho_0 (t_0' - t_0) / 60 \quad \text{BTU/hr} \quad (C-14)$$

where, ρ_i and ρ_0 are hot gases and air densities in $(\text{lb}_m / \text{ft}^3)$, respectively. They are functions of the gas temperature, and pressure ($\rho = p/RT$).

For the two-pass overall-counterflow recuperator shown in Figure C-2, all the design parameters and hot gases and air input temperatures (t_{iI} , t_{0II}) are assumed known:

To find the outlet temperature of the working gases and also the heat flux, using equations (C-1, C-13, and C-14), a fixed point iteration technique will be used [12]. It is an iterative technique in the form of $t_{j+1} = g(t_j)$. If t_j is assumed t_{j+1} could be evaluated from the function g , until the difference between two successive iterations will be less than a pre-determined accuracy. The following procedure is suggested.

1. Assume $t_{0I}'' | j$
2. ~~Assume $t_{0I}'' | j$~~ ; use (C-13) and (C-14) to obtain I and t_{iI}'' . Using t_{iI}' , t_{0I}'' and t_{iI}'' in equation (C-1) gives $t_{0I}'' | j+1$. The fixed point iteration technique (FPI) is then applied until no improvement is possible within our accuracy limit. Therefore, t_{0I}'' and t_{iI}'' are now known based on the assumed $t_{0I}'' | j$.
3. Now t_{iI}'' equals t_{iII}' , and t_{0II}' is known. Using the same procedure as in (2), t_{0II}'' and t_{iII}'' can be estimated.
4. Returning to state I, t_{iI}' , t_{iI}'' and t_{0I}' are known. Therefore, $t_{0I}'' | j+1$ can be calculated. Repeating the same procedure starting from (1), setting $t_{0I}'' | j = t_{0I}'' | j+1$, and continuing until the difference between the estimated (j) and the calculated (j+1) is permissible.

In short, we have the three equations (C-1), C-13)

and (C-14). If they are applied twice for pass I and II, six unknowns $t_{0_I} = t_{0_{II}}$, $t_{i_I} = t_{i_{II}}$, $t_{i_{II}}$, t_{0_I} , q_I and q_{II} may be determined. In a similar way, for the case of three-pass overall-counterflow recuperator, we will have nine unknowns for the three passes.

C.2 Flow Friction and Pressure Drop Across the System.

The evaluation of flow friction with sufficient accuracy is essential for the setting of the optimal operating conditions for a given apparatus.

First we will consider the minor losses which occurred in a flow due to bends, elbows, sudden expansion or contraction, etc. Sudden expansion in a pipeline to a reservoir causes a pressure drop equal to, Figure C.4

$$\Delta P_1 = \frac{v_1^2}{2g} \rho_1 = \frac{(4V_{Fan}/\pi d_D^2)^2}{2g} \rho_1 \quad (C-15)$$

That is, the complete kinetic energy in the flow is converted into thermal energy, in which v_1 is the air velocity at entrance, ρ_1 is the air density at $t_{0_{II}}$ temperature. We shall assume that the pressure drop due to the flow changing direction from one pass to another to be equivalent to a flow through two standard elbows.

$$\Delta P_3 = \frac{v_3^2 f_3}{2g} K \quad (C-16)$$

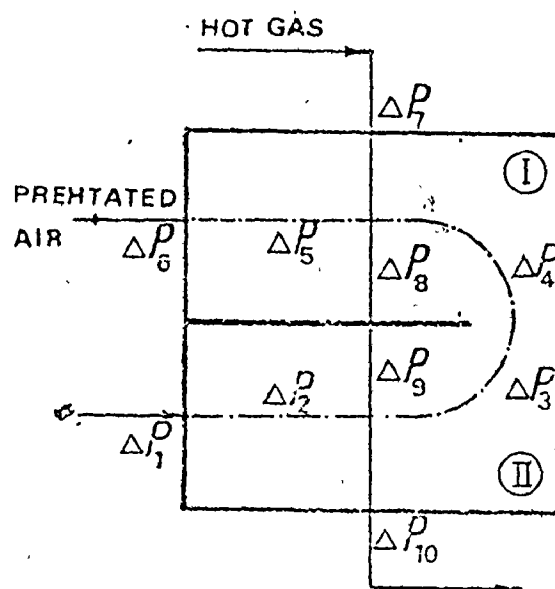


Figure C.4. Pressure Drop in Two-Pass Exchanger

$$\Delta P_4 = \frac{v_4^2}{2g} K \quad (C-17)$$

where, K is standard elbow head loss coefficient. It is assumed equal to 0.9, in accordance with experiment results of Gibson [Reference [2], 11], page 306]. v_3 and v_4 are the air velocities leaving pass II and entering pass I. The head loss at the entrance to a pipeline from a reservoir is usually taken as [21].

$$\Delta P_6 = \frac{v_6^2}{2g} \cdot 0.5 \quad (C-18)$$

where, the opening is assumed to be square-edged. v_6 is the air velocity in the pipe. Both ΔP_2 and ΔP_5 pressure losses, due to the air flowing through the tube bundles normal to their axis for pass II and I respectively, can be evaluated using Appendix D, Section 6.

The hot gas with pressure drops as it flows through the recuperator tubes to the stack are determined as follows. Abrupt contraction and expansion pressure-losses, ΔP_7 and ΔP_{10} , are explained in detail at Appendix D, Section 7. The drop in pressure through the recuperator tubes due to friction can be determined as follows

$$\Delta P_8 = f_t \frac{L_I}{d_i} \frac{v_9^2}{2g_c} \rho_9 \quad (C-19)$$

$$\Delta P_9 = f_t \frac{L_{II}}{d_i} \frac{v_{10}^2}{2g_c} \rho_{10} \quad (C-20)$$

where, f_t is the tube friction factor. It is given in Appendix D Section 4. ρ_9 and ρ_{10} are the hot gases densities at different mean temperatures for passes I and II.

Having determined the total pressure drop across the recuperator and knowing the rate of flow, it is easy to determine the power required to maintain the flow of the gases through the apparatus.

APPENDIX D
SOME PHYSICAL PROPERTIES

This appendix contains reference gases and materials thermodynamic properties.

D.1 Viscosity of a Multicomponent Gas Mixtures as a Function of Temperatures:

The semiempirical formula of Wilke, ([19], page 24), is quite adequate to evaluate the viscosity of a mixture of gases, μ_{mix} , as follows:

$$\mu_{\text{Mix}} = \sum_{i=1}^n \frac{\alpha_i \mu_i}{\sum_{j=1}^n \alpha_j \phi_{ij}} \quad (\text{D.1})$$

in which

$$\phi_{ij} = \frac{1}{\sqrt{8}} \left(1 + \frac{M_i}{M_j} \right)^{-\frac{1}{2}} \left[1 + \left(\frac{\mu_i}{\mu_j} \right)^{\frac{1}{2}} \left(\frac{M_j}{M_i} \right)^{\frac{1}{4}} \right]^2 \quad (\text{D.2})$$

Here n is the number of chemical species in the mixture; α_i and α_j are the mole fractions of species i and j ; μ_i and μ_j are the viscosities of species i and j at the system temperature and pressure; and M_i and M_j are the corresponding molecular weights. The viscosity coefficient of gases as

a function of temperature is determined by Sutherland's formula, ([18], page 349), as follows

$$\mu = 559. (\mu_0) \frac{1 + (C/273) [T/273]^{\frac{1}{2}} \times 10^{-8}}{1 + (C/T)} \text{ Ib}_m/\text{ft. sec}$$

(D.3)

in which

$$T = \frac{5.0}{9.0} (t - 492.0) + 273. \quad \text{(D.4)}$$

t is the gas average temperature $^{\circ}\text{F}$

The values of μ_0 and C are given in Table D-1 for the gases of interest. In engineering calculations, the dependence of gas viscosity on pressure up to 10 atmospheric may be neglected.

D.2 Specific Heat as a Function of Temperature

To accurately evaluate the amount of heat carried by the gases under varying temperatures, the specific heats of these gases, which vary with temperature, must be known. For the particular case at hand, we are interested in knowing the specific heat for the products of combustion of Blast Furnace (BFG) and Coke Oven Gas (COG), and also for air. They are all mixtures of simple gases, for which the behaviour of their specific heats is well known ([22], page 638).

The specific heats for the constituents in $\text{BTU}/\text{Ib}_m^{\circ}\text{F}$ are:

$$C_{P_{O_2}} = (8.9465 + .0048044\alpha^{1.5} - 42.679\alpha^{-1.5} + 56.615\alpha^{-2})/32.0 \quad (D-5)$$

$$C_{P_{N_2}} = (9.3355 - 122.56\alpha^{-1.5} + 256.38\alpha^{-2} - 196.08\alpha^{-3})/28.016 \quad (D-6)$$

$$C_{P_{CO_2}} = (-0.8929 + 7.2967\alpha^{.5} - 0.9807\alpha + 0.0057835\alpha^2)/44.014 \quad (D-7)$$

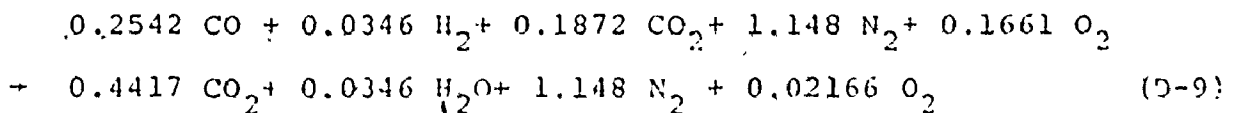
$$C_{P_{H_2O}} = (34.19 - 43.868\alpha^{.25} + 19.778\alpha^{.5} - 0.88407\alpha)/18.016 \quad (D-8)$$

in which

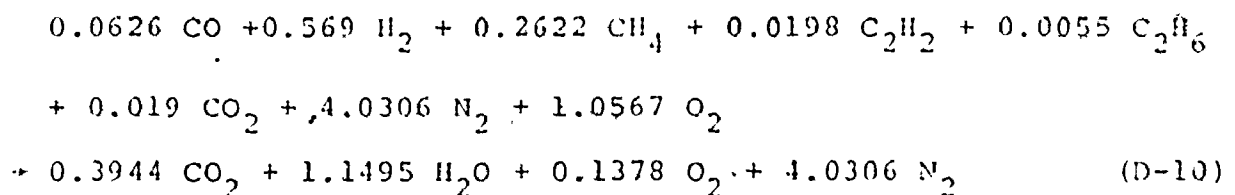
$$\alpha = (\text{temperature in degrees Rankine})/180$$

Knowing the average volumetric proportion of the constituents for (BFG), and (COG) and air, and also the combustion equations for both (BFG) and (COG), the specific heat values of them can be determined as follows:

The Combustion equation for BFG at 15% excess air is; (24).



The combustion equation for COG at 15% excess air is:



Using equations D-5, D-6, D-7, D-8, D-9 and D-10, the specific heats for BFG, CQG product of combustion, (PC), and air are as follows:

$$C_{P_{BFG|PC}} = [0.021021(18.016) C_{P_{H_2O}} + 0.268354(44.014) C_{P_{CO_2}} + 0.1316(32) C_{P_{O_2}} + 0.697465(28.016) C_{P_{N_2}}] / 32.15$$

(D-11)

$$C_{P_{COG|PC}} = [0.20123(18.016) C_{P_{H_2O}} + 0.06905(44.014) C_{P_{CO_2}} + 0.02412(32) C_{P_{O_2}} + 0.7056(28.016) C_{P_{N_2}}] / 27.196$$

(D-12)

$$C_{P_{air}} = [0.21(32) C_{P_{O_2}} + 0.79(28.016) C_{P_{N_2}}] / 28.17$$

(D-13)

D.3 Prandtl Number

Tabulated data for the values of Prandtl number at different temperatures, [18], for both dry air and flue gases (13% CO₂, 11% H₂O and 76% N₂) at atmospheric pressure, were fitted into a fifth order linear polynomial with a maximum residual of (0.001) from the experimental tabulated values.

$$N_{Pr_0} [Air] = 0.707 - 0.212 \times 10^{-3} B + 0.2957 \times 10^{-6} B^2 + 0.4353 \times 10^{-9} B^3 - 0.855 \times 10^{-12} B^4 + 0.3482 \times 10^{-15} B^5$$

(D-14)

$$N_{P_{r_i}} [\text{Hot Gases}] = 0.72 - 0.3495 \times 10^{-3} \beta + 0.5604 \times 10^{-6} \beta^2 - 0.5645 \times 10^{-9} \beta^3 + 0.2487 \times 10^{-12} \beta^4 - 0.3524 \times 10^{-16} \beta^5 \quad (\text{D-15})$$

in which

$$\beta = (t(^{\circ}\text{F}) - 492.0) / 9$$

The above two equations are valid for the range [32-2300^oF].

D.4 Friction Factor

An empirical transition function for commercial pipes for the region between smooth pipes and the complete turbulence zone has been developed by Colebrook [Reference [21], page, 283), which is the basis for the Moody diagram in Figure D.1.

$$\frac{1}{\sqrt{f}} = -0.86 \ln \left(\frac{\epsilon/d_i}{3.7} + \frac{2.51}{N_{R_N} \sqrt{f}} \right) \quad (\text{D.16})$$

in which

f = friction factor

ϵ = roughness height, ft

d_i = pipe inner diameter ft

N_{R_N} = Reynolds number

A fixed point iteration technique, [12], could be used to evaluate the value of f , using equation (D-16) to obtain a given precision. However, a starting value for f is essential to guarantee convergence. An empirical explicit form,

TABEL D.1. CONSTANTS C AND μ_0 FOR USE IN EQUATION (D-3) FOR VISCOSITY

GAS	C	μ_0
1. AIR	122	1.755
2. NITROGEN	107	1.708
3. OXYGEN	138	1.962
4. CARBON DIOXIDE	250	1.402
5. WATER VAPOUR	673	0.87

TABEL D.2. FIRECLAY BRICK THERMAL CONDUCTIVITY, (28).

TEMPERATURE (°F)	392	1112	1832	2552
THERMAL CONDUCTIVITY (BTU/ft hr °F)	0.53	0.85	0.95	1.02

TABEL D.3. COG AND BFG COMPOSITION AND THEIR PRODUCTS OF COMBUSTION

COKE OVEN GAS (COG) TYPICAL COMPOSITION				(COG) PRODUCTS BLAST FURNACE OF COMBUSTION GAS (BFG)				(BFG) PRODUCTS OF COMBUSTION	
CON- STIT- UENT	VOLU- METRIC %	CON- STIT- UENT	VOLU- METRIC %	CON- STIT- UENT	VOLU- METRIC %	CON- STIT- UENT	VOLU- METRIC %	CON- STIT- UENT	VOLU- METRIC %
H ₂	56.90	C ₂ H ₆	0.55	O ₂	2.41	CO	25.42	O ₂	1.316
CH ₄	26.22	CO ₂	1.9	H ₂ O	29.12	H ₂	3.46	H ₂ O	2.102
CO	6.26	O ₂	0.45	CO ₂	6.91	CO ₂	18.75	CO ₂	26.831
C ₂ H ₄	1.98	N ₂	5.74	N ₂	70.56	N ₂	52.37	N ₂	69.751
MOLECULAR WEIGHT [lb/Mole]			10.395	27.2	39.1	32.15			
DENSITY [lb/ft ³ , at 60°F]			0.0274	0.0719	0.0838	0.0847			
CALORIFIC VALUE [BTU/scf]			500.	—	93.	—			

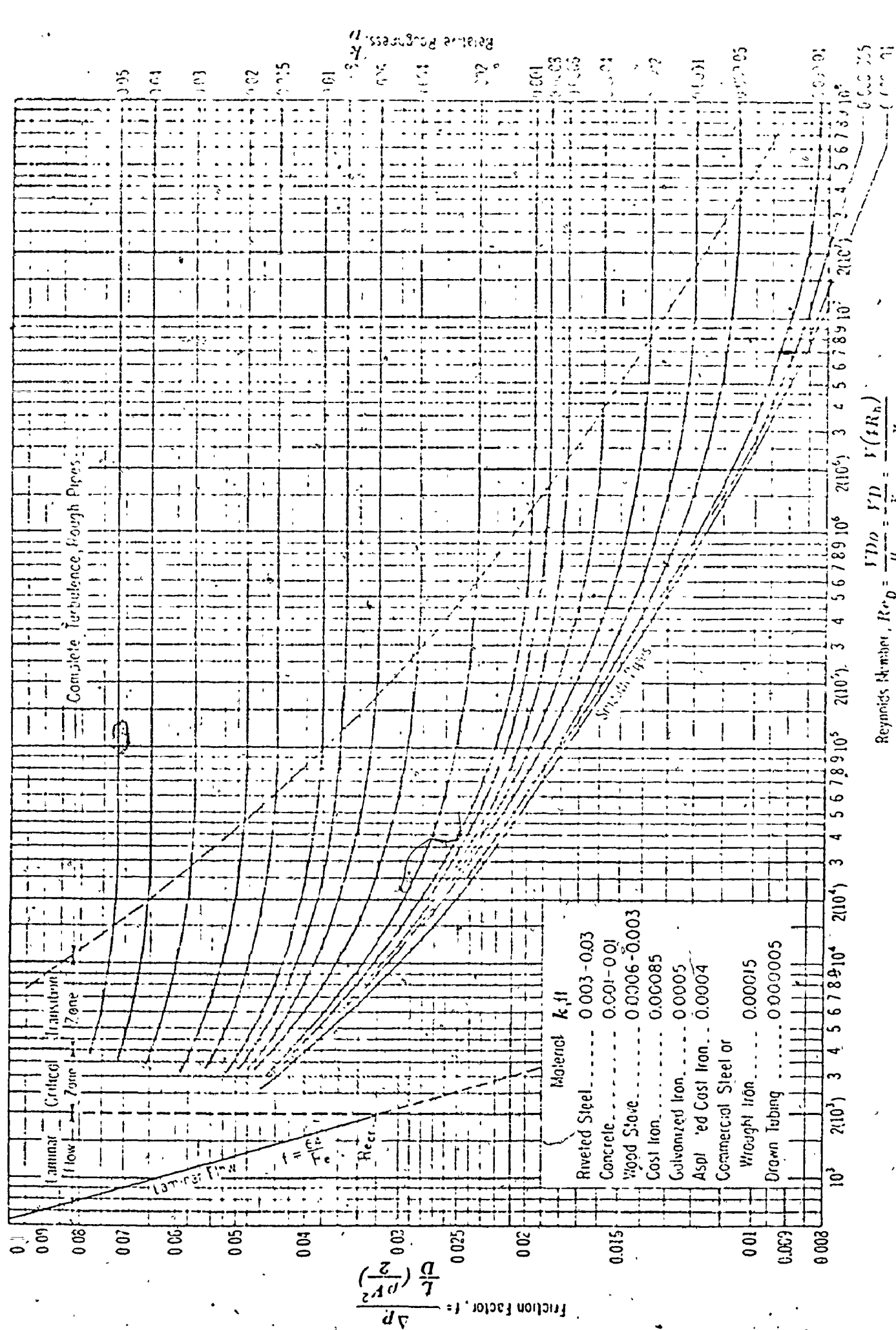


FIG. D-1 Friction factors for commercial pipe. (From "Friction Factors for Pipe Flow," by L. F. Moody, Trans. ASME, Vol. 65, 1943, with permission of the publishers, The American Society of Mechanical Engineers.)

developed by Wood [25], can be used.

$$f = 0.094 (\epsilon/d_i)^{0.225} + 0.53 (\epsilon/d_i) + 88. (\epsilon/d_i)^{0.44} N_{R_N}^{-1.62} (1.62 (\epsilon/d_i)^{0.13}) \quad (D-17)$$

Equations D-16 and D-17 are valid only for Reynolds number greater than 10^5 . However, Blasius formula ([21], page 295) can be used for a Reynolds number upto 10^5 .

$$f = 0.316 / N_{R_N}^{0.25} \quad (D-18)$$

D.5 Semi-Silicon Carbide Thermal Conductivity

No experimental data was available for semi-silicon carbide thermal conductivity. Therefore, the available Fire-clay brick (Missouri) thermal conductivity values, Table D.2, were used as an equivalent substitute. A third order polynomial is used for fitting.

$$K = 0.4132 + 0.4812\alpha - 0.0965\alpha^2 \quad \text{BTU/hr ft}^0 \text{F} \quad (D-19)$$

in which $\alpha = t/1000$, where t is in degrees Fahrenheit.

D.6 Staggered Tube Banks, Drag Coefficient:

The pressure loss, Δp , for a fluid flowing through a tube bundle normal to its axis, is conventionally expressed by

$$\Delta p = N_B f_t \rho \frac{U^2}{2} \quad (D-20)$$

where N_B = number of tube rows in flow direction
 ρ = density of fluid
 U = average velocity through area between tubes
 f_t = drag coefficient, or friction factor

The friction factor, f_t , depends on the geometric arrangement of the tubes. Experimental results are mainly available for two arrangements, i.e., tubes either aligned or staggered in the flow direction. However, we are interested only here, in a symmetrical staggered arrangement. The friction factor, f_t , was plotted by Zhukauskas ([26], page 41) versus Reynolds number, N_{R_N} for different tube spacing ratios, A , as shown in Figure D.2. Four nonlinear equations were fitted for four different values of, A , as a function of the flow Reynolds number, N_{R_N} . Nonlinear curve fitting is discussed in Appendix E in detail.

$$f_t (A=1.25) = [\text{Exp } 8.380 - 2.827\lambda + 0.3497\lambda^2 - 0.0275\lambda^{2.763}] \quad (D-21)$$

$$f_t (A=1.5) = [\text{Exp } 6.868 - 2.501\lambda + 0.3162\lambda^2 - 0.02289\lambda^{2.804}] \quad (D-22)$$

$$f_t (A=2.0) = [\text{Exp } 5.123 - 2.030\lambda + 0.2781\lambda^2 - 0.0263\lambda^{2.722}] \quad (D-23)$$

$$f_t (A=2.5) = [\text{Exp } 6.434 - 2.665\lambda + 0.3529\lambda^2 - 0.02379\lambda^{2.837}] \quad (D-24)$$

where $\lambda = \ln(N_{R_N})$

A linear interpolation or extrapolation can be used for different values of A .

D.7 Abrupt Contraction and Expansion Pressure-Loss Coefficients

Heat exchanger usually involves a flow contraction at its core entrance and a flow expansion at its core exit. This problem has been discussed by Kays [23].

The entrance pressure drop is made up of two parts. The first is the pressure drop which would occur due to flow-area change alone, without friction. The second is the pressure loss due to the irreversible free expansion that always follows an abrupt contraction. The entrance pressure drop, Δp_{en} , can then be expressed as

$$\Delta p_{en} = \frac{\rho V^2}{2} (1 - \sigma_e^2) + K_C \frac{\rho V^2}{2} \quad (D-25)$$

where, V is the velocity in the tubes inside the heat exchanger core, and σ_e is the core free-flow by frontal area ratio. The irreversible component of the pressure drop is contained in the abrupt contraction coefficient, K_C . The exit pressure rise, Δp_{ex} , is similarly broken into two parts and can be expressed as follows

$$\Delta p_{ex} = \frac{\rho V^2}{2} (1 - \sigma_i^2) - K_e \frac{\rho V^2}{2} \quad (D-26)$$

where K_e is the abrupt expansion coefficient.

K_C and K_e are functions of the Reynolds number in the tubes and of the contraction and expansion geometry, as

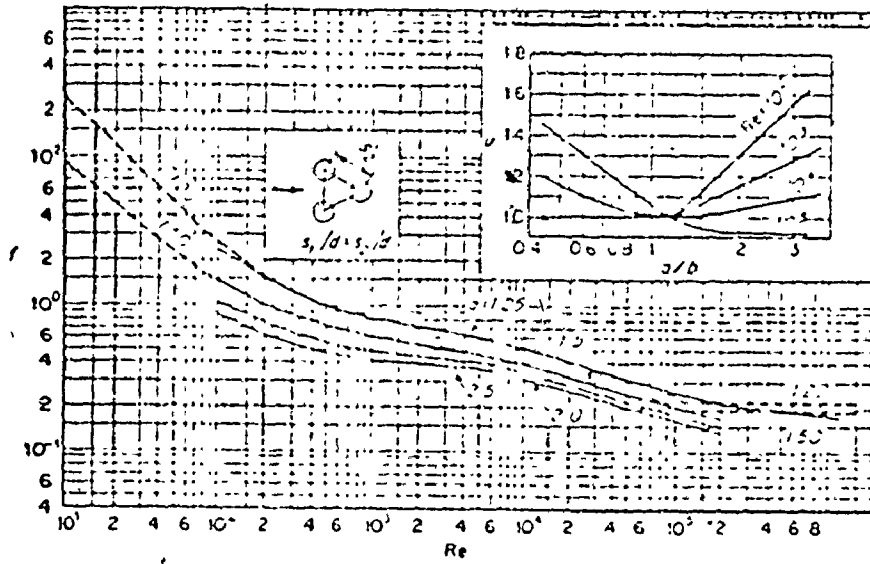


Figure D-2. Friction Factor f for Staggered Tube Banks Reference [23].

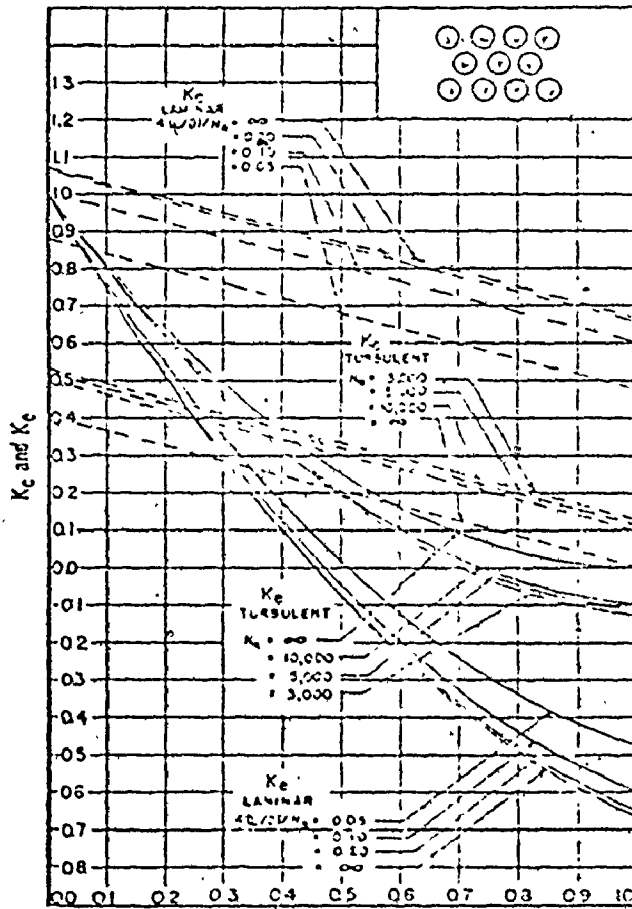


Figure D-3. Entrance and Exit Pressure Loss Coefficients for a Heat Exchanger [23].

presented in Figure D-3. They are expressed in a linear form as a function of σ for different values of Reynold's number with turbulent flow as follows .

$$K_e (N_{R_N} = 3000) = 1.0 - 2.058\sigma + 0.8444\sigma^2 + 0.0923\sigma^3 \quad (D-27)$$

$$K_C (N_{R_N} = 3000) = 0.52 - 0.38\sigma \quad (D-28)$$

$$K_e (N_{R_N} = 5000) = 1.0 - 2.115\sigma + 1.059\sigma^2 - 0.0521\sigma^3 \quad (D-29)$$

$$K_C (N_{R_N} = 5000) = 0.51 - 0.39\sigma \quad (D-30)$$

$$K_e (N_{R_N} = 10,000) = 1.0 - 2.091\sigma + 1.029\sigma^2 - 0.03546\sigma^3 \quad (D-31)$$

$$K_C (N_{R_N} = 10,000) = 0.5 - 0.4\sigma \quad (D-32)$$

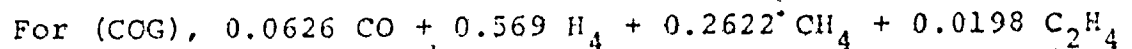
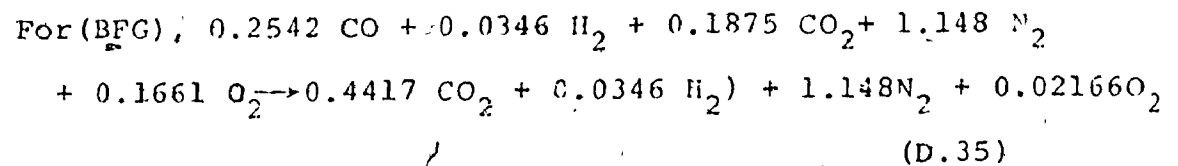
$$K_e (N_{R_N} = \infty) = 1.0 - 1.941\sigma + 0.8807\sigma^2 + 0.06367\sigma^3 \quad (D-33)$$

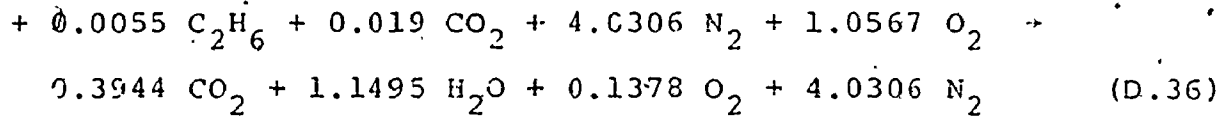
$$K_C (N_{R_N} = \infty) = 0.4 - \sigma \quad (D-34)$$

Linear interpolation could be applied for the values of N_{R_N} in between.

D.8 Combustion of Blast Furnace Gas and Coke Oven Gas

Volumetric analyses of typical samples of Blast Furnace Gas (BFG) and Coke Oven Gas (COG) were assumed to have the typical volumetric composition shown in Table D.3. Combustion equations for both (BFG) and (COG) at 15% excess air will have the following forms:





Therefore, one mole of (BFG) uses 0.791 moles of air to produce 1.646 moles of products of combustion; and one mole of (COG) uses 5.02 moles air to produce 5.712 moles of products of combustion.

D.9 Ceramic Recuperator Air and Hot Gases Volume Flow Rates

Leakage occurs evenly throughout the ceramic recuperators because of the porous walls and weak joints of the tubes. For a two-pass overall counterflow recuperator, for example, the leakage system can be simplified and considered as a constant mean percentage of the higher pressure gas leaks to the lower pressure side. The preheated air volume flow rate, V_{air} , and the percentage volumetric gases leakage, $l\%$ are assumed to be known or specified. The hot gases will be treated as a mixture of blast furnace gas, (BFG)_{POC}, and coke oven gas, (COG)_{POC}, products of combustion at 15% excess air. We assume that the volumetric coke oven gas ratio to the total fuel gas mixture, x_{fuel} , is known. Therefore, using COG and BFG combustion equations (D.36 and D.35), the hot gases (products of combustion) volume flow rate, V_{POC} , can be evaluated as follows

$$\begin{aligned}
 V_{\text{POC}} &= V_{\text{air}} [5.712x + 1.646(1-x)] / \\
 &\quad [5.02x + 0.791(1-x)] \\
 &= V_{\text{air}} (4.066x + 1.646) / (4.41x + 0.791) \quad (\text{D-38})
 \end{aligned}$$

Referring to Figures D-4 and D-5, the leaking air volume flow rates (y_1 , y_2 , y_3 , and y_4), could be evaluated as following

$$y_1 = l_8 V_{\text{air}} / (1-l_8) \quad (\text{D-39})$$

$$y_2 = l_8 V_{\text{air}} / (1-l_8)^2 = y_1 / (1-l_8) \quad (\text{D-40})$$

$$y_3 = l_8 V_{\text{air}} / (1-l_8)^3 = y_2 / (1-l_8) \quad (\text{D-41})$$

$$y_4 = l_8 V_{\text{air}} / (1-l_8)^4 = y_3 / (1-l_8) \quad (\text{D-42})$$

Therefore, the average pass (I) air volume rate, V_{o_I} , is

$$V_{o_I} = V_{\text{air}} + y_1 + y_2/2 \quad (\text{D-43})$$

The average pass (I) hot gases volume flow rate, V_{i_I} , is

$$V_{i_I} = V_{\text{POC}} + y_2/2 \quad (\text{D-44})$$

The average pass (II) air volume flow rate, $V_{o_{II}}$, is

$$V_{o_{II}} = V_{o_I} + y_2/2 + y_3/2 \quad (\text{D-45})$$

The average pass (II) hot gases volume flow rate, $V_{i_{II}}$, is

$$V_{i_{II}} = V_{i_I} + y_2/2 + y_3/2 \quad (\text{D-46})$$

The axial flow fan air volume flow rate, V_{Fan} , is

$$V_{\text{Fan}} = Q = V_{o_{II}} + y_3/2 + y_4 \quad (\text{D-46})$$

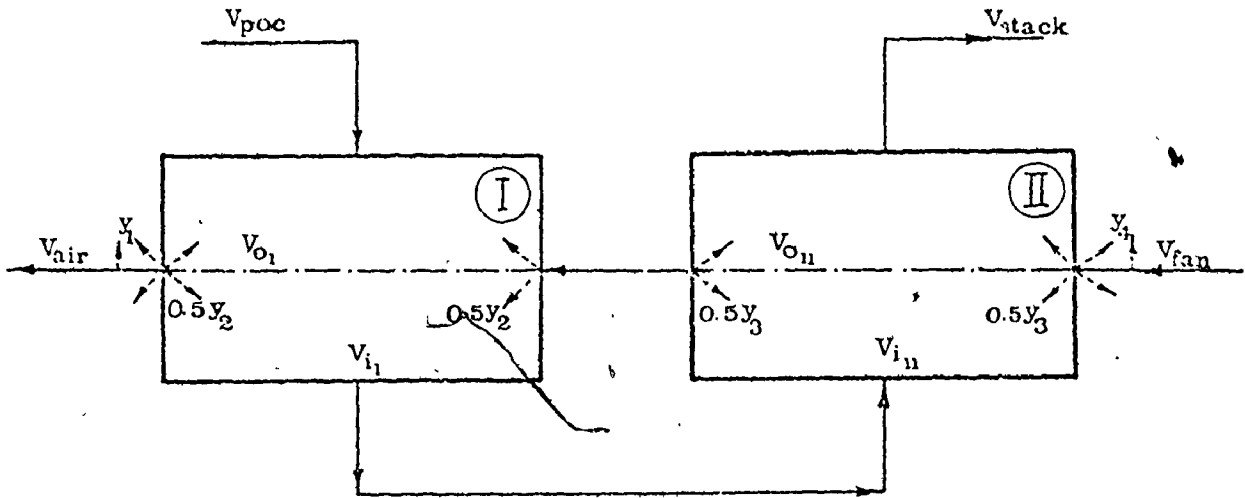


Figure D.4. Two-pass Overall-counterflow-Recuperator Volume Flow Rate Distribution.

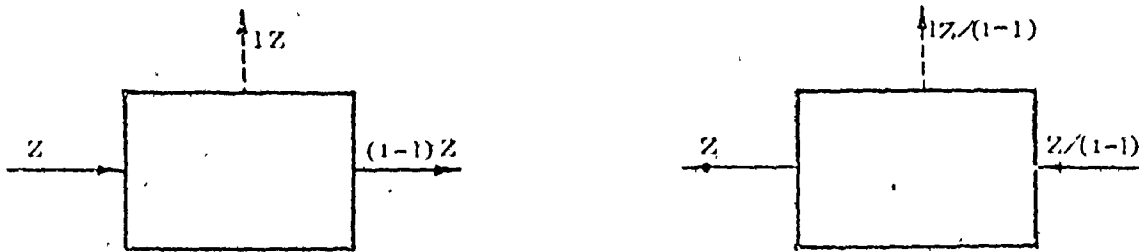


Figure D.5. Block Diagram of Leakage.

and, the stack hot gases volume flow rate, V_{stack} , is

$$V_{\text{stack}} = V_{i_{\text{II}}} + y_3/2 \quad (\text{D-48})$$

Finally, it is worthwhile here to mention that the coke oven gas volume flow rate, V_{COG} , equals

$$V_{\text{COG}} = x V_{\text{air}} / (4.41x + 0.791) \quad (\text{D-49})$$

while the blast furnace gas volume flow rate, V_{BFG} , equals,

$$V_{\text{BFG}} = (1-x) V_{\text{air}} / (4.41x + 0.791) \quad (\text{D-50})$$

D.10 Stack Draft and Pressure Loss

Due to the temperature difference between the hot gases travelling through the stack and the ambient temperature, a draft will be created, which can be calculated from the following formula, [32].

$$\text{stack draft} = 2.7124 H_{\text{st}} P_{\text{amb}} \left(\frac{1}{T_{\text{amb}}} - \frac{1}{T_{\text{st}}} \right) \quad (\text{D-51})$$

psi ✓

where,

H_{st} = stack height, ft

P_{amb} = ambient pressure, psi

T_{amb} = ambient temperature, $^{\circ}\text{R}$

T_{st} = average stack temperature, $^{\circ}\text{R}$

To obtain the actual draft for a stack, however, the losses that occur with flow must be deducted from the theoretical draft, equation (D-51). These losses are both frictional

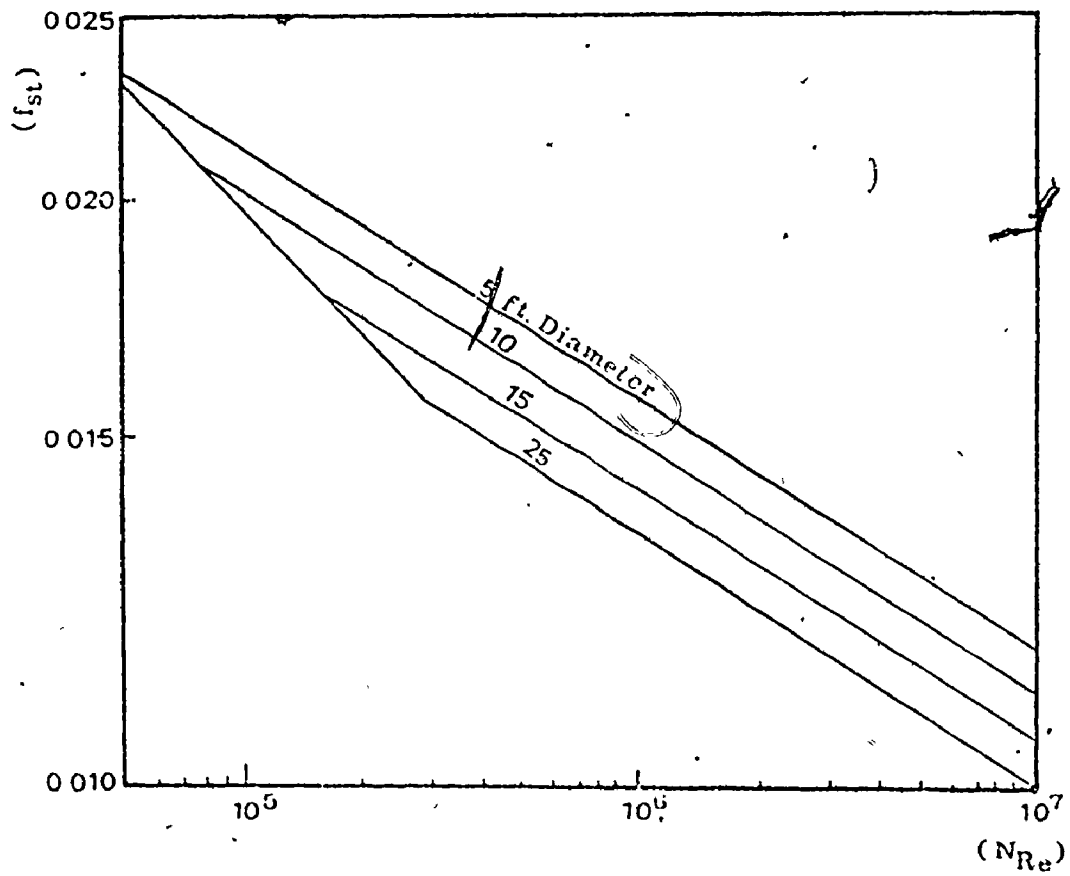


Figure D.6. Friction Factors For Stacks, F_{st} .

type and exit velocity in nature. They may be evaluated by the following equation [32].

$$\text{Stack flow loss} = 0.4902 \frac{T_{st}}{d_{st}} \left[\frac{6 \rho V_{st}}{10,000} \right]^2 \left[1 + \frac{f_{st} H_{st}}{d_{st}} \right] \text{ PSI (D-52)}$$

where,

d_{st} = stack diameter, ft

V_{st} = hot gases volume flow rate, cfm

ρ = hot gases density, lb/ft³

f_{st} = friction factor, see Figure D-6

To apply Figure D-6, the Reynolds number can be calculated by the equation

$$N_{Re} = \frac{1,656,000 \rho V_{st}}{T_{st} d_{st}} \quad (\text{D-53})$$

The overall draft can be obtained by subtracting the friction losses, equation D-52, from the theoretical draft, equation (D-51). This quantity is known as the natural draft of the stack since it is produced without mechanical means.

APPENDIX E
NONLINEAR CURVE FITTING

E.1 General

The best way to summarize a mass of multifactor data is by a simple equation instead of doing interpolation or extrapolation between the available mass of data. This Appendix is a summary, mainly by examples, of our efforts to fit a set of optimization function values, $U(\bar{y})$, with one, two, or more independent variables, \bar{y} , to a non-linear equation. As the number of variables increases, the problems become more complex. The curve, surface or hypersurface which needs to be fitted is a trade-off curve Type B defined and described in Chapter 2 in this piece of work. The trade-off curve independent variable, \bar{y} , is the relaxed hard specification which affected the design and was considered to be a junction between the minor sub-system under analysis and the master sub-system, as explained in Chapter 3.

A single equation is required to relate the optimization function values, u_j , to the relaxed junction specifications, y_{ji} . The subscript i designates the independent variable or specification, while subscript j defines the optimum point corresponding to i^{th} specification. If the number of data points exceeds the number of the fitted equation constraints

which have to be estimated, the least-squares method can be used to minimize the sum of the squared deviations of the data values, u_j , from those predicted by the equation, $U(\bar{y})$. However, some assumptions or requirements have to be stated first, [5].

E.2 Assumptions

(a) The data is typical. That is to say, it is a representative sample from the whole feasible range of situations about which we are interested. For one independent variable, y_1 , a vector of dependent variables, $U(y_1)$, has to be available for the entire feasible, practical range of y_1 , while for two independent variables, y_1 and y_2 , a matrix of dependent variables, $U(y_1, y_2)$, not necessary square, has to be accessible. In the limit, for (I) independent variables, (y_1, y_2, \dots, y_I) a tensor of order I of the dependent variables, $U(y_1, y_2, \dots, y_I)$ has to exist.

(b) The correct form of the fitted equation is assumed to be chosen, otherwise convergence of residuals will not be achieved. Therefore, more than one fitting model should be tested and identified.

(c) Preliminary estimates of all the nonlinear fitting model parameters, θ , must be available.

The term nonlinear, as applied to models in this part of the thesis is nonlinear in the parameters (coefficients)

to be estimated (and more than likely is also nonlinear in the independent variables, y). For example,

$$U(y_1, y_2) = \theta_1 y_1^{\theta_2} y_2^{\theta_3} \quad (E.1)$$

is a nonlinear fitting model. If the estimates of, $\bar{\theta}$, are not close "enough", the computed estimates will not converge on the best values.

E.3 Models

In general, more than one fitting model is possible or proposed. It is preferable to select the "best" model, based on one or a combination of the following criteria.

1. It is desirable to have a minimum number of coefficients consistent with reasonable error.
2. The simplest possible form is desirable consistent with reasonable error.
3. The model should be rational, based on physical grounds.
4. The variance, $S^2_{\bar{y}}$, should be a minimum.

For illustration, only two independent variables, (y_1, y_2) , are used. The following polynomial type model is one of the easiest empirical equations to fit. Two models will be demonstrated here in a polynomial form; the first being linear while the second is nonlinear; both are developed by the author.

Model I

$$U_I^* = \theta_0 + \theta_1 y_1 + \theta_2 y_1^2 + \dots + \theta_{n_1} y_1^{n_1} \quad (E-2)$$

$$\text{where, } \theta_i = \beta_{i0} + \beta_{i1} y_2 + \beta_{i2} y_2^2 + \dots + \beta_{in_2} y_2^{n_2}$$

$$, i=0, n_1 \quad (E-3)$$

Model II

$$U_{II}^* = \theta_0 + \theta_1 y_1 + \dots + \theta_{n_1-1} y_1^{n_1-1} + \theta_{n_1} y_1^{n_1+1} \quad (E-4)$$

$$\text{where, } \theta_i = \beta_{i0} + \beta_{i1} y_2 + \dots + \beta_{in_2-1} y_2^{n_2-1} + \beta_{in_2} y_2^{n_2+1}$$

$$, i = 0, n_1 \quad (E-5)$$

At this stage, n_1 and n_2 are assumed to be predetermined integer powers of y_1 and y_2 . Model I is a simple linearization of an n_1 degree polynomial as a function of the first independent variable, y_1 ; multiplied by a second n_2 degree polynomial which is function of the second independent variable, y_2 . On the other hand, Model II is the same as Model I except for the last nonlinear term. The number of the linear Model I parameters, β_{ij} , equals $[(n_1+1)(n_2+1)]$; while the number of the nonlinear Model II parameters, including the β_{ij} 's and θ_{n_1+1} , equals $[(n_1+1)(n_2+2) + 1]$.

E.4 Method

A well established linear least-squares technique was used to determine the linear model parameters, β 's. The same technique was used to determine the preliminary estimates of the nonlinear model parameters, β_{ij} and θ_{n_1+1} . However, a nonlinear least-squares technique was used to determine the optimum parameters values in the Model II. An iterative technique can be used; where the estimates at each iteration are obtained by a method due to Marquardt (1963), [5] which combines the Gauss (Taylor series) method and the method of steepest descent. Gradient nonlinear search methods, however, can be implemented to refine final parameters values, with minimum square residuals as an objective. Final function values using the predicted models, residuals and its sum, approximate confidence limits for each function values, and individual confidence limits for each parameter based on linear hypothesis and 95 per cent confidence limits were calculated.

E.5 Choice of Model

We now turn to methods of discrimination among models that apply equally well to linear or nonlinear models. Many different comparison tests can be executed depending upon the specific hypothesis selected. To select among two estimated regression equations, U_I^* and U_{II}^* , one can use the symmetric

test of Williams and Klot, (page 216, [30]). The null hypothesis is that the two regression equations are of equal ability in predicting the values of U . The test carried out to find the slope λ of the equation which passes through the origin:

$$z \equiv U - 0.5(U_I^* + U_{II}^*) = \lambda(U_I^* - U_{II}^*) \quad (E-6)$$

where U represents the empirical data, U_I^* , and Z is the test dependent variable. A plot of $[U - \frac{1}{2}(U_I^* + U_{II}^*)]$ versus $(U_I^* - U_{II}^*)$ should have a slope of approximately $(-\frac{1}{2})$ if the hypothesis about Model II being correct is true. We can infer that a significant negative indicates that U_{II}^* is a better estimated regression equation than U_I^* ; hence Model II is better than Model I. A similar analysis with the supposition that U_I^* is the correct equation leads to the conclusion that, ($\lambda = \frac{1}{2}$). That is to say, a significant positive slope should be found. If λ is not significantly different from zero, no choice can be made between U_I^* and U_{II}^* . Another test parameter has to be defined; which gives a measure of the deviation about the regression line. The residual root mean square RRMS,

$$\lambda = \frac{n \sum_{i=1}^n \alpha_i \gamma_i - \sum_{i=1}^n \alpha_i \sum_{i=1}^n \gamma_i}{(n \sum_{i=1}^n \alpha_i^2 - (\sum_{i=1}^n \alpha_i)^2)} \quad (E-6a)$$

$$\text{where, } \alpha_i = U_{I_i}^* - U_{II_i}^* \quad (E-6b)$$

$$\gamma_i = U_i - 0.5(U_{I_i}^* + U_{II_i}^*) \quad (E-6c)$$

n = total number of data points

can be stated as follows

$$\begin{aligned} \text{RRMS} &= \sqrt{\text{Residual sum of squares/degrees of freedom}} \\ &= \sqrt{\sum_{i=1}^n (U_i - U^*)^2 / f} \end{aligned} \quad (\text{E-7})$$

where, f = number of data points (n) - number of parameters

E.6 Example

Consider the set of optimum data points, shown in Table E-1 generated by optimizing a ducted axial flow fan for different operating conditions of head loss, H (in. water), and, air volume flow rate, Q (cfs), where the dependent variable, P.V.A.C., will be the unit present value average cost as described in Chapter 2.

It is advisable to normalize the input data sets, to avoid the problem of computer over flow and/or loss of accuracy due to truncation and rounding off errors. Therefore, H , Q and (P.V.A.C.) values, which are used to generate the trade-off surface as shown in Figure 2.20, will be considered as input data for creating a trade-off surface, and will be divided by 5., 50,000., and 2000., respectively. The resulting semi-normalized values are shown in Table E-1, H' , Q' , and (P.V.A.C.)' where it is simple to refer back to the original values. The total number of data points available

Table E.1 Input Data Used in Linear and Nonlinear
Regression Example

P.V.A.C. [Present Value Average Cost (2,000. dollars)]				
$H \backslash Q$	0.4	1.0	1.6	2.2
0.1	0.04036	0.08865	0.13361	0.179825
0.2	0.09710	0.183145	0.27528	0.361410
0.5	0.23704	0.48987	0.752875	1.027895
1.0	0.525945	0.989755	2.166525	3.021475
1.5	0.867405	2.182775	6.508995	11.25693
2.0	1.30768	3.291650	11.396070	36.48236
2.5	1.88377	7.59322	21.35380	106.4097

is 28, however, cubic spline interpolation can be used to increase the number of data points. An interpolated set of (70) points, which is shown in Table E-2, is also used in the following analysis and discussion.

Consider now the following three linear models:

Model 1

$$U_I^* = \ln [(P.V.A.C.)] = \beta_0 + \beta_1 Q + \beta_2 H + \beta_3 H^2 Q \quad (E-8)$$

Model 2

$$U_2^* = \ln [(P.V.A.C.)] = \beta_0 + \beta_1 Q + \beta_2 Q^2 + \beta_4 HQ + \beta_5 HQ^2 + \beta_6 H^2 + \beta_7 H^2 Q + \beta_8 H^2 Q^2 \quad (E-9)$$

Model 3

$$U_3^* = \ln [(P.V.A.C.)] = \beta_0 + \beta_1 Q + \beta_2 Q^2 + \beta_3 Q^3 + \beta_4 H + \beta_5 HQ + \beta_6 HQ^2 + \beta_7 HQ^3 + \beta_8 H^2 + \beta_9 H^2 Q + \beta_{10} H^2 Q^2 + \beta_{11} H^2 Q^3 + \beta_{12} H^3 + \beta_{13} H^3 Q + \beta_{14} H^3 Q^2 + \beta_{15} H^3 Q^3 \quad (E-10)$$

Before going any further, let us examine the effect of increasing the number of data points, Tables E-1 and E-2, on the model root residual mean square, RRMS, equation (E-7) as a measure of deviation of the assumed models from the input fitted data. Since, the input trade-off surface has a smooth trend, the spline method is a good way of interpolating. Also, the percentage difference in RRMS for different linear

Table E-2. Input Interpolated Data Used in Regression

$\frac{H}{Q}$	(P.V.A.C.) [Present Value Average Cost (2,000 Dollars)]										
	0.4	0.6	0.8	1.0	1.2	1.4	1.6	1.8	2.0	2.2	
0.1	.04036	.05674	.07291	0.0886	0.1038	0.1187	0.1336	0.1488	0.1642	0.1798	
0.2	0.0971	0.1252	0.1537	0.1831	0.2137	0.2447	0.2753	0.3047	0.3333	0.3614	
0.5	0.2370	0.3207	0.4049	0.4899	0.5761	0.6637	0.7529	0.8436	0.9355	1.0279	
1.0	0.5259	0.6179	0.7568	0.9898	1.3432	1.7610	2.1665	2.5009	2.7760	3.0215	
1.5	0.8674	1.0763	1.4574	2.1928	3.3640	4.8700	6.5090	8.1243	9.7004	11.2569	
2.0	1.3077	1.8209	2.4451	3.2917	4.5871	7.0204	11.3961	18.2321	26.8994	36.4824	
2.5	1.8838	4.5591	6.6553	7.5932	7.6711	10.6964	21.3538	42.8630	72.5836	106.4097	

models, due to the use of 60% more data points in about 4% which can be neglected. Therefore, an interpolated data points set can be used without sacrificing accuracy making it possible to try using higher order polynomials with more parameters in order to achieve the best fitting model.

One nonlinear model only will be considered here; which has the shape of (Model II) described by equation (E-4) and (E-5).

Model 4

$$U_4^* = \ln [(P.V.A.C)^*] = \beta_0 + \beta_1 Q^{*\beta_4} + \beta_2 H^{*\beta_5} + \beta_3 H^{*\beta_6} Q^{*\beta_7}$$

(F-11)

E.7 Results

The preceding four models parameters, β 's, are listed here with their 95% confidence intervals. The residual root mean square, RRMS is also computed for each model as a primary criterion for selection.

Confidence Intervals on the "Model 1" β 's.

$$\beta_0 = -2.669 \pm 0.3550$$

$$\beta_1 = 1.132 \pm 0.2540$$

$$\beta_2 = 0.5854 \pm 0.2502$$

$$\beta_3 = 0.6092 \pm 0.1782$$

Degree of Freedom (f) = 66

Sum of Residuals Squares (SRS) = 8.8307

Residual Root Mean Square (RRMS) = 0.3658

Confidence Intervals on the "Model 2" B's

$$\beta_0 = -3.449 \pm 0.651$$

$$\beta_1 = 2.145 \pm 1.38$$

$$\beta_2 = -0.2472 \pm 0.5353$$

$$\beta_3 = 1.258 \pm 1.121$$

$$\beta_4 = 1.193 \pm 2.377$$

$$\beta_5 = -0.5359 \pm 0.922$$

$$\beta_6 = -0.2411 \pm 0.4231$$

$$\beta_7 = -0.2790 \pm 0.897$$

$$\beta_8 = 0.228 \pm 0.348$$

Degrees of Freedom (f) = 61

Sum of Residuals Squares (SRS) = 3.3181

Residual Root Mean Square (RRMS) = 0.2332

Confidence Intervals on the "Model 3" B's.

$$\beta_0 = -4.2672 \pm 1.354$$

$$\beta_1 = 5.2190 \pm 5.701$$

$$\beta_2 = -1.967 \pm 5.3609$$

$$\beta_3 = 0.1989 \pm 1.557$$

$$\beta_4 = 2.3097 \pm 3.905$$

$$\begin{aligned}
 \beta_5 &= 0.2923 \text{ +/-} 16.458 \\
 \beta_6 &= -3.8652 \text{ +/-} 15.465 \\
 \beta_7 &= 1.6088 \text{ +/-} 3.916 \\
 \beta_8 &= -0.9695 \text{ +/-} 3.292 \\
 \beta_9 &= -0.5704 \text{ +/-} 13.870 \\
 \beta_{10} &= 4.1977 \text{ +/-} 13.032 \\
 \beta_{11} &= -1.6745 \text{ +/-} 3.301 \\
 \beta_{12} &= 0.1806 \text{ +/-} 0.8374 \\
 \beta_{13} &= 0.1102 \text{ +/-} 3.529 \\
 \beta_{14} &= -1.0534 \text{ +/-} 3.316 \\
 \beta_{15} &= 0.4385 \text{ +/-} 0.840
 \end{aligned}$$

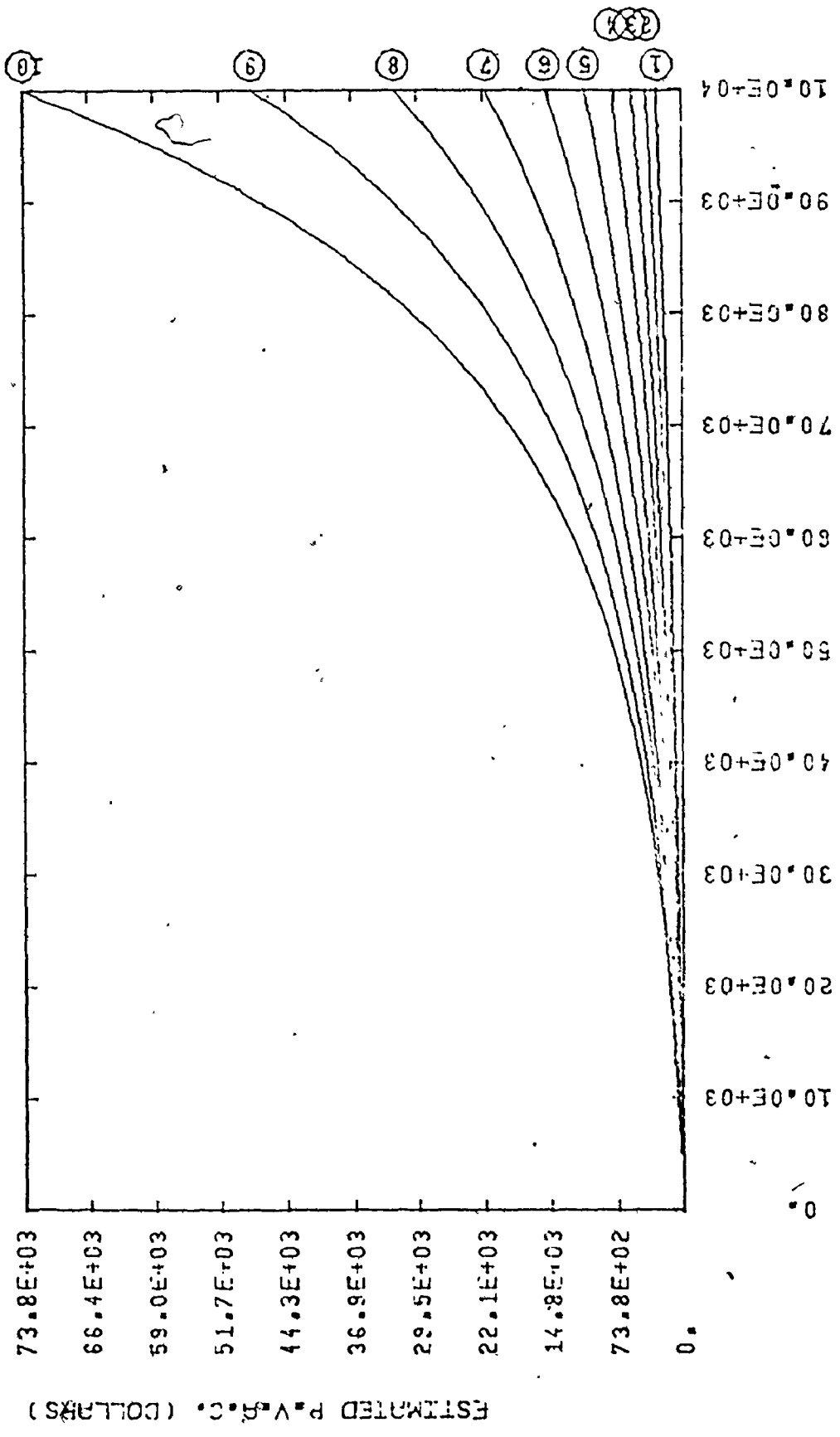
Degrees of Freedom (f) = 54

Sum of Residuals Squares (SRC) = 1.457

Residual Root Mean Square (RRMS) = 0.1643

Confidence Intervals on the "Model 4" β 's:

$$\begin{aligned}
 \beta_0 &= -13.6784 \text{ +/-} 31.99 \\
 \beta_1 &= 7.0880 \text{ +/-} 2.922 \\
 \beta_2 &= 6.5962 \text{ +/-} 20.274 \\
 \beta_3 &= 0.1442 \text{ +/-} 0.088 \\
 \beta_4 &= 0.1790 \text{ +/-} 0.088 \\
 \beta_5 &= 0.1221 \text{ +/-} 0.378 \\
 \beta_6 &= 1.9750 \text{ +/-} 0.477 \\
 \beta_7 &= 1.5468 \text{ +/-} 0.310
 \end{aligned}$$



CURVE NUMBER...	HEAD RISE (IN. WATER)	VOLUME FLOW RATE (CFM)
1	20.0E-01	10.0E+03
2	30.0E-01	10.0E+03
3	40.0E-01	10.0E+03
4	50.0E-01	10.0E+03
5	60.0E-01	10.0E+03
6	70.0E-01	10.0E+03
7	80.0E-01	10.0E+03
8	90.0E-01	10.0E+03
9	10.0E+00	10.0E+03
10	11.0E+00	10.0E+03

Figure F.1.1. Surface Generated by the Empirical Formula "Model 4".

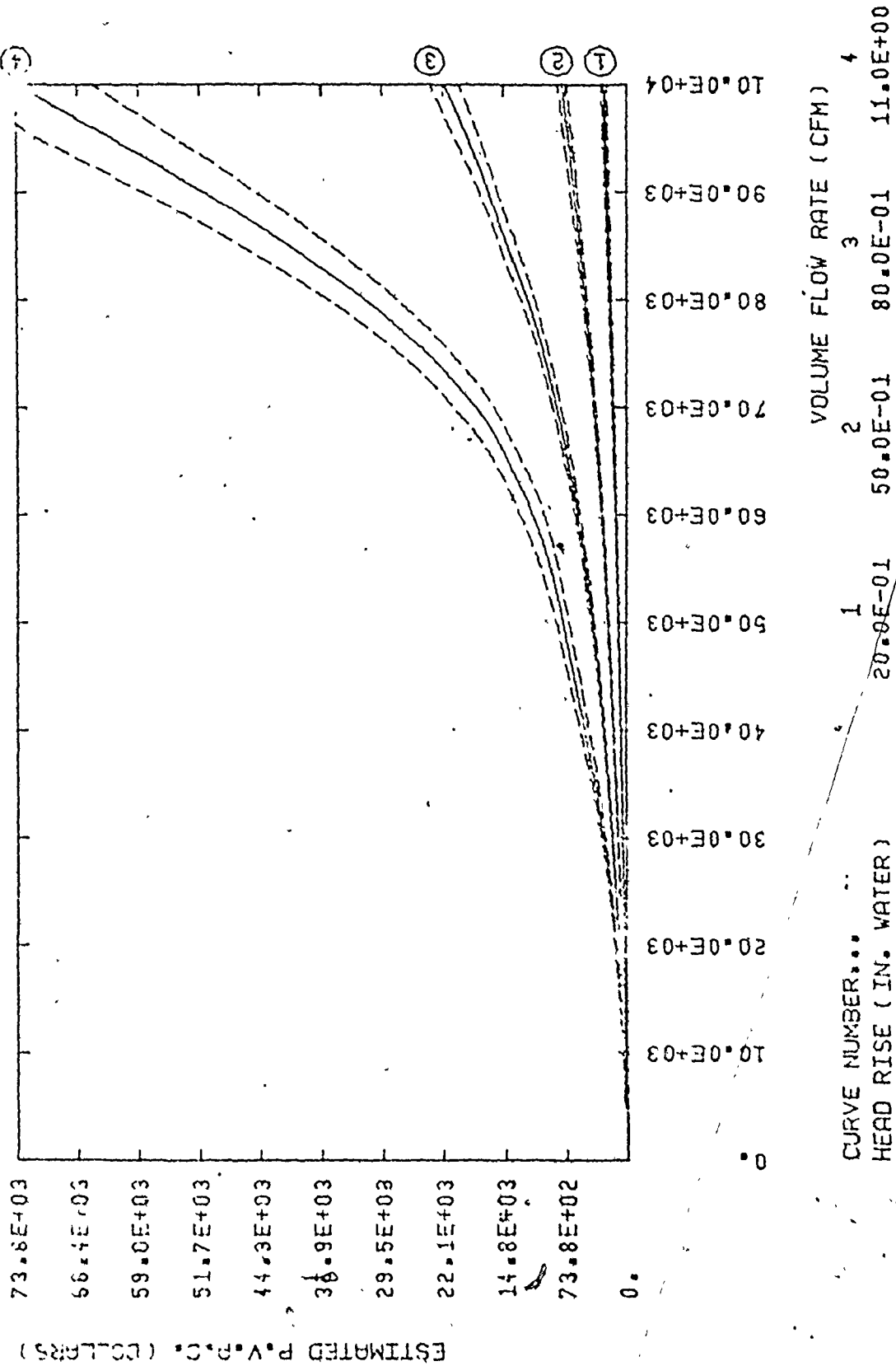


Figure E.2. Confidence Limits of the "Model4" Function Value.

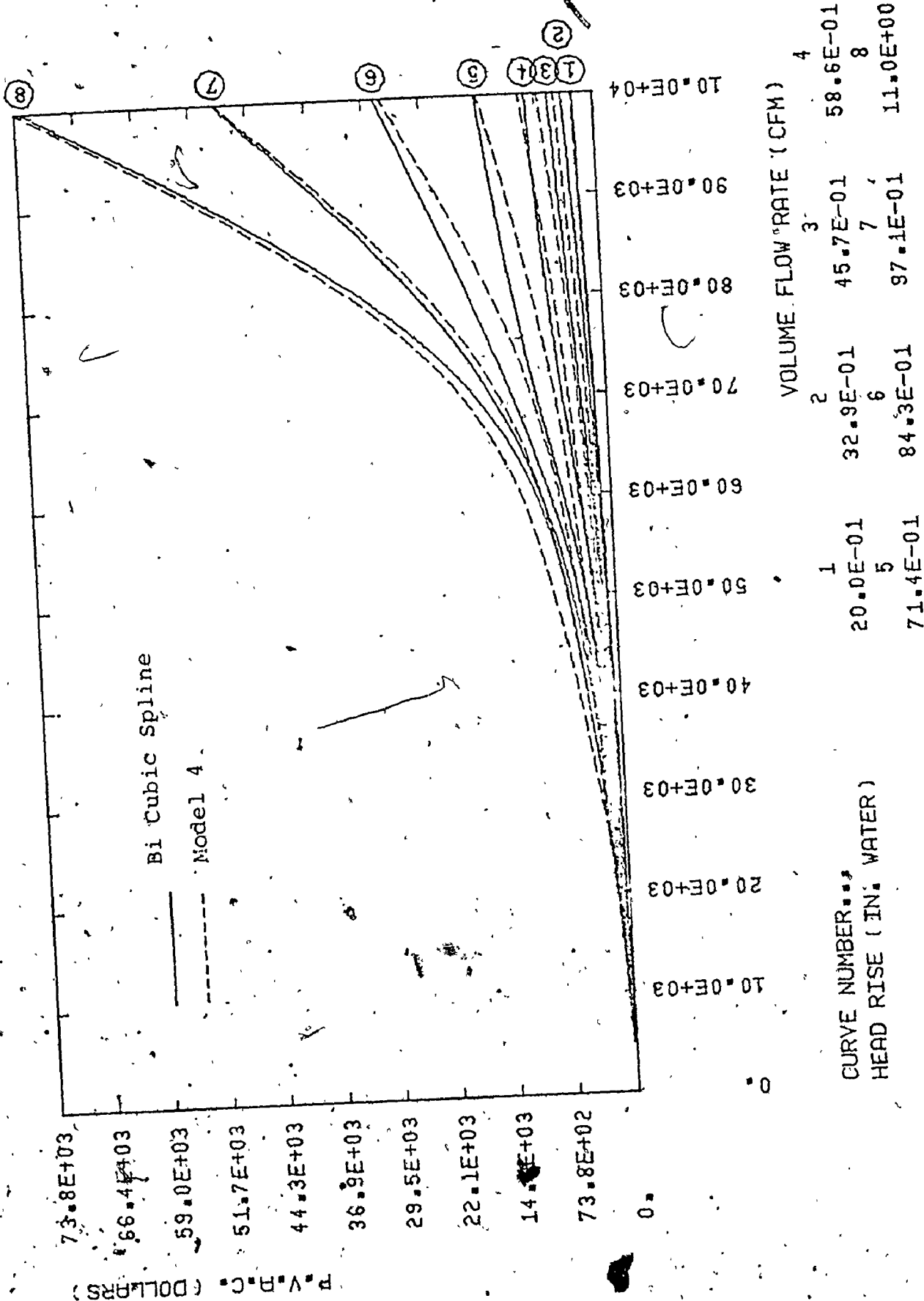


Figure E.3. Comparison Between Model 4 and Bi-cubic Spline Fits.

Degrees of Freedom (f) = 62
Sum of Residuals Squares (SRS) = 1.2496
Residual Root Mean Square (RRMS) = 0.142

Table E-4 lists the sum of the squares of the residuals for each model and the respective root mean squares. There appears to be no significant differences in the fits of the models. By arbitrarily eliminating the first linear model with the largest variance, the choice of models is reduced to a choice between Model 2 and Model 4 and between Model 3 and Model 4. We shall use the test of Williams and Klot to ascertain which of the three models is the best.

Table E-5 lists the data and calculations needed for Equation E-6. The slopes of the best fitting lines through the original, computed from equations (E-6a, E-6b and E-6c), are -0.5383 and -0.2394 for Models 2-4 and Models 3-4, respectively. Therefore, we might conclude that Model 4 represents the data best. However, a non-linear model with a higher order will lead to a better regression with a less variance.

Table E-6 lists the input data points, the estimated points using Model 4 equation, and their deviation from the input points. On the other hand, Table E-6 also shows the original data before taking the natural logarithm of the P.V.A.C. values, compared with those computed from Model 4,

Table E-3. Effect of increasing the sample size on the deviation from linear regression.

Number of Data Points	20			72		
Linear Model	1	2	3	1	2	3
Degree of freedom	24	19	12	66	61	54
Sum of Residual Squares (SRS)	3.4879	1.1152	0.4843	8.8307	3.3181	1.457
(RRMS)	0.3812	0.2423	0.2009	0.3658	0.2332	0.1643

Table E-4. Identification of the Best Model; Based on (RRMS)

Model	Degrees of Freedom (f)	Sum of Residuals Squares (SRS)	Residual Root Mean Squares (RRMS)
1	66	8.8307	0.3658
2	61	3.3181	0.2332
3	54	1.457	0.1643
4	62	1.2496	0.1420

TABLE E-5 CALCULATIONS FOR THE WILLIAMS AND KLOOT TEST

i	U_i ln(P. V.A.C)	U_2^* MODEL	U_3^* MODEL	U_4^* MODEL	γ_{24} $U_i \frac{-(U_2^* + U_4^*)}{2}$	γ_{34} $U_i \frac{-(U_3^* + U_4^*)}{2}$	a_{24}^2 $U_2^* - U_4^*$	a_{34}^2 $U_3^* - U_4^*$	
1	-0.210	-2.780	-2.990	-3.026	-0.302	-0.172	0.336	0.096	
2	-2.423	-2.131	-2.263	-2.323	-0.165	-0.097	0.254	0.117	
3	-2.013	-1.724	-1.863	-1.989	-0.157	-0.027	0.255	0.126	
4	-1.716	-1.508	-1.541	-1.703	-0.110	-0.094	0.195	0.026	
5	-2.332	-2.485	-2.458	-2.465	0.143	0.174	-0.021	-0.084	
6	-1.698	-1.842	-1.839	-1.757	0.101	0.100	-0.085	-0.083	
7	-1.290	-1.405	-1.445	-1.349	0.087	0.106	-0.057	-0.096	
8	-1.013	-1.176	-1.152	-1.045	0.093	0.081	-0.131	-0.108	
9	-1.440	-1.892	-1.513	-1.511	0.217	0.072	-0.299	-0.002	
10	-0.714	-1.041	-0.821	-0.772	0.193	0.049	-0.269	-0.049	
11	-0.284	-0.513	-0.339	-0.307	0.126	0.054	-0.206	-0.062	
12	0.028	-0.219	-0.122	0.079	0.097	0.049	-0.298	-0.201	
13	-0.643	-0.832	-0.542	-0.569	0.103	-0.038	-0.163	0.127	
14	-0.010	-0.072	0.189	0.150	-0.049	-0.139	-0.222	0.039	
15	0.773	0.755	0.927	0.759	0.010	-0.070	0.035	0.167	
16	1.106	1.243	1.238	1.357	-0.197	-0.199	-0.103	-0.104	
17	-0.142	-0.075	-0.121	-0.115	-0.048	-0.023	0.049	-0.096	
18	0.781	0.997	0.712	0.810	-0.073	0.020	0.098	-0.093	
19	1.372	1.784	1.736	1.612	0.174	0.173	0.171	0.175	
21	0.263	0.470	0.291	0.313	-0.123	0.011	0.157	-0.112	
22	1.181	1.465	1.177	1.364	-0.029	-0.079	1.101	-0.136	
23	2.433	2.541	2.429	2.398	-0.036	0.024	0.143	0.023	
24	3.397	3.693	3.524	3.698	-0.056	0.026	0.090	-0.073	
25	0.683	0.892	0.576	0.669	-0.122	-0.139	0.133	0.293	
26	2.697	1.745	2.014	1.864	0.239	0.093	-0.119	0.149	
27	0.051	3.933	0.041	3.164	-0.040	-0.041	-0.123	-0.123	
28	1.357	3.531	0.597	3.759	-0.053	-0.159	-0.073	0.135	
					Σ	-0.275	-0.371	-0.097	-0.039
					λ_{24}	-0.0003			
					λ_{34}	-0.0003			
					Σ				

TABLE E-6 PERCENTAGE DEVIATION

i	U_i $\ln(\frac{PV_i}{AC})$	U_4^*	$(U_i - U_4^*)$ R_i	% DEV- IATION	$(PVAC)$ $(PVAC/29)$	$(PVAC)^*$ $\text{Exp}(U_4^*)$	$(PVAC)$ $PVAC$ R_i	%DEV- IATION
1	-3.210	-3.086	-0.124	3.86	0.040	0.046	0.005	11.65
2	-2.423	-2.383	-0.039	1.59	0.089	0.092	0.003	3.78
3	-2.013	-1.989	-0.024	1.19	0.134	0.137	0.003	2.37
4	-1.716	-1.703	-0.013	0.75	0.180	0.182	0.002	1.29
5	-2.032	-2.465	0.133	5.69	0.097	0.085	0.012	14.18
6	-1.698	-1.737	0.059	3.48	0.133	0.173	0.011	6.09
7	-1.299	-1.349	0.059	4.56	0.275	0.269	0.016	6.06
8	-1.018	-1.045	0.028	2.71	0.361	0.352	0.010	2.89
9	-1.449	-1.511	0.072	4.97	0.237	0.221	0.016	7.49
10	-0.714	-0.772	0.058	8.18	0.490	0.462	0.028	6.01
11	-0.284	-0.397	0.023	3.17	0.733	0.736	0.017	2.34
12	0.023	0.079	-0.052	--	1.027	0.959	0.078	5.03
13	-0.643	-0.669	0.026	4.05	0.526	0.512	0.014	2.64
14	-0.010	0.159	-0.169	--	0.990	0.852	0.138	14.80
15	0.773	0.760	0.013	1.68	2.167	2.139	0.028	1.30
16	1.196	1.357	-0.251	22.67	3.0213	3.883	0.886	22.14
17	-0.142	-0.114	-0.028	19.61	0.867	0.692	0.023	2.75
18	0.789	0.309	-0.029	3.69	2.133	2.247	0.064	2.34
19	1.872	1.612	0.261	13.95	6.509	5.013	1.496	29.80
20	2.421	2.487	-0.066	2.73	11.257	12.025	0.768	6.49
21	0.268	0.313	-0.045	16.73	1.308	1.368	0.060	4.49
22	1.191	1.364	-0.172	14.45	3.292	3.910	0.618	15.81
23	2.433	2.323	0.036	1.47	11.396	19.997	0.399	3.60
24	3.597	3.698	-0.011	0.31	36.432	36.839	0.407	1.10
25	0.633	0.659	-0.025	5.37	1.334	1.952	0.063	3.47
26	2.027	1.854	0.163	8.83	7.593	6.951	1.122	17.71
27	3.151	3.164	-0.193	3.06	21.354	23.697	2.613	9.29
28	4.667	4.759	-0.092	1.97	106.71	116.64	10.13	8.89

PERCENT DEVIATION FROM MEAN = 7.00%

Table E-7. Estimated Function Value and its Confidence Limit

		Estimated Function Value and Pairs of Confidence Limits By Using Model 4.				
Q	H	0.4	1.0	1.6	2.2	
0.1		-3.0859+/- .1506	-2.3845+/- .1018	-1.9888+/- .0887	-1.7028+/- .1253	
0.2		-2.4646+/- .1362	-1.7566+/- .0728	-1.3488+/- .0651	-1.0454+/- .1112	
0.5		-1.5113+/- .1294	-0.7720+/- .0795	-0.3070+/- .0688	0.0792+/- .0970	
1.0		-0.6686+/- .1099	0.1500+/- .0693	0.7601+/- .0602	1.3565+/- .1099	
1.5		-0.1144+/- .1065	0.8094+/- .0622	1.6120+/- .0695	2.4870+/- .1307	
2.0		0.3132+/- .1213	1.3635+/- .0686	2.3976+/- .0776	3.6079+/- .1332	
2.5		0.6686+/- .1451	1.8642+/- .0922	3.1641+/- .1197	4.7591+/- .2083	

where the actual percentage deviations are given.

E-8 Conclusion

The following sequence of procedures is suggested by the author for successful execution of a multi-variable nonlinear fitting with reasonable accuracy.

1. Knowing in advance the shape of the input data curve, surface of hypersurface, (depending upon the number of independent variables), a natural logarithm or exponential of the dependent variable is likely to be successful.

2. For better computation accuracy, it is advisable to normalize both the dependent and independent variables.

3. Spline interpolation could be used to increase the normalized input data set.

4. A preliminary estimate of the nonlinear model parameters, β , are computed using an equivalent linear model, Model I, by least square technique. For example, the preliminary estimates of Model 4 parameters are ($\beta_0 = -2.669$, $\beta_1 = 1.132$, $\beta_2 = 0.5854$, $\beta_3 = 0.6092$, and $\beta_4 = \beta_5 = \beta_6 = \beta_7 = 1.0$), which were obtained from Model 1.

5. A nonlinear technique finally has to be applied until a conversion is achieved to an optimum minimum square residuals sum.

6. Statistical analysis of the model parameters and estimated function values have to be carried out. If the

suggested model variance is more than a permissible limit a higher order nonlinear model might be tried.

Finally, we can conclude that Model II is a good multi-variable nonlinear fitting equation form. For example, for a case of three independent variables, Y_1 , Y_2 , and Y_3 , and for a first order model, ($n_1 = n_2 = n_3 = 1$, Equations E-4 and E-5), Model II can be written as follows:

$$U_{II}^* = \beta_0 + \beta_1 Y_1 + \beta_2 Y_1^2 + \beta_3 Y_2 + \beta_4 Y_2^2 + \beta_5 Y_3 + \beta_6 Y_3^2 + \beta_7 Y_1 Y_2 + \beta_8 Y_1 Y_2^2 + \beta_9 Y_1^2 Y_2 + \beta_{10} Y_1 Y_3 + \beta_{11} Y_1^2 Y_3 + \beta_{12} Y_1 Y_2 Y_3 + \beta_{13} Y_2^2 Y_3 + \beta_{14} Y_1 Y_2^2 Y_3 + \beta_{15} Y_1^2 Y_2 Y_3 + \beta_{16} Y_1 Y_2 Y_3^2 + \beta_{17} Y_1^2 Y_2 Y_3 + \beta_{18} Y_1 Y_2^2 Y_3 + \beta_{19} Y_1^2 Y_2^2 Y_3 \quad (E-12)$$

An important aspect for further research in the area of nonlinear curve fitting applied to Type B trade-off hypersurfaces is the establishment of the model order, in improving the programing convergence, and in searching for a convenient feasible way of model discrimination. Such characteristics can only be studied through difficult and tedious statistical and optimization analysis. We have however, obtained reasonable success in the present work, and our suggested nonlinear model give quite reasonable deviations from the original data set.

APPENDIX FUSER'S MANUAL TO GENERATE ANDPLOT A TRADE-OFF SURFACE

SUBROUTINE TRAD2 (N, RMAX, RMIN, XSTRT, NCONS,
 NEQUS, IPRINI, IDATA, IGEN, NY1,
 NY2, NSP1, NHY1, NHY2, NHU, SCALE,
 UT, Y1, Y2, HY1, HY2, HU, UTP, W)

Purpose

To plot a trade-off surface $U(y_1, y_2)$ versus two input design specifications designated y_1 and y_2 . The trade-off surface, which can be developed explicitly or introduced by the user, is a locus of all optimum design generated by

$$U(x_1, x_2, \dots, x_n) \rightarrow \text{Minimum}$$

subject to

$$\begin{aligned} \phi_k(x_1, x_2, \dots, x_n) &\geq 0 & k=1, p \\ \psi_j(x_1, x_2, \dots, x_n) &= 0 & j=1, m \end{aligned}$$

where, y_1 and y_2 occur in one or more of the constraint functions, and/or the optimization function. Cubic spline technique is used to interpolate between the generated optimum design points.

Input Variables

- Y1(I) . array of discrete values for first input specifications, dimensioned with the value of NY1. The values must be equally spaced in ascending order.
- Y2(I) array of discrete values for second input specifications, dimensioned with the value of NY2. The values must be in ascending order.
- NY1 } number of first specification values.
- NY2 } number of second specification values.
- UT(I,J) optimum function values corresponding to Y1(I) and Y2(J), dimensioned with the value of NY1, NY2. It is an input matrix for IGEN=0, and a working array otherwise.
- NSP1 number of points used in smoothing each of the NY2 curves. A value between (50-100) is adequate.
- NHY1 number of characters to be plotted Y1 label.
- NHY2 number of characters to be plotted Y2 label.
- NHU number of characters to be plotted UT label.
- SCALE scale factor for plot size, (equals one for 7 x 4 in. frame).
- HY1(I) Hollerith Y1 label, dimensioned with the value of IFIX (1. + FLOAT (NHY1)/10).
- HY2(I) Hollerith Y2 label, dimensioned with the value of IFIX (1. + FLOAT (NHY2)/10.).

HU(I) Hollerith UT label, dimensioned with the value of
 IFIX (1. + FLOAT(NHU)/10.).

IGEN = 0, optimum trade-off surface points are introduced
 by the user.

= 1, SEEK1 optimization subroutine is used to generate
 the trade-off surface.

= 2, SEEK3 optimization subroutine is used to generate
 the trade-off surface.

= 3, ADRANS optimization subroutine is used to gene-
 rate the trade-off surface.

The foregoing input variables must be specified in every case.
 However, the following input variables need only to be speci-
 fied if IGEN is unequal to zero.

N number of design or independent variables.

NCONS the number of inequality constraints.

NEQUS the number of equality constraints.

IPRINT prints results every IPRINT minimizations, set=0 for
 no intermediate output.

IDATA = 1, all input data is printed out.
 = 0, input data is not printed out.

RMAX(I) estimated upper bounds on X(I), dimensioned with
 the value of N.

RMIN(I) estimated lower bounds on X(I), dimensioned with
 the value of N.

XSTRT(I) starting value for X(I) used only with Y1(1) and
 Y2(1), dimensioned with the value of N.

Output Variable

UTP(I,J) interpolated UT values, dimensioned with the values of (NSP1, NY2).

Working Array

W(I) dimensioned with K
 where, $K = N + NCONS + NEQUS + 2*NY2 + 6*NSP1 + MAX(3*NY1 + 4*NY2)$
 for, IGEN = 0, the values of N, NCONS, and NEQUS are also set at zero.

Programming Information

If IGEN is not zero, the following common statement must be attached to the UREAL, CONST, and EQUAL subroutines,

COMMON/A/ SY1, SY2

where, SY1 and SY2 are the two input design specifications in question, and may occur in any of the functions.

The output fully labelled plot can be obtained either by the Benson-Lehner or Versatec using suitable control cards.

NY2 solid curves will be plotted for the feasible range of Y1, while an extrapolated dashed line will be plotted for the infeasible regions.

UT(1,1) must be feasible.

Subroutines called are SEEK1, SEEK3, ADRANS, ANSWER, UREAL, EQUAL, MAP2, T2, IBCIEU, PLOT, UNITTC, DDASHM, PLTMPL

	SUBROUTINE TRAD2 (N, RMAX, RHIN, XSTRT, NCONS, NEQUS, IPRINT, IDATA, IGEN, NY1, NY2, N	TRA	10
	=====		
	NY1, NY2, NSP1, RHY1, RHY2, RHU, UT, Y1, Y2, HY1, HY2, HU, UTP, W)	TRA	20
	DIPERSON RMAX(1), RHHC(1), XSTRT(1), HY1(1), HY2(1), HUC(1), UT(NY	TRA	30
	11, 1), UTP(RSP1, 1), WC(1), Y1(1), Y2(1)	TRA	40
	IC=1	TRA	50
	IF (N.EQ.0) GO TO 1	TRA	60
	IA=0+10	TRA	70
	GO TO 2	TRA	80
1	CONTINUE	TRA	90
	IA=10+1	TRA	100
2	IF (NCONS.EQ.0) GO TO 3	TRA	110
	IB=IA+NCONS	TRA	120
	GO TO 4	TRA	130
3	IB=IA+1	TRA	140
4	IF (NEQUS.EQ.0) GO TO 5	TRA	150
	IC=IB+NEQUS	TRA	160
	GO TO 6	TRA	170
5	IC=IB+1	TRA	180
6	I1=IC+RSP1	TRA	190
	I2=I1+RSP1	TRA	200
	I3=I2+RSP1	TRA	210
	I4=I3+RSP1	TRA	220
	I5=I4+RSP1	TRA	230
	I6=I5+RSP1	TRA	240
	I7=I6+NY2	TRA	250
	I8=I7+NY2	TRA	260
	IGEN=RMAX(3*NY1, 4*NY2)	TRA	270
	IO=I8+RHN	TRA	280
	CALL T2 (N, RMAX, RHIN, XSTRT, NCONS, NEQUS, IPRINT, IDATA, IGEN, NY1, NY2, N	TRA	290
	ISP1, RHY1, RHY2, RHU, UT, Y1, Y2, HY1, HY2, HU, UTP, WC(10), WC(11), WC(12),	TRA	300
	WC(13), WC(14), WC(15), WC(16), WC(17), WC(18))	TRA	310
	RETURN	TRA	320
	END	TRA	330

```

SUBROUTINE T2 (N, RMAX, RMIN, XSTRT, NCONS, NEQUS, IPRINT, IDATA, IGEN, NY1 T20 10
=====
1, NY2, NSP1, NHY1, NHY2, NHU, UT, Y1, Y2, HY1, HY2, HU, UTP, X, PHI, PSI, W1, W2, W3 T20 20
2, W4, W5, SP1, W6, WM, W7) T20 30
DIMENSION Y1(1), Y2(1), RMAX(1), RMIN(1), XSTRT(1), X(1), PHI(1), T20 40
IPSI(1), W1(1), W2(1), W3(1), W4(1), W5(1), W6(1), SP1(1), UT(NY1,1 T20 50
2), UTP(NSP1,1), W7(1), WK(1) T20 60
COMMON /A/ SY1, SY2 T20 70
COMMON /OPT1/ KO, NINDEX T20 80
IK=1 T20 90
SCALE=1. T20 100
IF (IGEN.EQ.0) GO TO 1 T20 110
IF (NSP1.GT.70) GO TO 1 T20 120
WRITE (6,30) T20 130
RETURN T20 140
1 CONTINUE T20 150
DO 2 I=1, NY2 T20 160
WK(I)=FLOAT(NSP1) T20 170
2 CONTINUE T20 180
IF (IGEN.EQ.0) GO TO 15 T20 190
KI=KJ=1 T20 200
3 CONTINUE T20 210
DO 13 J=KJ, NY2 T20 220
DO 11 I=KI, NY1 T20 230
SY1=Y1(I) T20 240
SY2=Y2(J) T20 250
GO TO (4,5,6), IGEN T20 260
4 CALL SEEK1 (N, RMAX, RMIN, NCONS, NEQUS, .01, .01, XSTRT, 9, 100, 300, IPRINT T20 270
1, IDATA, X, U, PHI, PSI, W1, W2, W3, W4) T20 280
GO TO 7 T20 290
5 CALL SEFK3 (N, RMAX, RMIN, NCONS, NEQUS, XSTRT, .01, .01, 1, .05, 300, 1, IPR T20 300
1INT, IDATA, U, X, PHI, PSI, W1, W2, W3, W4) T20 310
GO TO 7 T20 320
6 CALL ADTRANS (N, RMAX, RMIN, NCONS, NEQUS, 100, P3, 50, XSTRT, IPRINT, IDATA, T20 330
IX, U, PHI, PSI, W1, W2, W3, W4) T20 340
7 IF (IPRINT.NE.0) CALL ANSWER (U, X, PHI, PSI, N, NCONS, NEQUS) T20 350
UT(I, J)=U T20 360
DO 8 II=1, N T20 370
XSTRT(II)=X(II) T20 380
8 CONTINUE T20 390
IF (L.GT.1) GO TO 10 T20 400
DO 9 II=1, N T20 410
W5(II)=X(II) T20 420
9 CONTINUE T20 430
10 IF (KO.EQ.1) IEXIT=IEXIT+1 T20 440
IF (I.EQ.1.AND.J.EQ.1) GO TO 14 T20 450
IF (I.EQ.NY1) GO TO 21 T20 460
IF (IEXIT.GE.2) GO TO 21 T20 470
11 CONTINUE T20 480
DO 12 II=1, N T20 490
XSTRT(II)=W5(II) T20 500
12 CONTINUE T20 510
13 CONTINUE T20 520
14 WRITE (6,31) T20 530
15 SP1(I)=Y1(I) T20 540
DSP1=(Y1(NY1)-Y1(I))/FLOAT(NSP1-1) T20 550
DO 16 I=3, NSP1 T20 560
SP1(I)=SP1(I-1)+DSP1 T20 570
16 CONTINUE T20 580
CALL IBCIEU (UT, NY1, Y1, NY1, Y2, NY2, SP1, NSP1, Y2, NY2, UTP, NSP1, W7, IE) T20 590
W2(1)=W2(2)=UTP(1, IK) T20 600
W1(1)=Y1(1) T20 610
W1(2)=Y1(NY1) T20 620
DO 17 I=1, NSP1 T20 630
DO 17 J=1, NY2 T20 640
IF (UTP(I, J).LT.W2(1)) W2(1)=UTP(I, J) T20 650
IF (UTP(I, J).GT.W2(2)) W2(2)=UTP(I, J) T20 660
17 W6(J)=UTP(NSP1, J) T20 670
CALL MAP2 (W1, W2, 2, HY1, HY2, HU, NHY1, NHY2, NHU, W6, Y2, NY2, SCALE) T20 680
DO 20 J=1, NY2 T20 690
MM=IFIX(WK(J)) T20 700
DO 18 I=1, NSP1 T20 710
W1(I)=UTP(I, J) T20 720
18 CONTINUE T20 730

```


	CALL PLTHPL (SP1,W1,IMM)	T20 740
	IF (MM.CE.NSP1) GO TO 20	T20 750
	IS=0	T20 760
	DO 19 I=MM,NSP1	T20 770
	IS=IS+1	T20 780
	CALL UNITTO (SP1(I),W1(I),W2(IS),W3(IS))	T20 790
19	CONTINUE	T20 800
	NDA=NSP1-IMM+1	T20 810
	CALL DDASHN (W2,W3,NDA,...1,0,.05,1.,IE,W4,W5)	T20 820
20	CONTINUE	T20 830
	CALL PLOT (12.,0.0,-3)	T20 840
	CALL PLOT (0.0,0.0,999)	T20 850
	RETURN	T20 860
21	IF (IEXIT.EQ.1) GO TO 28	T20 870
	IF (I.LT.4) GO TO 25	T20 880
	I1=I-1	T20 890
	DIF=UT((I-2),J)-UT((I-3),J)	T20 900
	IF (I.EQ.4) GO TO 23	T20 910
	RAT=DIF-(UT((I-3),J)-UT((I-4),J))	T20 920
	DO 22 IU=11,NY1	T20 930
	UT(IU,J)=UT((IU-1),J)+DIF+RAT	T20 940
	RAT=RAT*2.	T20 950
22	CONTINUE	T20 960
	GO TO 29	T20 970
23	DO 24 IU=11,NY1	T20 980
	UT(IU,J)=UT((IU-1),J)+DIF	T20 990
24	CONTINUE	T20 1000
	GO TO 29	T20 1010
25	IF (J.EQ.1) GO TO 27	T20 1020
	DO 26 IU=11,NY1	T20 1030
	UT(IU,J)=UT((IU-1),J)+UT(IU,(J-1))-UT((IU-1),(J-1))	T20 1040
26	CONTINUE	T20 1050
	GO TO 29	T20 1060
27	WRITE (6,32) UT(1,IK),Y1(1),Y2(1)	T20 1070
	RETURN	T20 1080
28	UT(I,J)=UT((I-1),J)+(UT((I-1),J)-UT((I-2),J))*2.-(UT((I-2),J)-UT((I-3),J))	T20 1090
29	IF (J.EQ.NY2) GO TO 15	T20 1100
	KJ=J+1	T20 1110
	WK(J)=(FLOAT((I-IEXIT)*NSP1)/FLOAT(NY1-1))+1.	T20 1120
	GO TO 3	T20 1130
C		T20 1140
C		T20 1150
30	FORMAT (5X,33H(NSP1) HAS TO BE GREATER THAN (N)/)	T20 1160
31	FORMAT (5X,33HSTARTING POINT HAS TO BE FEASIBLE)	T20 1170
32	FORMAT (5X,4HDECREASE THE INDEPENDENT VARIABLES STEP SIZE,/,5X,55	T20 1180
	1UWHEN THE PROGRAM HUNG UP THE ONLY FEASIBLE POINT WAS U=,E12.5,/,5	T20 1190
	24X,6HAT Y1=,E12.5,7HAND Y2=,E12.5)	T20 1200
	END	T20 1210
		T20 1220

	SUBROUTINE MAP2 (X, Y, H, HX, HY, HO, NHX, NHY, NHO, WY, WV, NYC, SCALE)	MAP 10
	=====	
C	DIMENSION X(1), Y(1), HX(1), HY(1), HO(1), WY(1), WV(1), W1(2)	MAP 20
	IF (SCALE.LE.1.) SCC=1.	MAP 30
	IF (SCALE.GT.1.) SCC=SCALE	MAP 40
	IC=1	MAP 50
	NX=10	MAP 60
	NY=10	MAP 70
	YYH=.05*SCC	MAP 80
	XXH=.07*SCC	MAP 90
	OH=.1*SCALE	MAP 100
	OX=.8*SCALE	MAP 110
	YHH=.15*SCALE	MAP 120
	DYE=.4*SCALE	MAP 130
	YHO=.9*SCALE	MAP 140
	XH=2.0*SCALE	MAP 150
	ZHY=2.3*SCALE	MAP 160
	ZW1=2.5*SCALE	MAP 170
	XHO=2.7*SCALE	MAP 180
	ZXD=2.9*SCALE	MAP 190
	YM=4.0*SCALE	MAP 200
	YL=8.0*SCALE	MAP 210
	XL=9.0*SCALE	MAP 220
	DXE=1.2*SCALE	MAP 230
	YE2=2.3*SCALE	MAP 240
	YE1=2.5*SCALE	MAP 250
	EXIT=1.0	MAP 260
	YOH=0.0	MAP 270
	HX1=NX+1	MAP 280
	HY1=NY+1	MAP 290
	NUL=NHX/10	MAP 300
	IF (NUL.EQ.0) NUL=1	MAP 310
	NCON=6-NUL	MAP 320
	XE1=FLOAT(NUL)*DXE+3.04*SCALE	MAP 330
	XE2=FLOAT(NUL)*DXE+2.54*SCALE	MAP 340
	DATA W1/10HCURVE NUMB,6HER...	MAP 350
	XX=XL-FLOAT(HHX)*0.1*SCALE	MAP 360
	ZZ=YL-FLOAT(HHO)*0.1*SCALE	MAP 370
	CALL DATE (D1)	MAP 380
	CALL LETTER (10,0.2,90,0.,3.5.,10H*TRAD-OFF*)	MAP 390
	CALL LETTER (10,0.1,90,0,0.6,3.5,D1)	MAP 400
	CALL PLOT (1.,0.0,-3)	MAP 410
C		MAP 420
C	WRITE (UT) LABLE	MAP 430
C		MAP 440
	CALL LETTER (NHO,OH,90.,OX,ZZ,HO)	MAP 450
	CALL FACTOR (H,X,Y,XL,YL,XH,YH)	MAP 460
C		MAP 470
C	PLOTTING GRAPHS FRAM	MAP 480
C		MAP 490
	CALL PLOT (XM,YH,3)	MAP 500
	CALL PLOT (XL,YH,2)	MAP 510
	CALL PLOT (XL,YL,1)	MAP 520
	CALL PLOT (XH,YL,1)	MAP 530
	CALL PLOT (YM,YH,1)	MAP 540
	XS=(XL-XD)/FLOAT(NX)	MAP 550
	YS=(YL-YD)/FLOAT(NY)	MAP 560
	XH=XI	MAP 570
	YH=YM	MAP 580
C		MAP 590
C	DIVIDING THE VERTICAL AXIS	MAP 600
C		MAP 610
	DO 1 I=1,NY1	MAP 620
	CALL PLOT (XH,YH,3)	MAP 630
	CALL PLOT (XH+XXH,YH,2)	MAP 640
C		MAP 650
C	WRITTING THE (UT) NUMERICAL VALUES	MAP 660
C		MAP 670
	CALL INCHTO (XM,YH,XP,YP)	MAP 680
	ENCODE (10,12,YD) YP	MAP 690
	CALL LETTER (10,OH,0.,YHO,YH-YYH,YD)	MAP 700
	YH=YH+YS	MAP 710
	IF (YH.GT.YL) YH=YL	MAP 720
1	CONTINUE	MAP 730

```

DO 2 I=1, NX1
CALL PLOT (XH, YL-XXH, 3)
CALL PLOT (XH, YL, 2)
XH=XH+XS
CONTINUE
YH=YL
DO 3 H=1, NY1
CALL PLOT (XL, YH, 3)
CALL PLOT (XL-XXH, YH, 2)
YH=YH+YS
CONTINUE

WRITE (Y1) LABEL

CALL LETTER (NHX, OH, 0.0, XX, XHO, HX)
IF=1

NUMBURING THE (NY1) CURVES

DO 6 I=1, NYC
XXX=XL+.2*OH
RC=.2*OH
RY=.15*SCALE
CALL UNITTO (XL, WY(1), XT, YHELP)
IF (YHELP.LE.(YCH1+YHH).AND.YHELP.GT.(YCH1-YHH).AND.IF.EQ.1) GO TO 4
IF=1
GO TO 5
XXX=XL+.45*SCALE
IF=2
CONTINUE
IF (I.GE.10) RY=RY-YYH
ENCODE (10, 13, C1) I
CALL SYMBOL (XXX, (YHELP-RY), OH, C1, 90., 10)
IF (I.GE.10) RC=RC+YYH
CALL CHAF (XXX-YYH, YHELP, RC, 3HCIR)
YCH1=YHELP
CONTINUE
XH=XL

WRITTING THE (Y1) NUMERICAL VALUS

DO 7 I=1, NX1
CALL PLOT (XH, YH+XXH, 3)
CALL PLOT (XH, YH, 2)
CALL INCHTO (XH, YH, XW, YW)
ENCODE (10, 12, XD) XW
CALL LETTER (10, OH, 90., XH+YYH, 2.9, XD)
XH=XH+XS
IF (CH.LE.XD) XH=XH
CONTINUE
IF (FLOAT(NYC)/FLOAT(6-NUL).LE.EXIT) GO TO 9
KPATH=0
GO TO 10
KPATH=1
NCON=NYC

WRITE (Y2) LABEL

CALL LETTER (NHX, OH, 0.0, XM, ZHY, HY)
CALL LETTER (16, OH, 0.0, XM, ZW1, W1)

WRITTING THE (Y2) NUMERICAL VALUS

DO 11 I=1, NCON
ENCODE (10, 13, B1) I
CALL SYMBOL (XE1, YE1, OH, B1, 0.0, 10)
ENCODE (10, 12, BW) WV(1)
CALL SYMBOL (XE2, YE2, OH, BW, 0.0, 10)
XE1=XE1+DXE
YE1=YE1+DYE
CONTINUE
IF (KPATH.EQ.1) RETURN
IF (EXIT.GE.6.0) RETURN

```

```

MAP 740
MAP 750
MAP 760
MAP 770
MAP 780
MAP 790
MAP 800
MAP 810
MAP 820
MAP 830
MAP 840
MAP 850
MAP 860
MAP 870
MAP 880
MAP 890
MAP 900
MAP 910
MAP 920
MAP 930
MAP 940
MAP 950
MAP 960
MAP 970
MAP 980
MAP 990
MAP 1000
MAP 1010
MAP 1020
MAP 1030
MAP 1040
MAP 1050
MAP 1060
MAP 1070
MAP 1080
MAP 1090
MAP 1100
MAP 1110
MAP 1120
MAP 1130
MAP 1140
MAP 1150
MAP 1160
MAP 1170
MAP 1180
MAP 1190
MAP 1200
MAP 1210
MAP 1220
MAP 1230
MAP 1240
MAP 1250
MAP 1260
MAP 1270
MAP 1280
MAP 1290
MAP 1300
MAP 1310
MAP 1320
MAP 1330
MAP 1340
MAP 1350
MAP 1360
MAP 1370
MAP 1380
MAP 1390
MAP 1400
MAP 1410
MAP 1420
MAP 1430
MAP 1440
MAP 1450
MAP 1460
MAP 1470

```

XE1=FLOAT(NUL)*DXE+3.04*SCALE
XE2=FLOAT(NUL)*DXE+2.54*SCALE
YE1=YE1-DYE
YE2=YE2-DYE
EXIT=EXIT+1.
IC=NCON+1
NCON=(6-NUL)*IFIX(EXIT)
GO TO 8

MAP1480
MAP1490
MAP1500
MAP1510
MAP1520
MAP1530
MAP1540
MAP1550
MAP1560
MAP1570
MAP1580
MAP1590

C
12
13

FORMAT (2PE10.2)
FORMAT (12)
END

	SUBROUTINE IBCIEU (F, IFD, X, NX, Y, NY, XL, NXL, YL, NYL, FL, IFLD, WK, JER)	IBC	10
	=====		
	DIMENSION F(IFD, NY), X(NX), Y(NY), XL(NXL), YL(NYL), FL(IFLD, 1), W	IBC	20
	K(1), BPAR(4)	IBC	30
	REAL BPAR, F, FL, WK, X, XL, Y, YL, ZERO	IBC	40
	DATA ZERO/0.0	IBC	50
	KER=0	IBC	60
	LER=0	IBC	70
	IF (IFD.LT.NX) GO TO 6	IBC	80
	IF (IFLD.LT.NXL) GO TO 7	IBC	90
	MER=0	IBC	100
	NXMI=NX-1	IBC	110
	NYMI=NY-1	IBC	120
	DO 1 I=1,4	IBC	130
	BPAR(I)=ZERO	IBC	140
1	CONTINUE	IBC	150
	DO 2 IY=1, NY	IBC	160
	CALL ICSICU (X, F(1, IY), NX, BPAR, WK(1), NXMI, JER)	IBC	170
	IF (JER.NE.0) GO TO 8	IBC	180
	CALL ICSEVU (X, F(1, IY), NX, WK(1), NXMI, XL, FL(1, IY), NXL, JER)	IBC	190
	IF (JER.NE.0) KER=37	IBC	200
2	CONTINUE	IBC	210
	KYL=NYMI*3	IBC	220
	KYLP1=KYL+1	IBC	230
	DO 5 IXL=1, NXL	IBC	240
	DO 3 IY=1, NY	IBC	250
	WK(KYL+ IY)=FL(IXL, IY)	IBC	260
3	CONTINUE	IBC	270
	CALL ICSICU (Y, WK(KYLP1), NY, BPAR, WK(1), NYMI, JER)	IBC	280
	IF (JER.NE.0) GO TO 9	IBC	290
	DO 4 IYL=1, NYL	IBC	300
	CALL ICSEVU (Y, WK(KYLP1), NY, WK(1), NYMI, YL(IYL), FL(IXL, IYL), 1, JER)	IBC	310
	IF (JER.NE.0) LER=38	IBC	320
4	CONTINUE	IBC	330
5	CONTINUE	IBC	340
	GO TO 10	IBC	350
6	MER=129	IBC	360
	GO TO 10	IBC	370
7	MER=130	IBC	380
	GO TO 10	IBC	390
8	MER=131	IBC	400
	IF (JER.EQ.131) MER=133	IBC	410
	GO TO 10	IBC	420
9	MER=132	IBC	430
	IF (JER.EQ.131) MER=134	IBC	440
10	ILR=MAX(MER, KER, LER)	IBC	450
	RETURN	IBC	460
	END	IBC	470

	SUBROUTINE ICSEVU (X,Y,NX,G,IC,U,S,M,IER)	ICS 10
C	=====	
	DIMENSION X(1), Y(1), C(1C,3), U(1), S(1)	ICS 20
	DATA 1/1/,ZERO/0.0/	ICS 30
	JER=KER=0	ICS 40
	IF (M.LE.0) GO TO 9	ICS 50
	NXM1=NX-1	ICS 60
	DO 8 K=1,N	ICS 70
	D=U(K)-X(1)	ICS 80
	IF (D) 1,5,3	ICS 90
1	IF (1.EQ.1) GO TO 6	ICS 100
	I=I-1	ICS 110
	D=U(K)-X(I)	ICS 120
	IF (D) 1,5,4	ICS 130
2	I=I+1	ICS 140
	D=DD	ICS 150
3	IF (1.GE.NX) GO TO 7	ICS 160
	DD=U(K)-X(I+1)	ICS 170
	IF (DD.GT.ZERO) GO TO 2	ICS 180
	IF (D.EQ.ZERO) GO TO 5	ICS 190
4	S(K)=((C(1,3)*D+C(1,2))*D+C(1,1))*D+Y(1)	ICS 200
	GO TO 8	ICS 210
5	S(K)=Y(1)	ICS 220
	GO TO 8	ICS 230
6	JER=33	ICS 240
	GO TO 4	ICS 250
7	IF (DD.GT.ZERO) KER=34	ICS 260
	D=U(K)-X(NXM1)	ICS 270
	I=NXM1	ICS 280
	GO TO 4	ICS 290
8	CONTINUE	ICS 300
	IER=MAX0(IER,KER)	ICS 310
9	CONTINUE	ICS 320
	END	ICS 330